Master's thesis

NTNU
Norwegian University of Science and Technology
Faculty of Engineering
Department of Geoscience and Petroleum

Arman Hiwa
Jonas Mannsverk
Vilde Romslo Meyer

Trajectory control, kick-detection and friction test: Transitioning to an automated drilling system.

Master's thesis in Petroleum Geoscience and Engineering
Supervisor: Tor Berge Gjersvik, Alexey Pavlov, Sigbjørn Sangesland
June 2020

NTNU
Norwegian University of
Science and Technology

Arman Hiwa
Jonas Mannsverk
Vilde Romslo Meyer

Trajectory control, kick-detection and friction test: Transitioning to an automated drilling system.

Master's thesis in Petroleum Geoscience and Engineering
Supervisor: Tor Berge Gjersvik, Alexey Pavlov, Sigbjørn Sangesland
June 2020

Norwegian University of Science and Technology
Faculty of Engineering
Department of Geoscience and Petroleum

NTNU

Kunnskap for en bedre verden

Abstract

This thesis was originally supposed to cover Phase II of the Drillbotics™ competition. However, it changed as a result of COVID-19. Work done prior to the outbreak is documented in appendices to convey the findings to next year's NTNU team. Henceforth, the content of this thesis will discuss the modified scope defined. The overall objective remains the same, respectively to "develop, test and validate technologies which enables autonomous directional drilling in the future". However, not limited to miniature scale.

Motives for utilizing automation includes releasing humans from performing repetitive and monotonous tasks, as well as developing new technology to keep the oil and gas industry economically feasible and most importantly improve overall safety. The transition from human labor to a fully automated drilling system should be carried out gradually. Three areas were chosen to further explore the automation potential, respectively trajectory control, kick detection and friction test. Models developed for all three areas utilizes OpenLab drilling simulator to collect necessary data.

As trajectory control was part of the original scope for Drillbotics© competition, the knowledge already acquired was used to investigate a solution for correcting unwanted deviation. Using the minimum-energy criterion a model for testing is created. Results show smooth well paths will increase overall borehole quality.

Uncontrolled kicks during a drilling operation have the potential to cause a well blowout. Therefore, an automated kick-detection model has been created and tested. Results indicate proper detection of actual kicks, however, it requires a reduction of false test results.

An autonomous friction test model has been designed with the intention to offload the human operator of repetitive tasks. The model is used to evaluate the hydraulic dependencies on the recordings. Findings indicate that flow rate greatly impacts the test results, while the impact of density is close to negligible.

Sammendrag

Denne masteroppgaven var originalt tiltenk å dekke Fase 2 av Drillbotics© konkurransen. Dette ble endret som følge av COVID-19 utbruddet. Arbeidet utført i forkant av COVID-19 er vedlagt, slik at det kan videreformidles til neste års NTNU lag. Videre vil denne oppgaven inneholde det nye omfanget, med nye problemstillinger. Hovedmålet forblir det samme, henholdsvis det å ≪utvikle, teste og validere teknologi som fremmer utvikling av autonom boring≫, men oppgaven er ikke lenger begrenset til miniatyr skala.

Motivasjonen for å benytte automasjon ligger i å frigjøre mennesker fra repetitive og monotone oppgaver, utvikle ny teknologi for å holde olje og gass industrien økonomisk bærekraftig, i tillegg til det viktigste aspektet - generell forbedring av sikkerhet. Overgangen fra menneskelig arbeidskraft til fullstendig automatiserte boresystemer burde foregå gradvis. Tre temaer ble valgt for videre undersøkelser i forhold til potensialet rundt automatisering, henholdsvis brønnbane kontroll, kick-gjenkjenning og friksjonstest. Modeller ble utviklet for alle tre temaene i MATLAB, og data ble innsamlet ved hjelp av OpenLab simulator.

Da brønnbane kontroll var en del av den originale oppgaven for Drillbotics© konkurransen, ble informasjonen som allerede var tilegnet brukt for å undersøke en løsning for korrigering av uønskede avvik. En modell ble utviklet basert på ≪minimum-energi-kriteriet≫ og viser at en jevn brønnbane vil øke brønnkvaliteten.

Ukontrollerbare kicks under boreoperasjoner har potensialet til å påføre en brønn utblåsning. Derfor har en automatisk kick-gjenkjenner blitt utviklet og testet. Resultatene indikerer korrekt registrering av reelle kicks, men trenger derimot optimalisering for å minske mengden falske resultater.

En automatisk friksjonstest modell har blitt utviklet med intensjonen å avlaste de menneskelige operatørene for repetitive oppgaver. Modellen er brukt for å evaluere resultatenes hydrauliske avhengighet. Observasjoner indikerer at strømningshastighet sterkt påvirker test resultatene, mens effekten av tetthet er tilnærmet neglisjerbar.

Acknowledgments

We want to express our greatest gratitude to our professors supervising; Alexey Pavlov, Tor Berge S. Gjersvik, Sigbjørn Sangesland and Sigve Hovda. Thank you for your continuous guidance and for sharing your knowledge and expertise, helping us solve the challenges encountered. We especially appreciate you assisting us in changing the scope due to COVID-19, and your swift adaptability.

Secondly, we would like to thank NORCE Energy for providing us with the OpenLab drilling simulator. A special thank you to Jan Einar Gravdal for providing help related to the use of the software.

Though the Drillbotics© was canceled, we want to show our appreciation to the people supporting in Phase II. Thank you to Noralf Vedvik and Steffen W. Moen for sharing your knowledge, as well as assisting with practical challenges encountered during Phase II of Drillbotics©.

We would like to express our appreciation to Lyng Drilling for assisting us in designing the drill bit and of course for manufacturing the bits for free. A special thank you to Are Funderud for inviting us to your premises, showing us around and answering all our questions when designing the bit.

We would like to acknowledge the Department of Geoscience and Petroleum at NTNU for providing us with the opportunity to work together as a multidisciplinary team to solve comprehensive engineering challenges providing valuable hands-on experience prior to our careers. Also, thank you to Drilling System Automation Technical Section (DSATS) for providing us students with this platform to solve highly relevant engineering challenges.

Lastly, we would like to give special recognition to BRU21 (Better Resource Utilization in the 21st century) for sponsoring the Drillbotics © project.

Table of Contents

List of Tables

List of Figures

Acronyms

ASM along string measurements.
BHA bottom hole assembly.
BOP blow-out preventer.
DLS dogleg severity.
DSATS drilling system automation technical section.
FRT free rotating torque.
FRW free rotating weight.
HSE health, safety and environment.
IIBOP instrumented internal blow-out preventer.
KOP kick-off point.
LOA level of automation.
LWD logging while drilling.
MAD mean absolute deviation.
MD measured depth.
MPD managed pressure drilling.
MWD measurements while drilling.
NPT non-productive time.
NTNU Norwegian University of Science and Technology.
PDM positive displacement motor.
PID proportional-integral-derivative.
PUW pick-up weight.
RC radius of curvature.
RKB rotary kelly bushing.
ROP rate of penetration.
RPM revolutions per minute.
RSS rotary steerable system.
SOW slack-off weight.
SPE society of petroleum engineers.
SPP standpipe pressure.
T&D torque and drag.
TVD true vertical depth.
UI user interface.
WDP wired drillpipe.
WOB weight on bit.

Chapter 1

Introduction

A main objective in the energy sector is developing and implementing digital technology and digitalization, as its potential and possible impact is of great significance. Transitioning into a low-carbon energy system is necessary to reach the 2 degree climate target[1], and an essential contributor to this is digital technology. Automation is amongst the digital technologies available today with the potential to make a difference, emphasized by already proven advantages. This technology is gradually replacing manual labor, with benefits including improved safety, increased productivity, higher production rates, better product quality and lower operational costs [2].

As oil and gas reservoirs are being depleted around the globe, the resources are becoming more challenging to extract. In order for the industry to still be economically feasible, new innovated solutions are essential. Partly to fully automated operations, specifically in drilling, is an important stepping stone for the petroleum industry to evolve. In 2008, society of petroleum engineers (SPE) established drilling system automation technical section (DSATS) to invest time and resources into drilling automation. DSATS' main objectives include increasing safety and drilling efficiency by developing technology that links downhole measurements and tools with topside [3]. As a continuance of DSATS - an international competition known as Drillbotics©, was introduced. The first competition was held in

[1] Keeping the global temperature rise this century below 2°[1].

2014, engaging university students at all levels in further developing and implementing drilling automation.

The odd situation caused by COVID-19 has affected this project, changing the overall scope. However, the long-term objective remains the same; ”develop, test and verify technologies that enables autonomous directional drilling in the future”. The outline of the Drillbotics© competition has since the beginning been to design and build a miniature drilling rig with the ability to autonomously drill a rock sample using control algorithms and downhole sensors [4]. With this in mind, the new scope's biggest change is that the team is no longer limited to the miniature scale and will use full-scale offshore operations as a basis.

With moving the focus to full-scale offshore operations at the end of March, the team regrouped and familiarized themselves with the topic. A new scope was defined in collaboration with the supervisors at the beginning of April.

The progress made by the team in regards to the Drillbotics© competition will be addressed in Appendix C.2, so the work will not go to waste and can be further developed by future Norwegian University of Science and Technology (NTNU) teams. However, the main parts of this thesis will discuss the new scope, including drilling automation today, three focus areas chosen to further investigate as well as autonomous models created and tested.

Chapter 2

Project Objectives

The original scope and associated objectives of this thesis had to be modified due to the impact of COVID-19. All of Norwegian University of Science and Technology (NTNU)'s campuses were closed down for all students on March 12th, the same day that the Norwegian Government initiated the strictest measures taken in peacetime. Unable to access the lab, the team was could not continue the work related to the drillstring mechanics, control system and the rig in general. As this is an extraordinary situation, the team and supervisors sat down and discussed possible scope adjustments that could be made such that prior work does not go to waste, and a comprehensive and copious thesis is still delivered at the original deadline. This chapter will give a description of progress made in regards to the Drillbotics© competition prior to the outbreak of COVID-19 in Norway; a supplementary detailed description is written in Appendix C.2. Thereafter, the new modified scope will be presented.

2.1 Drillbotics©: Progress Made Before the Outbreak of COVID-19

The outline and scope of the Drillbotics© competition heavily depend on collaboration, and it encourages to assemble a multidisciplinary team with a maximum of five students. Going back to August of 2019, NTNU gathered a team of five stu-

dents with different academic backgrounds; respectively two cybernetic students specializing in autonomous systems and three petroleum students specializing in drilling engineering. This would have been NTNU's fourth year competing in the international competition with outstanding results from the previous years, respectively second place in 2017, first in 2018 and ranked first in the preliminary rounds in 2019.

The competition is divided into two phases; Phase I (the design phase) and Phase II (the building and testing phase). During the fall semester, or Phase I, the team decided on a design, which was submitted in a detailed report to the committee [5]; a synopsis is given in Appendix C.1. Based on this report the NTNU team qualified for the 2020 Drillbotics© competition and was invite to Celle, Germany at the end of June.

2.1.1 Problem Statement for the 2020 Competition

The problem statement of the 2020 Drillbotics© is as follows: "Design a rig and related equipment to autonomously drill a well, using downhole sensors, that is able to hit multiple directional targets, as quickly as possible while maintaining borehole quality and integrity of the drilling rig and drillstring" [4].

The design is therefore required to be able to build an inclination angle as well as changing azimuth. Also, the committee asked the teams to focus more on the autonomous aspect of the design by implementing closed-loop control.

2.1.2 Phase II

Starting Phase II on a good note, the team received positive feedback from the Drillbotics© committee and was accepted as one of the finalists in the international competition. To ensure efficient workflow, the team discussed expectations for the upcoming phase right of the bat. The project was divided into smaller tasks and a priority list was made. Thereafter, the tasks were distributed amongst the team based on interest, experience and competence to take advantage of each team member's strength. As new challenges came to light, they were divided appropriately

amongst the team members. A time planner, with associated risk, was also created.

The top mechanical priority was to design and produce a sustainable positive displacement motor (PDM). Based on the literature study conducted in Phase I, the team worked in Solidworks to develop a design for the rotor and stator. Samples were 3D-printed early on to both get familiar with the printer, in addition to the printing process being time-consuming. Multiple types of plastic were used when printing, providing the opportunity to print PDMs with a variation in mechanical properties. Based on learning's from testing the 3D-printed parts in plastic, a final design was to be manufactured. To limit problems related to wear, the team was planning on using a plastic stator and steel rotor. Final lobe configuration is determined based on learning's obtained from the testing phase.

Though it is not as complex and time consuming as the PDM, the bent sub is highly prioritized. The challenge associated with the sub is possible leakage, which is a bigger problem with an adjustable solution as opposed to a fixed. After consulting with the mechanical lab engineer and considering the path limits versus the possibility of leakage, the team was leaning towards changing the original design. This entails a fixed sub, with a fixed angle, which possibly would limit the team to hit the competition target(s).

Baker Hughes provided each team with two generic directional polychrystalline-diamond compact (PDC) micro-bits designed specifically for the Drillbotics© competition. The guidelines still allowed for the teams to design their own drill bit if desired, which the NTNU team was motivated to do. Continuing the collaboration with Lyng Drilling from previous years, the team began designing a drill bit using Solidworks. Lyng Drilling offered to manufacture the drill bit designed for free of charge.

A detailed description of progress made in Phase II is presented in Appendix C.2.

2.2 Affects of COVID-19

The same day as NTNU locked down all campuses, the Drillbotics© committee announced that the competition was still scheduled as planned, but with conditions changing rapidly, a continuous risk assessment would be performed [6].

Shortly after the campus was closed down, the student team and supervisors sat down discussing options. Though the competition was not canceled at this point it was decided that NTNU would not participate regardless due to the circumstances; Drillbotics© was officially canceled on April 10th [7]. Obviously, this was a huge set back as the team had already spent a significant amount of time working towards the competition in June. Furthermore, it was decided to split the team into two groups based on disciplines, respectively separating between petroleum and cybernetics. With the obvious time constraints each group had to modify the current scope swiftly and quickly adapt to the situation.

2.3 Modified Scope and Objectives

The overall objective, for the petroleum team, will still remain as ”develop, test and validate technologies which enables autonomous directional drilling in the future”. The main difference is that the team will scale up looking at full-size offshore drilling operations. Thesis objectives will include:

- Give an overview of automation implemented in drilling operations today.
- Consider different parts of the operations that will benefit becoming autonomous.
- Create models for testing and simulation.

These objectives are wide and very much open for self-interpretation. The team quickly familiarized themselves on the progress of drilling automation today, and possible gaps to try and fill. With the limited time left, the team has chosen to

focus on three parts of the drilling operation, and explore the automation potential of these:

- Trajectory Control.
- Kick Detection.
- Friction Test.

Chapter 3

Health, Safety and Environment (HSE)

Health, safety and environment (HSE) is the number one priority in the oil and gas industry. In recent times, risk reduction, avoiding errors and overall less human interaction are the main objectives. The goal is to always reduce number of accidents, especially those involving physical injuries. This thesis discusses implementation of drilling automation in full-scale operations, which obviously comes with many benefits. The leading benefit, in regard to safety, is removing humans from the site, especially away from the red zone[2]. However, as it is further investigated there are also consequences to be aware of with reducing human involvement as the technology is complex. It is essential that an automated system is reliable and has undergone excessive testing before completely removing the human connection.

3.1 Mode Confusion

Iversen et al. [9] define mode confusion as a downside of automation. Mode confusion entails that an automated system behaves differently than what is expected in such a way that the operator is not aware or does not comprehend what the

[2] A defined zone of the drill floor where the crew could be exposed to dropped objects, and in close reach to remotely operated pipe handling equipment, such as drilling machinery [8].

system is doing. The phenomenon is of high relevance today, with the increasing implementation of autonomous- and advisory systems in the oil and gas industry.

There are two categories of error as a consequence of mode confusion; error of commission and error of omission. Error of commission relates to when the operator is not aware of which mode the system is operating in. The human operator performs the appropriate action for one operational mode when the system is operating in another mode. Subsequently, error of omission consists of errors where the human operator fails to detect and/or react to an undesired system behavior [9]. Studies and experience from the aviation industry have shown that the latter types of errors are the dominant forms. Because these system behaviors are unexpected, the operator is less likely to pay enough attention and detect the undesired behavior [10].

3.1.1 Human Operator Error

A series of test cases were performed by Iversen et al. [9] in a drilling test facility to understand the potential of human error in different automation scenarios. Observations made provide further insight into the benefits and challenges automation encounters today.

More automation cause higher risk of operator error

A series of cases where different levels of automation (LOAs) for tripping, specifically to avoid surge and swab, were conducted. Observations from the study suggested that transitioning towards more system control, i.e. a higher LOA, increased the incidents of error when human interaction was first initialized. A hypothesis exercised is that the causes of these errors could correlate to the increased difficulty for the operators to understand the state of the system at all times [9]. The hypothesis is based upon Billings' [11] work about automation in the aviation industry, where he discovered a correlation between automated planes and human response, which Iversen conveyed on to the petroleum drilling industry.

Operator error increases if too much freedom of choice

In another series of test cases conducted, the driller was given the freedom to adjust the drilling parameters defined by the automated system. It was observed that though the driller desired to operate the system more conservatively, the automated system's advice was followed. This observation corresponds with other studies indicating people generally follow the advice given by an automated system, as opposed to trusting their own instinct [9]. Comparing these findings with the previous case-observations, it appears that the operator suspects that the automated system is wrong and chooses to not take the appropriate actions. Furthermore, this indicates that though the operator has the knowledge to adjust the system parameters, their confidence in automated systems prevents them from taking necessary manual action to mitigate unwanted behavior.

Higher levels of automation, increased efficiency

The final observation conducted from the study suggested that a higher LOA increased the overall efficiency of the operation. A probable reason for this is that the driller switches their area of focus from controlling the drilling operation to focus on the process as a whole. This increases the possibility of detecting problems at an early stage and solve the challenges encountered.

An aspect worth mentioning in regards to higher LOAs is the potential of the driller not actually paying attention to the process, and as a consequence not detecting unexpected circumstances. Though it is not addressed in the study, it should be considered when implementing automated operations [9].

3.2 Human Operator's Role

When designing an automated system, it is with the intention to increase the overall operational HSE. As mentioned above, the introduction of automation does not directly lead to increased safety and efficiency. Most automated systems are in need of a monitoring operator, which is capable of taking appropriate action in case of unwanted system behavior. When implementing an automated system, a critical

aspect is to decide to what extent the human operator should be a part of the system. This includes both the operator's level of expertise as well as his knowledge of the system's operating modes. Appropriately determining these factors is important as it might decrease the probability of mode confusion.

3.2.1 Human Factors Influence

A case study for drilling automation conducted by Moralez et al. [12] focused on the human operator's behavior and perception related to automated systems. The observations related to the human operator's experience is presented below.

Misunderstanding of goals and benefits

Studies suggest that when implementing an automated system, the operators have not been fully aware of the goals and benefits of automating a process. In regards to drilling performance, it has been observed that operators believe the main and only goal with automation is increasing system efficiency.

A study performed on tubular tripping cases, where tripping time per stand was recorded using an automated system and compared to manual tripping performance. The results conducted from the study provides an explanation as to why human operators might not be convinced of the benefits with automated systems, as the time per stand when manually tripping usually was shorter. However, though the manual tripping speed was faster, the automated system delivered steadier tripping performance which increased the overall efficiency [12].

Different operational sequences

The possibility for error of commission increases if a system performs an operation different from what the operator is taught to do. Additionally, if the operator has mistrust in the system executing the operation, it leads to discomfort and distrust. An operator with distrust to a system is then less likely to interact in case of actions needed to be taken [12].

Repetitive and monotonous tasks

Mainly operations with high LOA implemented in the industry today apply to repetitive tasks. Such repetitive and monotonous tasks will over time be difficult to maintain on a high level of performance and can lead to "out of the loop syndrome", where the probability of errors of omission increases [13].

3.2.2 Human Operator: Integral Part of System

The overall goal of automating the drilling industry is not to get rid of human labor completely, but rather remove human interaction from hazardous and dangerous operations. Respectively transition humans from performing the operations to a monitoring and generating function. The previous sections touched on different safety aspects that should be addressed when automating an operation, mostly in regards to the human-computer interaction.

An automated system is never 100% reliable, and will subsequently always require human interaction to some extent to maintain a high level of HSE. In order for a human operator to interact when needed, it is essential for them to hold the necessary expertise and knowledge about the system. Introducing and educating the human operator on the closed-loop system is of high priority, as it will improve the operator's knowledge about the system in addition to keep the engagement of the operator at the desired level.

Chapter 4

Automation

Automation has traditionally been defined as the use of automatic devices and controls instead of human labor. This definition has with time broadened to cover a wider range of mechanical processes, also human labor expanded to include both physical- and mental labor [14]. This leads to the need for a modernized definition of automation. Sheridan [15] defines automation as:

- Mechanical action.
- The mechanical sensing of environmental variables and the integration of those.
- Data processing and decision making.
- Communication of processed information to people.

The automotive and aeronautical industries have utilized automation in repetitive or dangerous operations for years. This chapter will cover how to define automated processes, the history of automation in the drilling industry, its current state and industry initiatives and technology development that might simplify the steps towards a higher level of automation (LOA).

4.1 Levels of Automation

The industry consists of a wide range of different operations and processes, which all have a specific degree of automation. Defining the different LOAs is impor-

tant for both analyzing the progress made in the industry today, as well as which LOA the different operations seek to reach. Endsley [16] created a LOA model which divides the operation into four different functions: monitoring, generating, selecting and implementing. Ten LOAs were created by assigning these functions to human-controlled, computer-controlled, or a combination of the two. Table 4.1 shows the ten LOAs, and it can be used to analyze the LOA for any operation.

Table 4.1: LOA10 system for levels of automation [16]. Color coded simplified LOA10 system; yellow (monitor), green (advice), pink (control) and orange (autonomous) [17].

	Functions (H = Human Controlled, C = Computer Controlled)			
Levels of Automation	**Monitoring**	**Generating**	**Selecting**	**Implementing**
1. Manual Control	H	H	H	H
2. Action Support	H/C	H	H	H/C
3. Batch Processing	H/C	H	H	C
4. Shared Protocol	H/C	H/C	H	H/C
5. Decision Support	H/C	H/C	H	C
6. Blended Decision Making	H/C	H/C	H/C	C
7. Rigid System	H/C	C	H	C
8. Automated Decision Making	H/C	H/C	C	C
9. Supervisory Control	H/C	C	C	C
10. Full Automation	C	C	C	C

The LOA10 system, expressed in Table 4.1, goes from fully manual control (L1) to fully automated control (L10), where the system gives feedback to the operator if necessary. This system is an advanced and detailed tool, helpful when analyzing automated processes. Furthermore, a more simplified system is developed where the ten LOAs are reduced into four correlating categories: monitor, advice, control and autonomous [17]. The simplified LOA10 system focuses on the computer's role in the process and is illustrated by colors in Table 4.1.

4.2 Automation in Drilling

Developing new technologies to increase productivity and efficiency, while still maintaining a high level of quality and safety, are always the main focus in the drilling industry. Replacing human labor operating in red zones with automated machinery is clearly a safety enhancement along with others discussed in chapter 3. Though it is not the main motivation, increasing economic feasibility in

terms of improved overall efficiency and deliver a better end product is definitely a desire to increase the overall LOA in the industry.

4.2.1 Evolution

In the early 1860s, the first innovation associated with automated drilling operations saw the light of day, an automated bit feed controller. This bit feed technology was to be used when drilling blast holes for European tunnels [18]. Throughout history, there have been many initiatives to improve the drilling operation, such as optimizing processes and improve safety. This evolution has led to how today's drilling operations are executed. The early attempts focused on mechanizing operations performed by humans.

In 1971, the use of computer controls for rig operations were investigated. The closed-loop control system was built up by a mixture of electrical and pneumatic components, measuring and controlling the weight on bit (WOB) and rotary speed by varying the engine throttle. To compare actual conditions with expected ones, the system used simulations and made changes accordingly [18]. The early attempts of computer control systems required a well-trained driller to operate the system, and it did not allow for problems to be solved in the field.

Computer control systems have come a long way from when they were first introduced. In addition to controlling the WOB, it can also maintain parameters, such as rate of penetration (ROP), constant hydraulic pressure and torque. A major evolution in drilling computer control system is the driller's consoles, moving the operator in to the doghouse with computer screens and joystick controls, and away from monitoring rudimentary weight and pressure gauges outside in harsh weather [18].

4.2.2 Current State

The petroleum industry in general is known to be conservative, especially offshore, when it comes to implementing new solutions and technologies. This is foremost related to the safety of the rig crew, but also the cost and complexity of performing

the rig modifications. Drilling automation has been on the agenda in the drilling community for some years, with growing interest. The society of petroleum engineers (SPE) established a technical section, known as the drilling system automation technical section (DSATS), with the purpose of accelerating the development and implementation of automated drilling systems [3]. Table 4.2 lists examples of automated products available today in the simplified LOA10 system.

Table 4.2: Examples of automated drilling solutions [17].

Monitor	Advice	Control	Autonomous
• Smart alarms • Wellsite monitoring systems	• Drilling dynamics diagnostic systems • Directional drilling advisors	• Stick-slip surface control • MPD control systems	• MWD RSS • LWD formation samplers • Auto-driller

Today's drilling automation encompasses a hierarchical system of automated subsystems. The lower ranks in the hierarchy are often those with the highest LOAs. Looking at the examples listed in Table 4.2, the drilling solutions with the highest LOAs are the ones programmed to perform the operator's tasks throughout the whole operational sequence. The existing technology performs its tasks initiated by the driller without awareness of the overall operational process. It relates only to what is happening right now, how to prevent breaches and to understand the current activity performed [2].

Challenges encountered by the industry today comprises of moving the overall drilling system from L2 of LOA10 to a higher LOA [17]. The main challenge for increasing LOA is for individual subsystems to work together, creating a quality borehole. Future automated drilling systems call for the technology to recognize all types of activities related to the operation, this includes current, present and future.

4.2.3 Technology Allowing for Automation

The current state of automation in the industry can be described as a manual drilling process, consisting of automated sub-processes [17]. Proceeding towards

a higher LOA in drilling operations depends on new technology development and close collaboration between companies involved. This section will cover some technology improvements and initiatives taken to give a foundation for transitioning into autonomous drilling operations.

Wired drillpipe

Real-time data acquired from downhole sensors while drilling is an essential part of the modern drilling system. Replacing the traditional wireline sensors with logging while drilling (LWD) and measurements while drilling (MWD) gives access to real-time measurements, usually providing more data with better quality, or nonetheless maintain it. Though there are lots of progress in the while-drilling sensor technology, it has been limited by the reliance on mud-pulse telemetry and its transmission speed of about 10-12 bits per second. Since the mid-nineties, a technology known today as wired drillpipe (WDP) has been in development. It is designed to overcome the mentioned shortcomings of mud-pulse telemetry and had its first commercial job in 2006 [19, 20].

WDP is equipped with an armored coaxial cable through each joint with a field removable and replaceable inductive coil at the pin and box side of the pipe, shown in Figure 4.1. The main application of WDP is equivalent to a conventional drillpipe, respectively maintain drilling efficiency and performance. Furthermore, it possesses additional applications such as its bi-directional ability, high-speed telemetry to exceed 57 600 bits per second and its high reliability providing uptimes of 98% [21]. WDP has supplied the drilling process tremendously, including improving safety, saving operating time, improving wellbore quality and extending reservoir sections.

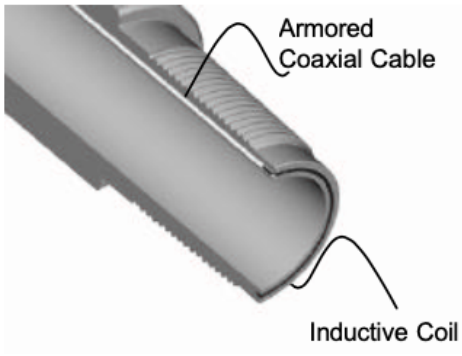

(a) Section view of WDP [19].

(b) Field replaceable WDP coil [20].

Figure 4.1: WDP design.

WDP has made it possible to achieve faster MWD and LWD telemetry rates, as well as instantaneous downlinking from topside to downhole tools. Moreover, this greatly contributes to the probability of fully automating the drilling system, where the high-frequency downhole data is fed to the control system to optimize drilling operations and ensure consistency [22].

Along with expanding the application envelope compared to existing technology, WDP allows for obtaining measurements along the string. Signal boosters along the drillstring are essential for the signal to be transported all the way to surface [20]. Conditions of the booster subs includes for the telemetry signal to improve the signal to noise ratio, and further improve efficiency between downhole components and surface. These booster subs can be customized to provide along string measurements (ASM), as well as boosting the telemetry signal. ASM enables for obtaining measurements such as bore- and annular pressure, temperature and three-axis vibration [22].

By integrating the WDP technology to a closed-loop drilling system, the applications of WDP expands far beyond a conventional drillpipe, and should therefore

be integrated into a closed-loop drilling system. Detecting small downhole pressure variations at multiple depths is made possible with the increased telemetry speed and downhole ASM. This is essential to facilitate for detection of mud-loss and early kick detection [20].

Engineering while drilling

Today's drilling operation is highly dependent on decisions and calculations made in the planning phase of a well program. During the planning phase, the drilling engineer plans the well design in accordance to a proposed well path, which often differs from the actual drilled path. The design plan is based on estimates of friction, pressure gradients, drillstring dimensions, and mud rheology. Though there is a pre-defined drill plan in place it is not sufficient enough for an automated drilling system, because it will often deviate from the actual well conditions. Until recently, the industry has lacked a system capable of continuously and accurately determine the dynamic wellbore changes. However, with increased computational power and improved models for solving complex finite difference equations, real-time models are available today [23].

Combining real-time access of downhole measurements and real-time models while drilling opens up for engineering while drilling. Moreover, this allows the operator to continuously make appropriate drilling decisions with higher certainty as they are based on actual downhole conditions.

Companies interoperability

Other industries have gone through or are currently in the transition phase of moving towards a partly- or fully-automated industry, as the drilling industry is today. Lessons learned from other industries highlight an important factor that lacks in the oil and gas industry, respectively interoperability [17]. Most drilling operations involve multiple companies collaborating, each with their own software and corresponding digital language. Progressing towards a fully automated drilling operation requires interoperability between the software involved, more specifically its ability to communicate with each other.

Early on DSATS' objective was to search for a digital infrastructure capable of promoting collaboration between the various companies interested in drilling automation [17]. This digital infrastructure should be able to incorporate various components from different equipment and easily connect them, interact with one another and share high-quality data. Such initiatives are of high importance in the steps towards a drilling operation operating at a higher LOA.

Chapter 5

Automated Drilling Subjects

As mentioned in section 2.3 the team has chosen three areas of the drilling operation to further explore their automation possibilities, respectively trajectory control, kick detection and friction test. These subjects were chosen with the mentioned overall objective in mind, ”develop, test and validate technologies which enables autonomous directional drilling in the future”. This chapter will discuss why these focus areas were chosen, in addition to introducing the simulation software used in the automated models created.

5.1 Motive for Choice of Focus Areas

After changing the scope, the team spent some time familiarizing themselves with the current state of automation in full-scale drilling operations. It was quickly realized that repetitive operational tasks encompass a great potential of being automated. Therefore, the team saw great potential in further investigating the repetitive tasks performed during a friction test.

Kick detection is chosen as the second focus area, primarily to improve health, safety and environment (HSE) by assisting the driller in detecting possible kicks. The motivation for further investigating kick detection includes utilizing the commercialized wired drillpipe (WDP) technology.

The third area chosen to investigate further is trajectory control, as this was a considerable part of the original Drillbotics© scope. Directional drilling is in recent times frequently used to reach feasible pay zones, as oil and gas resources are becoming less accessible. Furthermore, as a directional driller has many tasks maintaining a high level of performance on all is close to impossible. Therefore, automating parts of the process is desired.

5.2 OpenLab Drilling Simulator

OpenLab Drilling is a free access digital infrastructure that offers access to a high fidelity drilling process simulator, developed by the drilling & well modeling group at NORCE Energy in collaboration with the University of Stavanger (UiS). The OpenLab infrastructure has since 2018 been publicly available, especially relevant for students, researchers and engineers working with technology development, demonstration and education. OpenLab simulation data can be accessed using MATLAB [24].

5.2.1 Configurations

A configuration in OpenLab is a model that defines the parameters affecting the circulation system and drillstring mechanics [24]. The configuration is made and edited using the OpenLab user interface (UI). It can be generated both from a predefined template, or the user is able to customize the configuration by editing the hole section, well path, drilling fluid properties, drillstring elements, formation properties and rig equipment.

Well path

The well path is generated by defining parameters at the survey stations along the trajectory. For each survey station, the user defines measured depth (MD), inclination and azimuth. Based on these inputs true vertical depth (TVD) and dogleg severity (DLS) are calculated at every survey station.

Hole section

The hole section tab defines the parameters related to the riser, casing design and an optional openhole section. The riser- and casing design specifies the start- and end depth(s), in addition to the outer- and inner diameter. The open hole section specifies its length and hole diameter. The configured hole section is the initial state of the well at simulation start.

Drilling fluid

A configuration can define two accessible drilling fluids for the simulation. The fluids are defined by the fluid density, rheology, gel strength, oil-water ratio and the base-oil PVT[3] data. During a simulation, it is possible to instantly change between the two fluids types.

Drillstring

The drillstring is constructed by defining lengths, weights and sizes of the bottom hole assembly (BHA) elements and the drillpipes. This is also where the BHA design is presented, consisting of the necessary technology to execute the simulations, as well as collars, heavy weight drillpipes, stabilizers, cross-overs and a float sub.

The technology available to choose from are components configured for along string measurements (ASM), measurements while drilling (MWD), logging while drilling (LWD) and a steerable rotary tool, which are defined as:

- The ASM feature is added as a joint either on the BHA or along the drillpipe. The configuration allows for several ASM joints to be placed on the BHA or along the drillstring. Continuously internal and annulus pressure measurements are obtained at the joint's exact depth.
- The MWD tool measures the physical properties and is located on the BHA. Measurements obtained include pressure, temperature and wellbore trajectory in a three-dimensional space [25].

[3] Pressure, volume, temperature.

- The LWD tool measures formation properties during the excavation of the hole. This gives the advantage of measuring formation properties before being invaded by the drilling fluid [25].
- The steerable rotary tool transforms the BHA into a rotary steerable system (RSS), which allows for deviated drilling.

Geology

In the geology tab, the geo-pressure and geothermal gradients are defined along with the formation strength properties. As for well path, parameters at each survey station are plugged in, specifying the gradients and strengths at the relevant TVDs.

Rig equipment

The rig parameters defines the limitations of the rig equipment. Some of the parameters are adjustable, such as the managed pressure drilling (MPD) and blow-out preventer (BOP) maximum choke change rates, maximum acceleration of mud- and MPD pumps, traveling block weight, maximum rotational acceleration of the top drive, maximum acceleration of the drawworks, mud loss in shaker and the tank volume of the main and reserve mud tanks.

5.2.2 MATLAB Simulation

The OpenLab simulator offers the possibility to execute and access simulation data via MATLAB. Procedures and scripts used to connect MATLAB to the simulator is set up by the OpenLab developers and can be obtained from the OpenLab website [26]. In order to initialize a simulation, it needs to be configured. The simulation configuration includes both model configurations and initial simulator set-points.

Simulation model configuration

A requirement for configuring a simulation model includes defining necessary model properties and parameters, starting with determining the initial bit depth. Thereafter, the simulator allows for choosing between two different physical models: steady-state torque and drag (T&D) and transient T&D. The steady-state

model is a simplified model, while the transient model is a more advanced physical model. Finally, the user can define possible drilling incidents to occur during the simulation, such as influx or loss in the well. The simulator allows for incidences of influx and loss to be turned off or activated based on geo-pressure gradients, in addition influx/loss can be controlled manually. Adjustable inputs of the simulation model are presented in Table 5.1, with its corresponding default values.

Table 5.1: Model configurations and its default values.

Model configuration	Description	Default value
Initial bit depth	Depth of bit at t = 0	Target depth
Reservoir model	Kick or influx simulation	false
Manual reservoir mode	Manual or geo-pressure controlled kick/influx	false
Manual mass rate	Mass rate for manual influx or loss	0 kg/s
Manual total mass	Total mass for manual influx or loss	0 kg
Manual depth	Depth for manual influx or loss	Initial bit depth
Reservoir kick-off time	Time when influx or loss occuring	60 s
Transient mechanical model	Use the transient torque & drag model	false

Set-points

In addition to configuring the simulation model, the simulator needs to be fed initial set-points. The set-points optional to define, includes the main pump flow rate, top-of-string velocity, rate of penetration (ROP), surface revolutions per minute (RPM), MPD properties, BOP status, and the volume and temperature of active- and reserve pit. The objective of the simulator is reaching the set-points, and the time it takes to reach them is limited by the rig equipment and other mechanical constraints. It is possible to change the set-points at any time-step of the simulation. If a set-point is not defined, the simulator will choose its default value, listed in Table 5.2.

Table 5.2: Simulator model set-points and its default values.

Set-points	Default value
Top of string velocity	0
Flow rate in	0
Surface RPM	0
MPD choke pump flowrate in	0
MPD choke opening	1 (open)
BOP choke opening	1 (open)
Inlet fluid density	Main fluid
ROP	0

5.2.3 Drilling Incidents

While running a simulation it is possible to generate several fictional events based on real-life drilling situations. These fictional events are initiated in the OpenLab UI via the incidents tab.

Pack off

Pack off is when the wellbore is plugged around the drillstring during drilling. Poor transportation of cuttings and cavings is the most common reason for pack off to occur, worst case it is caused by a portion of the wellbore wall collapsing around the drillstring [25].

The pack off incident can be initiated in the simulator with a wide range of pack off conditions. Amongst properties used to define pack off incidents critical hole cleaning flow rate, RPM and cuttings proportion are the most important. In addition it is possible to define a reopening rate, such that it is possible to counteract the pack off incident in the simulator.

Pipe washout

A washout in an openhole section results in an enlarged region of the wellbore. This enlargement can be caused by excessive bit jet velocity, formation properties,

mechanical damage along with others [25].

In order to use the washout feature, it has to be configured as part of the simulation model, this includes the washout location and its distance from the bit as well as washout volume. It is not possible to use this configuration while simulating via MATLAB. The OpenLab simulator is able to regulate the washout fraction from 0 to 100%.

Manual influx/loss

It is possible to initiate simulations of manual influx or loss via MATLAB; this is also possible to activate via the OpenLab simulation UI. Applying this feature requires the simulator to be set to a manual reservoir mode, referring to Table 5.1.

Manual scenarios of influx/loss are initiated by defining the MD, in addition to the mass rate and total mass.

Friction

Friction is defined as the force resisting drillstring motion in the wellbore. The simulator offers the opportunity to modify the friction coefficients prior as well as during the simulation. Wellbore friction consist of five friction coefficients, respectively hydraulic string friction and annulus friction, steady-state T&D rotational and sliding friction in addition to steady-state T&D hydraulic efficiency. The default values of the wellbore frictions are listed in Table 5.3.

Table 5.3: Simulator wellbore friction coefficients default values.

Friction coefficient	Value
Hydraulic string	1
Hydraulic annulus	1
Steady-state T&D rotational	0.25
Steady-state T&D sling	0.25
Steady-state T&D hydraulic efficiency	0.25

Bit plugging

Lastly, the option of plugging the bit can be used as one of the OpenLab drilling incidents from the simulation UI. This causes the simulation to perform a clogging of the bit-nozzles and initiates disruption in the wellbore. Options for this feature, include the percentile opening of the bit nozzles ranging from 0 to 100%, where 0% is no flow through nozzles, while 100% represents fully opened nozzles.

5.2.4 Shortcomings of Simulating via MATLAB

The team has experienced some difficulties with the shortcomings associated with using MATLAB in accordance with OpenLab.

First of, the OpenLab UI has an option making adjustments in the ”Inital Condition” tab. Five parameters can be changed, including bit depth, top of string position, main and reserve pit volume as well as the temperature in the respectable pits. However, in MATLAB only the bit depth can be changed.

Another shortcoming of using Openlab with MATLAB is that it is not possible to extract the well configuration data, mentioned in section 5.2.1. One can however manually extract the data-sheets from the well in the Openlab UI as a counteracting solution.

Chapter 6

Trajectory Control

The world's oil and gas reservoirs are continuously being depleted, hence becoming less accessible and more challenging to produce. As a result, extended-reach and horizontal drilling are highly relevant to access the pay zones. This section will cover some basic theory and terminology on directional drilling, how to achieve a smooth transition to automated trajectory control, some control theory as well as testing of a trajectory control method.

6.1 Directional Drilling

Directional wells are known to be an efficient solution to reach challenging or impossible drilling targets. A downside with directional drilling is higher operational cost, but this again is partly compensated with minimized surface construction.

Directional drilling is defined as a method to direct a wellbore to the desired target(s) along a predetermined trajectory [27]. A well with inclination less than 5°is defined as a vertical well, while a high deviation well has an inclination greater than 60°; horizontal wells have an inclination greater than 85°. Applications of directional drilling include [28]:

- Drilling multiple wells from one offshore installation or limited areas onshore.

- Drilling single wells to less- or in-accessible reservoirs.
- Using the well path to connect multiple targets by utilizing side-tracking.
- Geo-steering.
- Steering away from challenging geological structures or formations, such as salt domes.
- The lateral length of a reservoir is usually notably greater than the vertical length, subsequently, a deviated or horizontal well will increase overall reservoir drainage area.
- Correcting unwanted well path deviations.

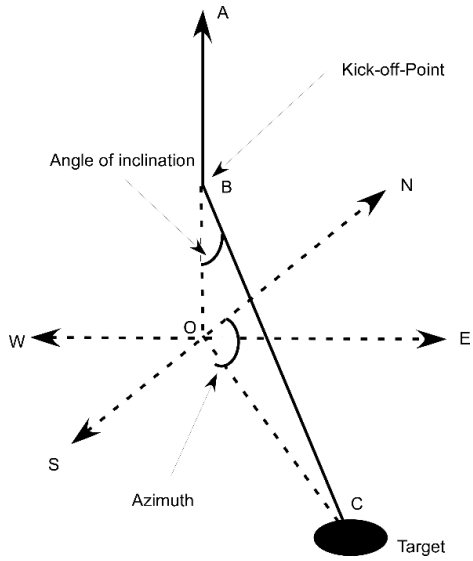

Figure 6.1: Relevant directional drilling parameters [27]

Figure 6.1 presents the main parameters of a deviated well, which are defined below together with other relevant terminology [27]:

- True vertical depth (TVD): The vertical distance from a point on the surface, usually the rotary kelly bushing (RKB), and to a point in the well.
- Measured depth (MD): Actual length of the wellbore.

- Tangent section: A section of the well path where a specific inclination is maintained constant. The intention is to increase both TVD and horizontal displacement.
- Kick-off point (KOP): The depth where deviation from the vertical is initiated.
- Azimuth: The compass direction of a directional survey, or the angle between north direction and the vertical line through the target and the wellhead.
- Inclination: The angle between the tangent section of the wellbore and a vertical line.
- Build-up rate: The rate at which the inclination angle is built. It is estimated from the difference between the inclination angle of two consecutive survey stations.
- Turn rate: The difference in azimuth angle between two consecutive survey stations.

6.1.1 Automation Potential in Directional Drilling

The tasks of a directional driller are many, and maintaining a high level of performance quality on all is nearly impossible; this is further elaborated in section 6.2. Inconsistent directional drilling performances have resulted in missed production potential, increased lifting costs, which essentially have contributed to the oil and gas industry losing billions of dollars in drilling costs [29]. Therefore, developing a sustainable wellbore trajectory control system is of the utmost importance, and should be prioritized in regards to drilling automation. Automated directional drilling services is proving to be a feasible solution, such as automated decision-making.

6.2 Transitioning into Automated Directional Drilling

As mentioned in chapter 4 the transition from human labor to automation is challenging in such a conservative industry. A drilling system automation roadmap

is created as a result of a joint industry project, to guide and assist the industry in understanding the direction of drilling system automation. Transitioning from humans to automation is suggested done in four cognitive functions, respectively acquiring information, analyzing and displaying information, deciding action, and implementing action. These four functions can also be recognized in the LOA10 system.

Historically, the most essential tasks of a directional driller have been to decide when to rotate the pipe from surface in an attempt to drill straight, subsequently when to stop rotating and point the bent-sub in the desired direction. The directional driller is also responsible for determining how long the downhole mud-motor should be the only source of rotational power. Performing these tasks accurately requires experience. A common problem amongst less experienced directional drillers, includes failing to compensate properly for variables such as motor yield variations, deflections, variations in rotary walk and build, target uncertainty, and tortuosity risks. Furthermore, even highly experienced directional drillers often fail to consider a reduction in potential hydrocarbon production which corresponds to drilling accuracy on a survey to survey basis. Consequently, there are simply too much real-time data to analyze for the directional driller to make appropriate decisions, and stay on the designed path.

Transitioning into a fully automated directional drilling operation should be done gradually, starting with partial automation. It should be mentioned that even partial automation is of value as it frees the directional driller of specific tasks. Ultimately, linking all automated tasks together will move the operation towards becoming fully automated. Based on the four cognitive functions, the following individual tasks in a bit guidance system have already been automated [29]:

1. Acquiring information.
    - Gather data recorded by the downhole sensors and electronic drilling recorders at surface. Specifically via wellsite information transfer standard Level 0.
    - Correction survey recordings, such as multi-station analysis and in-

field referencing.

2. Analyzing and displaying information.

    - Determining activity on the rig.
    - Calculation of bottom hole assembly (BHA) tendencies, performance and potential of the motor.
    - Geo-steering integration.
    - Correlation of gamma-ray, or formation top detection.
    - Factual and precise reporting of performance indicators.
    - Real-time data is a visual display available to all stakeholders of the well.
    - Real-time data from rig activity, motor performance, BHA tendencies, etc. are utilized to determine bit position and trajectory.

3. Deciding action.

    - Automated solutions for rotating and sliding decision-making are available. These models consider millions of probable solutions, which are based on lost production potential, tortuosity risks and cost related to drilling time.

4. Implementing action.

    - Applications such as stick-slip mitigation and auto-driller have been implemented to optimize rotation sequences automatically.
    - Technology able to execute tasks, such as toolface orientation, return to bottom and oscillation have been automated. This technology has been introduced in recent time and is utilized during sliding.

A workflow of the automated tasks described above is presented in Figure 6.2.

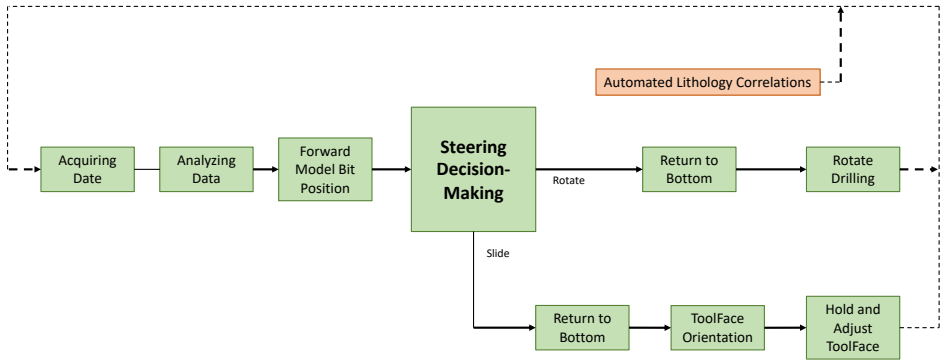

Figure 6.2: Automated directional drilling workflow [29].

6.3 Control Methods

Control theory is essential and must be utilized in an autonomous controller. These sections will cover control methods and corresponding theory, relevant for directional drilling.

6.3.1 PID Controller

The most commonly used closed-loop control algorithm in automation is a proportional-integral-derivative (PID) controller. Due to its robust performance with a broad selection of operating conditions and furthermore its simple functionality. The output of the PID controller is calculated by summing the three terms, respectively proportional, integral and derivative [30]:

$$u(t) = K_p e(t) + K_i \int_0^t e(\tau)d\tau + K_d \frac{d}{dt} e(t) \tag{6.1}$$

Where K_p is the proportional gain, K_i is the integral gain and K_d is the derivative gain; these three are also known as the tuning parameters. The control error, $e(t)$, is associated with the drilling-path-deviation vector, and t is the instantaneous time. τ is the integration variable and takes values from the time zero to the present time, t. Figure 6.3 illustrates the schematics of a PID controller.

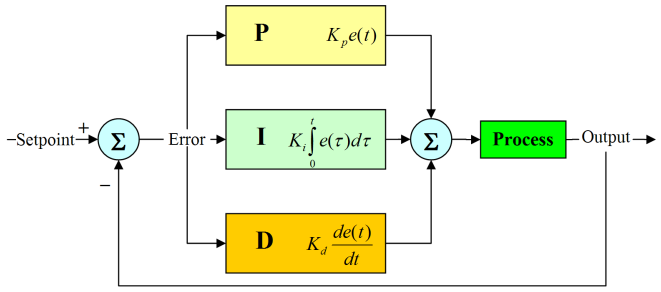

Figure 6.3: Schematic of a PID controller [31].

A PID controller requires cautious adjustment (or tuning) of the K_p, K_i and K_d parameters. The tuning process is complex and the input can be unstable if these parameters are incorrectly chosen. Instability is caused by excess gain, especially when there is significant lag [32].

6.3.2 Fuzzy Control

A fuzzy controller is not necessarily based on a precise physics-based model, rather this controller is a rule-based method. Where the system outputs, or controllables, correlates mathematically and systematically to the system inputs, known as observables.

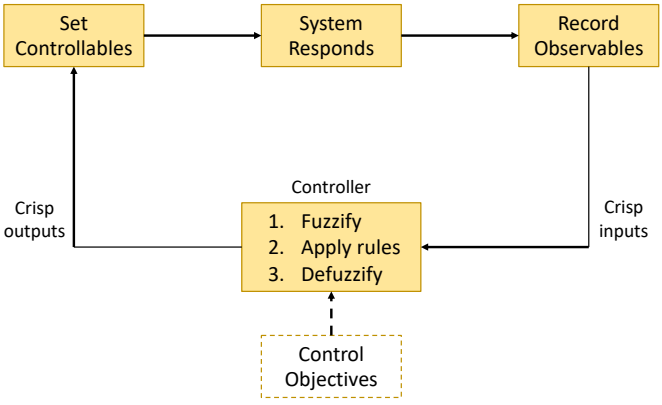

Figure 6.4: Schematic of closed-loop fuzzy-control system [33].

The controller is developed to utilize common sense and learn from experience, with fuzzy logic as the basis. Two fuzzy controllers relevant for directional drilling

are presented below.

- Stoner [33] developed a fuzzy-logic drilling-direction controller, applicable for a closed-loop rotary-direction-drilling system. The controller uses 100 control rules and a weighting factor, to project eight control observables into two controllables. The observables correlate to the linear and angular deviations between a planned well path and the actual drilling path. Moreover, the controllables are relative changes to the eccentricity settings of a non-rotating adjustable stabilizer. These outputs should be defuzzied entirely using numerical integration.

- A more recent controller was developed by Xue et al. [34] with the deviation angle, deviation-vector-change rate and deviation angle as control variables. With significantly fewer observables, compared to Stoner's eight, this model appears to be simpler. The fuzzy control algorithm simulates a step response, and compared to a traditional PID control it showed great advantages such as no overshooting and faster response. Additionally, results suggested that the fuzzy controller effectively tracks the well path design and has strong adaptability.

Briefly summarizing a fuzzy controller, the method is rather subjective since its intention is to mimic subjective decisions made by the directional driller. Consequently, its performance greatly depends on selecting appropriate observables, controllables, controller-input parameters and weighting factors in regards to defuzzification.

6.4 Mechanical Limits

The main objective of a wellbore trajectory controller is to correct the drilling direction when the actual drilling path deviates from the planned path [35]. To do so, a smooth correction path must be suggested before taking any correctional actions to change or adjust the steering direction. Furthermore, when deciding on a correction path, certain mechanical limits should be considered. Mechanical limits associated with designing a path, specifically for a deviated well in this case,

includes maximum allowable dogleg severity (DLS) and the drillstring mechanics, such as pipe bending and fatigue.

Dogleg severity (DLS)

All well paths are developed from a reference point to the desired target(s), and these points are expressed with coordinates {x, y, z} with corresponding units {meter North, meter East, meter TVD}. Considering the entire well path, the first section drilled should be vertical, until reaching a formation which can withstand the additional strain applied with directional drilling. The measured depth at which the drillstring initially begins to build angle is referred to as KOP. Though the 3D-curved well path generated is developed based on inclination- and azimuth-change, it cannot be separated into the two, due to turning and building. Therefore to avoid inaccurate coordinates it will be presented as DLS with unit $[°/m]$, which is estimated with the following equation [28]:

$$DLS = \frac{\phi}{CL} \tag{6.2}$$

Where the dogleg angle is expressed as $\phi[°]$ and $CL[m]$ is the course length and is defined as:

$$CL = \frac{RC\pi(I_2 - I_1)}{180} \tag{6.3}$$

$RC[m]$ is the radius of curvature, I_1 is the inclination at the first survey station, or the reference point, and I_2 is the inclination obtained from the survey station at the desired target.

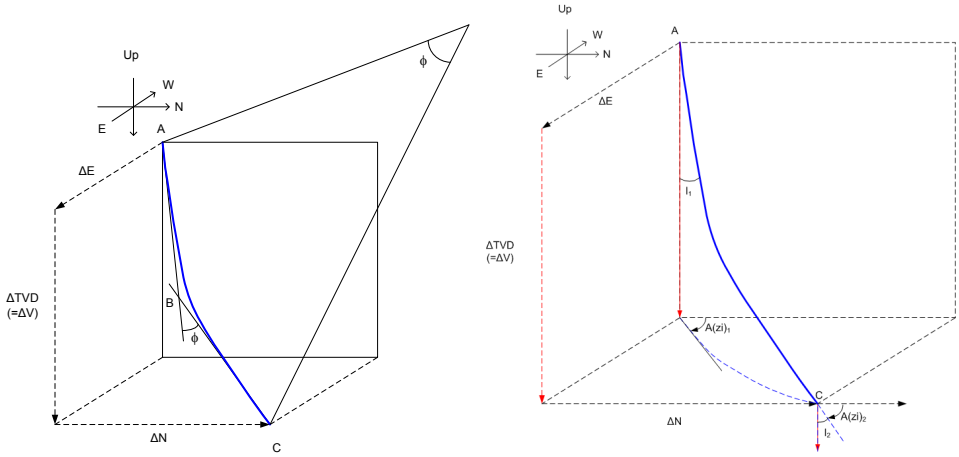

(a) Dogleg Angle (ϕ) **(b)** Inclination (I) and Azimuth (A)

Figure 6.5: Parameters relevant for developing a well path [28].

In conjunction with trajectory control, the correction path suggested should not have a smaller radius of curvature (RC) than the defined minimum RC. The minimum RC value is based on the material yield strength, and if the actual RC drops below the defined value, the drillpipe will fall out of the material's elastic zone. Furthermore, to avoid drillstring failure the corresponding DLS should not exceed the maximum value defined.

Pipe bending

With directional drilling the drillpipe will be exposed to bending, which induces bending stress, or axial stress. However, as long as the drillpipe stays within its elastic zone, as mentioned above, some pipe bending can be tolerated. The maximum drillpipe bending stress is divided into three different cases: no contact, point contact and arc contact. The derivations are shown in Appendix A.2 and results in three equations describing the maximum bending stress of a drillpipe [36]:

$$\sigma_b = \frac{ED}{2}[(C+q)\frac{kL}{sin(kL)} - q] \tag{6.4}$$

$$\sigma_b = \frac{ED}{2}[C_c cos(kL_m) + s_o sin(kL_m) - q] \tag{6.5}$$

$$\sigma_b = \frac{ED}{2}[C_c cos(kL_m) + s_o sin(kL_m) - q] \tag{6.6}$$

Equation 6.4 through 6.6 is applicable for the respective cases of no contact, point contact and arc contact.

Briefly discussing pipe bending in concurrence with trajectory control, the solution of the correction path should not cause the drillpipe to exceed its elastic limits. Subsequently, the total axial stress can not exceed the material yield strength. Total axial stress adds up axial stresses resulting from pipe bending, internal pressure and weight on bit (WOB). Therefore, the correction path should not require the drillpipe to bend such that the total axial stress exceeds the materials elastic limits.

Pipe Fatigue

The most frequent consequential drillstring failure is known as fatigue, which unfortunately is also the most costly. Drillstring fatigue is defined as stress cycles repeatedly applied on the drillstring initiating microcracks, which with time will propagate to macrocracks. In principle, fatigue only occurs in the presence of axial curved sections when the drillstring is rotating; the curved section witnesses one stress cycle per revolution [37].

The amplitude of the stress cycles generated from the curvature is directly proportional to the degree of curvature. Furthermore, the cyclic stress is equivalent to the bending stress, which is predicted using Equation 6.4 through 6.6. Increasing drillpipe outer diameter corresponds to increasing bending stress, meaning to mitigate fatigue damage decreasing drillpipe diameter is desired.

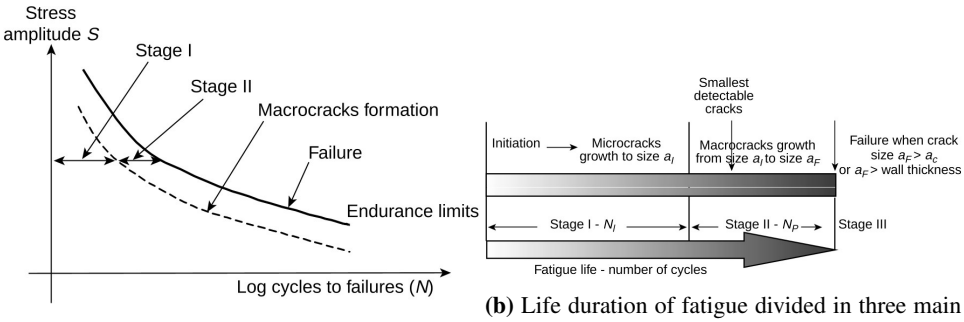

(a) S-N curve with the corresponding fatigue life.

(b) Life duration of fatigue divided in three main stages.

Figure 6.6: S-N curve and life duration of fatigue [38].

A material's fatigue limit is decided by correlating its S-N curve[4]. The endurance stress limit associated with the fatigue S-N curve should not be exceeded by the calculated bending stress, since the number of rotations is not limited. Indicating that if the plastic limit of a material is reached as a result of too high stress applied, fewer cycles of stress are necessary for the material to break. Figure 6.6 shows the S-N curve and the life duration of fatigue in three stages.

Fatigue is a phenomenon that develops over time, therefore the correction path alone should not trigger fatigue failure. However, increasing the number of stress cycles will move it further along. Moreover, the same approach as mentioned for pipe bending should be practiced to avoid pipe fatigue in a trajectory controller.

6.5 Well Path Deviation

To maximize production, a well path is planned prior to starting the drilling operation to hit the reservoir target(s) defined by the geologists and reservoir engineers (Figure 6.7). This is essential to avoid consequences, such as [29]:

- *Landing short.* To correct this deviation, a large dogleg is required, subsequently reducing production potential or worst case it could require plug and sidetrack. Either way, operational costs will increase.
- *Landing long.* This results in less production potential.

[4]Stress amplitude (S) versus maximum allowable number of cycles ($\log N_f$). [38]

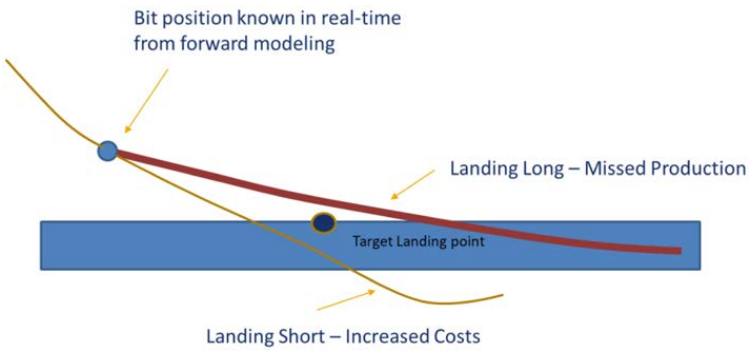

Figure 6.7: Effects of landing short or long from the target position [29].

The planned well path will act as a reference for the drilling operation, however in practice it is impossible to follow it without at least small deviations. When the deviations become too large, it is essential to perform appropriate corrective actions. Again, an appropriate well path must be suggested, this time a correction path.

A deviation correction path will guide the actual drilling path back to the planned well path. The well path deviation itself is expressed by a deviation vector and its corresponding deviation angle, which is illustrated in Figure 6.8; where AB is the deviation vector and θ is the deviation angle. Beginning in position A on the actual drilling path, the deviation vector AB points to position B, which is the cross point of the deviation plan and the planned trajectory. The deviation plan is perpendicular to the planned path and goes through position A. AB is also referred to as the error, ε. The deviation angle θ is defined by two unit-length tangential vectors, $\mathbf{T}_a$ and $\mathbf{T}_b$, which corresponds to the deviation vector AB. From position A, the deviation correction path is developed in two sections AC and CR.

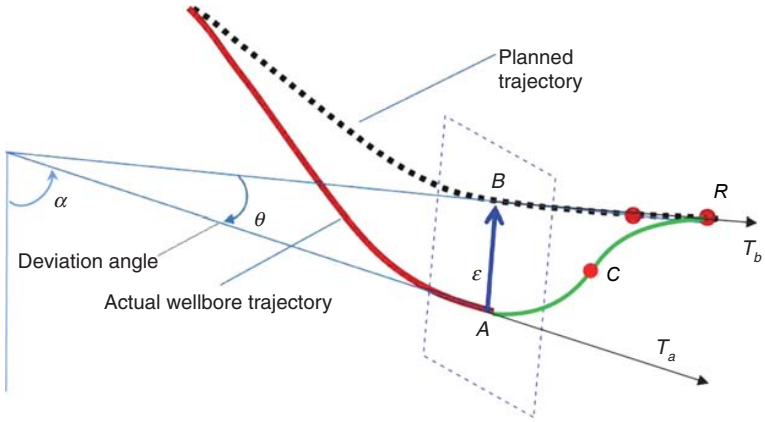

Figure 6.8: Well path deviation schematic, showing the deviation vector AB, deviation angle θ and the correction trajectory $A - C - R$ [35].

There are multiple options for deciding the correction path, such as a PID control algorithm or a fuzzy controller which are both described in section 6.3. However, this section will investigate a method based on the minimum well-profile-energy criterion to develop the correction path.

6.5.1 Minimum Well-Profile-Energy Criterion

The concept of well-profile-energy, known as the Samuel criterion, uses curvature bridging to better quantify the complexity of the well paths. For this method, mathematical reasoning is used rather than geometrical reasoning. Here, the wellbore-profile-energy is dependent on the ”thin elastic line” analogy of the well path, expressed as a drilling difficulty or complexity index. With the assumption that the drillstring is an elastic beam, the total strain energy of the wellbore path is [39]:

$$E_w = \int_0^L [\kappa(x)^2 + \tau(x)^2]dx \tag{6.7}$$

Where $\kappa(x)$ is the curvature and $\tau(x)$ is torsion.

The minimum-energy curve, in a nonlinear curve model, is the thin elastic line that bends the least when passing through a given set of points. The advantage of

this method is its simplicity for producing smooth curves. In addition, it can be more effectively emphasize the undulation of tortuous well paths.

A target point should be defined, such as R in Figure 6.8, and parameters of a returning path should be calculated using the minimum-incremental well-profile-energy. The target point is predicted based on limitations such as maximum allowable DLS. However, maximum allowable DLS together with the orientation-angle error, or the deviation angle θ, is not sufficient enough as it will only correct the angular deviation. In addition, the linear deviation $|AB|$ should also be corrected.

Two sections make up the deviation-correction path, AC and CR, with lengths ΔD_{AC} and ΔD_{CR} respectively; illustrated in Figure 6.8. The inclination-change rate, defined as κ_I, and the azimuth-change rate κ_{Az} are kept constant in the two sections, which correlates to the derivatives of κ_I and κ_{Az} being zero. Position A is the starting point of the correction path, and from this the path is determined based on predicting six unknown parameters. These are ΔD_{AC}, ΔD_{CR}, $\kappa_{I_{AC}}$, $\kappa_{I_{CR}}$, $\kappa_{Az_{AC}}$ and $\kappa_{Az_{CR}}$. Using these variables, the incremental well-profile-energy is [35]:

$$\Delta E = (\kappa_{AC}^2 + \tau_{AC}^2)\Delta D_{AC} + (\kappa_{CR}^2 + \tau_{CR}^2)\Delta D_{CR} \tag{6.8}$$

Where $\tau_i = \frac{\kappa_{Ii}\dot{\kappa}_{Azi} - \kappa_{Azi}\dot{\kappa}_{Ii}}{\kappa_i^2} sin(I_i) + \kappa_{Az_i}\left(1 + \frac{\kappa_{Ii}^2}{\kappa_i^2}\right) cos(I_i)$ and
$\kappa_i = \sqrt{\kappa_{I_i}^2 + \kappa_{Azi_i}^2 sin^2(I_i)}$.

Here, the integer i is either AC or CR, and ΔD_i is the incremental MD of each section. The inclination angle is expressed as I_i, further κ is the wellbore curvature, and τ_i is the borehole torsion.

By utilizing Equation A.1 through Equation A.5 from Appendix A.1, ΔD_{AC} can be expressed as function of ΔD_{CR}:

$$\Delta D_{AC} = \frac{(\Delta X^2 + \Delta Y^2 + \Delta Z^2) - \Delta D_{AC}(\Delta X sin(I_R)\ cos(Az_R) + \Delta Y sin(I_R)\ sin(Az_R) + \Delta Z cos(I_R))}{\Delta D_{CR}\left(\frac{1-u}{2}\right) + (\Delta X sin(I_A)\ cos(Az_A) + \Delta Y sin(I_A) sin(Az_A))} \tag{6.9}$$

Where ΔX is the difference in x-direction between the start position A and end position R. Successively, ΔY is the difference in y-direction and ΔZ in z-direction. Furthermore, $u = cos(I_A)\, cos(I_R) + sin(I_A)\, sin(I_R)\, cos(Az_R - Az_A)$. The four remaining unknown parameters defining inclination- and azimuth-change rates for both sections, respectively $\kappa_{I_{AC}}$, $\kappa_{I_{CR}}$, $\kappa_{Az_{AC}}$ and $\kappa_{Az_{CR}}$, are predicted using Equation 6.10 through Equation 6.13.

$$\kappa_{I_{AC}} = \frac{I_C - I_A}{\Delta D_{AC}} \tag{6.10}$$

$$\kappa_{I_{CR}} = \frac{I_R - I_C}{\Delta D_n} \tag{6.11}$$

Where $I_C = \pm arccos\left(\frac{\Delta Z - \Delta D_{AC}\, cos(I_A) - \Delta D_{CR} \cos(I_R)}{\Delta D_{AC} + \Delta D_{CR}}\right)$.

$$\kappa_{Az_{AC}} = \frac{Az_C - Az_A}{\Delta D_{AC}} \tag{6.12}$$

$$\kappa_{Az_{CR}} = \frac{Az_R - Az_C}{\Delta D_{CR}} \tag{6.13}$$

Where $Az_C = arctan\left(\frac{2\Delta Y - \Delta D_{AC}\, sin(I_A)\, sin(Az_A) - \Delta D_{CR}\, sin(I_R)\, sin(Az_R)}{2\Delta X - \Delta D_{AC}\, sin(I_A)\, cos(Az_A) - \Delta D_{CR}\, sin(I_R)\, cos(Az_R)}\right)$.

6.6 Creating a Trajectory Controller

The trajectory controller created in MATLAB is based on the minimum well-profile-energy criterion elaborated above. This section will describe the process of creating an autonomous trajectory controller to correct an unwanted deviation.

6.6.1 Predicting the Correction Path

The main objective of the controller created is predicting a correction path so that the unwanted deviation between the actual drilling path and reference path cancels out. Figure 6.8 shows a correction path, respectively the illustrated green line, which has a starting point in A and ends in R. Position A is located on the actual drilling path, while position R is on the referenced path. Furthermore, it is made up of two curved sections, AC and CR, with lengths ΔD_{AC} and ΔD_{CR}.

Figure 6.8 also shows the deviation vector AB which corresponds to the deviation error, ε, which furthermore is divided into the three dimensions ε_x, ε_y and ε_z. The trajectory controller uses the deviation error together with data for the reference and actual well path as a basis for further calculations. A lower limit for the deviation error is set, meaning deviation below this limit is tolerated and does not require corrective actions. All obtained survey recordings for both the reference- and actual well path are at the same TVD. For simplicity, it is therefore assumed that the vertical deviation error, ε_z, is zero. The deviation error is the length of vector AB which is calculated using the following expression:

$$AB = \sqrt{(x_A - x_B)^2 + (y_A - y_B)^2 + (z_A - z_B)^2} \tag{6.14}$$

Where position A is expressed with the following coordinates $\{x_A, y_A, z_A\}$ and position B is $\{x_B, y_B, z_B\}$.

Determining the starting point of the correction path, or position A, entails comparing survey recordings at the respective TVD and find the deviation error. If the error estimated is greater than the error limit defined, position A is found. Thereafter, position R is defined such that neither of the two correction path sections exceeds the maximum allowable DLS. Survey recordings from the two positions, A and R, include parameters such as position coordinates, inclination- and azimuth angles, DLS and MD.

As described in section 6.5.1 there are six unknown parameters, ΔD_{AC}, ΔD_{CR}, $\kappa_{I_{AC}}$, $\kappa_{I_{CR}}$, $\kappa_{Az_{AC}}$, $\kappa_{Az_{CR}}$. ΔD_{CR} can be determined using the minimum well-profile-energy criterion, respectively finding ΔE_{min} by estimating ΔE for different values of ΔD_{CR} and comparing them. A unique ΔD_{CR} correlate with ΔE, which is estimated using Equation 6.8. Furthermore, the remaining five unknown parameters are estimated using Equation 6.9 through 6.13. Position coordinates for C can now be estimated.

6.6.2 MATLAB Scripts

MATLAB is used when creating the trajectory controller. The controller consists of a main script `TrajectoryController.m`, in addition to four sub-scripts for obtaining well path, respectively `SurveyRecordings.m`, `Equations.m`, `WellpathPlots.m` and `PlotPosC.m`. All scripts can be found in Appendix B.1. Furthermore, the input variables are all survey recordings and correlating parameters, as well as defining an error limit.

`TrajectoryController.m` connects all sub-scripts, starting with the `SurveyRecordings.m` which imports all well path survey station data to MATLAB. Thereafter, it determines position A based on the error limit.
`WellpathPlots.m` is used to plot the reference well path, actual drilling path, position A and position R using the imported survey data and estimated position coordinates. A vector with n number of data points for ΔD_{CR} is generated and a unique value of ΔD_{CR} is decided as it correlates with ΔE_{min}. `Equations.m` contains Equation 6.8 through Equation 6.13, which is used for predicting the five remaining unknown parameters. Finally, `PlotPosC.m` plots the estimated position C.

6.6.3 Data Set Used for Testing

The OpenLab user interface (UI) was used to collect the necessary data sets, specifically well path data at each survey station, for testing; a detailed description of OpenLab is presented in section 5.2. A well-template of a generic offshore well provided by the developer was used to configure a 2500 meter well. A well path with both changes in inclination and azimuth was generated, with data points collected at a total of 190 survey stations, which was used as the reference path.

To initiate a deviation from the referenced well path, variables such as MD $[m]$, inclination $[^{\circ}]$ and azimuth $[^{\circ}]$ for random survey station were changed, and this will be referred to as the actual drilling path. Figure 6.9 shows the hole section or casing design of the wellbore and the reference well path; both images are collected from the OpenLab UI.

Parameters reported at each survey station includes MD, inclination, azimuth, TVD $[m]$, DLS $[°/30m]$, as well as N/S[5] and E/W[6] position $[m]$. They are collected from the OpenLab UI to excel, and imported to MATLAB accordingly. All data needed to predict the correction path is now available to use.

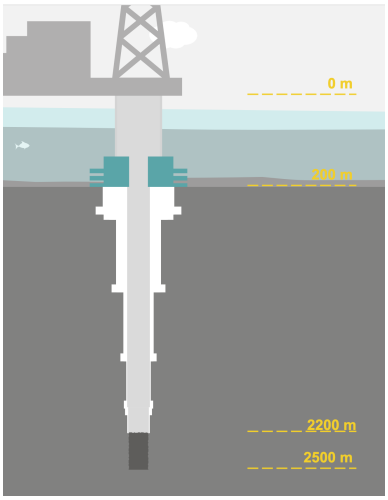

(a) Hole section.

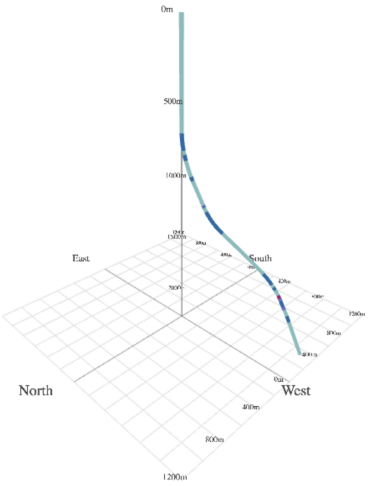

(b) Reference well path.

Figure 6.9: Reference path configuration for trajectory controller collected from OpenLab.

6.7 Results and Discussion

This section will cover results from testing the trajectory controller created, as well as some discussion in that regard.

6.7.1 Results

The data set collected from the OpenLab UI to excel, contains well path data for both the reference well path and the actual drilling path. The number of data points, n, for ΔD_{CR} are set to 10,000. The lower limit for deviation error is defined to

[5] North/South
[6] East/West

be less than 5 meters, or $\varepsilon < 5$. Exact value of the error ε, or AB, is presented in Table 6.1. The error is also divided to x-, y- and z-direction.

Table 6.1: Exact value of deviation errors; ε, ε_x, ε_y and ε_z.

Parameter	MATLAB	Value	Unit
Deviation error, ε	*err*	6.1342	m
Error x-direction, ε_x	*errX*	2.786	m
Error y-direction, ε_y	*errY*	5.465	m
Error z-direction, ε_z	*errZ*	0	m

With the specific errors estimated, position A is located at 801 mTVD which corresponds to survey station #55 on the actual well path. Position R is at 871 mTVD at survey station #62 on the reference path, which is associated with an acceptable correction path DLS. The reference well path, actual drilling path, position A and position R are plotted in Figure 6.10. An additional 2-dimensional plot showing x- versus y-direction is presented in Figure 6.11.

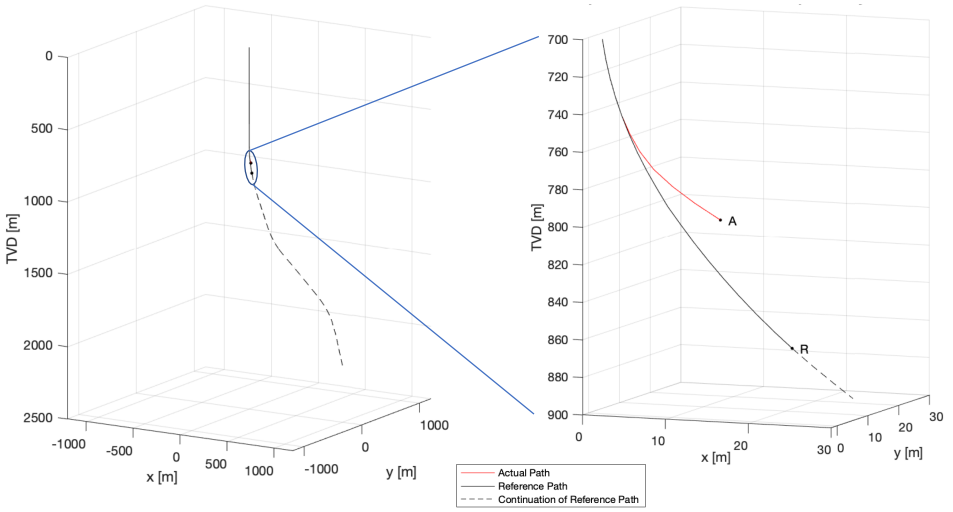

Figure 6.10: 3D schematic of the actual well path deviation from the referenced path.

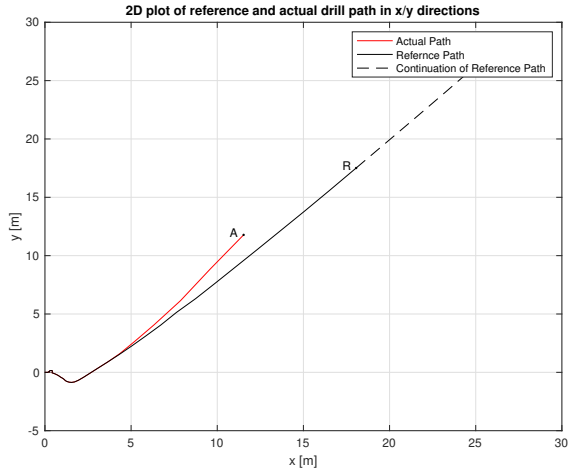

Figure 6.11: 2D schematic of the actual well path deviation from the referenced path.

Now that position A and R are determined, their corresponding parameters can be collected from the respective survey stations. Table 6.2 and 6.3 presents the position coordinates as well as the other known parameters for position A and R.

Table 6.2: Parameters for Position A located on the actual well path.

Parameter	**MATLAB**	**Value**	**Unit**
Survey station	*PosA*	55	
Coordinates	*A*	$\{11.53, 11.78, 801\}$	m
Inclination	*incA*	20.11	$^\circ$
Azimuth	*aziA*	240.12	$^\circ$
DLS	*dlsA*	5.38	$^\circ/30m$
MD	*mdA*	802.8	m

Table 6.3: Parameters for Position R located on the reference well path.

Parameter	MATLAB	Value	Unit
Survey station	*PosR*	62	
Coordinates	*R*	$\{18.06$, 17.51, $871.0\}$	m
Inclination	*incR*	14.36	$^\circ$
Azimuth	*aziR*	231.27	$^\circ$
DLS	*dlsR*	2.40	$^\circ/30m$
MD	*mdR*	873.1	m

When the starting- and ending point of the deviation correction path are estimated the next objective is to estimate position C; see Figure 6.8. As described in detail in section 6.5.1, there are a total of six unknown parameters to calculate. Respectively, the inclination- and azimuth-change rates of both sections, κ_I and κ_{Az}, in addition to the lengths of both sections, ΔD_{AC} and ΔD_{CR}. Thereafter, position coordinates can be estimated.

The automated trajectory controller goes through and calculates ΔE for all values of ΔD_{CR}. For every ΔD_{CR} the five remaining unknown parameters are calculated using Equation 6.9 through 6.13. When these are obtained, ΔE can be predicted. An array stores the five unknown parameters, inclination- and azimuth angle at position C, and ΔE for every ΔD_n. The program goes through the array and strips it of imaginary value parameters if any are present. Furthermore, all scenarios with negative ΔE are removed. A unique ΔD_{CR} is found from obtaining the minimum-incremental well-profile-energy, ΔE_{min}. The remaining five parameters are calculated for the particular test, and the results are presented in Table 6.4.

Table 6.4: Results.

Parameter	MATLAB	Value	Unit
Length of CR, $\Delta D_{CR} = \|CR\|$	*dCR*	48.2538	m
Length of AC, $\Delta D_{AC} = \|AC\|$	*dAC*	28.6373	m
Inclination @ position C	*incC*	30.3371	$^\circ$
Azimuth @ position C	*aziC*	49.0515	$^\circ$
Inc.-change rate @ AC, $\kappa_{I_{AC}}$	*k_incAC*	0.3571	$^\circ/m$
Inc.-change rate @ CR, $\kappa_{I_{CR}}$	*k_incCR*	-0.3311	$^\circ/m$
Azi.-change rate @ AC, $\kappa_{Az_{AC}}$	*k_aziAC*	-6.6720	$^\circ/m$
Azi.-change rate @ CR, $\kappa_{Az_{CR}}$	*k_aziCR*	3.7763	$^\circ/m$
Wellbore curvature @ AC, κ_{AC}	*k_AC*	3.3888	$^\circ/m$
Wellbore curvature @ CR, κ_{CR}	*k_CR*	0.3411	$^\circ/m$
Section AC borehole torsion, τ_{AC}	*t_AC*	-5.8223	$^\circ/m$
Section CR borehole torsion, τ_{CR}	*t_CR*	7.1046	$^\circ/m$
Position C coordinates	*C*	{13.82, 12.97, 826.80}	m

Based on the results obtained when using the minimum-energy solution, exact {x, y, z} coordinates of position C is predicted, also presented in Table 6.4. Position C is plotted in Figure 6.12.

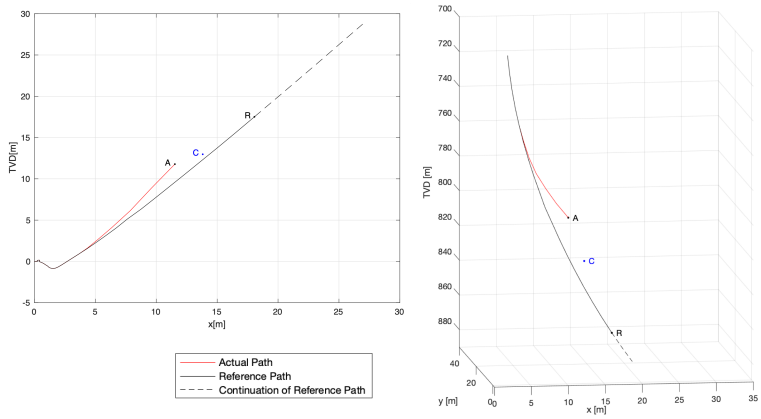

Figure 6.12: 2D- and 3D-schematics of the well path and position C.

The correction path determined is illustrated in Figure 6.13, which clearly appears

smooth. This however is reasonable as the actual length from position A to R is 70.5 meters, and the sum of the two section lengths $\Delta D_{AC} + \Delta D_{CR}$ are 76.9 meters.

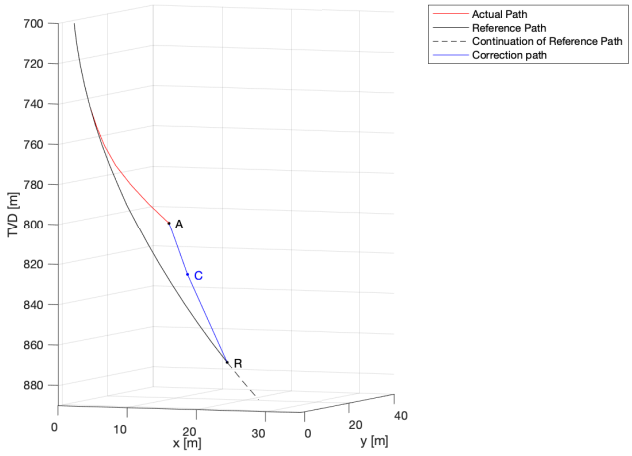

Figure 6.13: 3D schematic of the correction path.

6.7.2 Discussion

Using the minimum well-profile-energy criterion creates a smooth correction path, which generally is positive for the borehole quality. Moreover, the drilling operation becomes more efficient, and costs related to completion of the well obviously decreases with a smooth well path [40].

Challenges emerging when the actual drilling path starts deviating from the reference path, are irregularities such as drastic DLS values. Furthermore, if DLS of the actual drilling path exceeds its maximum allowable limit, drillstring failure is more likely to occur. Therefore, it is essential to take the appropriate corrective actions. To autonomously calculate a correction path a control algorithm must defined.

Minimum Energy Criterion compared to traditional control algorithms

Utilizing the minimum well-profile-energy to estimate the correction path as oppose to a PID- or fuzzy controller, has been shown by Liu [35] to create smoother wellbore paths.

A PID algorithm, as elaborated in section 6.3.1, requires tuning which will make the entire system unstable if not performed correctly. Furthermore, the findings by Liu shows that the wellbore energy generated from a PID controller is greater compared to testing done for the minimum-energy-method. A spike in DLS is observed immediately after initiating an action to correct the deviation. Challenges associated with the spike must be canceled out for the PID to prevent unstable steering. Generally there are more uncertainties related to the PID, especially in correlation with sudden changes in the drilling parameters.

The fuzzy control algorithm, similar to PID controller, generates a spike in DLS right after initiating a corrective action to steer the actual well back to the reference path. As mentioned the fuzzy controller is a rule-based method, which means the spike in DLS probably corresponds to rule stating that the system should respond with a large build-/drop-rate if a large deviation is detected. Thus, the fuzzy controller must also learn how to properly handle DLS spikes.

Benefits with the minimum energy method

As the minimum well-profile-energy criterion generates a smoother well path, the overall borehole quality is improved or nonetheless maintained at its current level. Generally, with smoother well paths and increasing borehole quality, the overall drilling process is improved. Associated with this are decrease in torque and drag, reduction in drillstring failure as mechanical limits are less likely to be exceeded, improved hole cleaning, and faster drilling rates [41].

Challenges with real world affects

In theory a smooth well path can be generated, however with unforeseen factors impacting the drilling performance, it can never be achieved in the real world. Fac-

tors affecting the drilling performance include reactions occurring between drilling fluid and formation, formation instabilities or downhole problems, as well as drill-string failure.

6.7.3 Closing Remarks

Obviously, it is not possible to achieve an ideal wellbore, this also applies for the correction path. However, the minimum well-profile energy criterion is a better foundation for determining the correction path oppose to other control methods considered, as it essentially will provide a smoother well path. Subsequently, DLS and tortuosity are less, which again will reduce wellbore friction.

The next step for the trajectory controller is to implement an action that calculates the toolface and bit tilt angle adjustments required to actually drill the correction path. Furthermore, appropriate controlling parameters can be customized to be used by a rotary steerable system (RSS). Ultimately, the commands given to the system should change the inclination- and azimuth-change rate for both sections of the correction path; both change rates are constant.

Chapter 7

Automated Kick-Detection

Kicks are a well-known phenomenon initiated downhole, which could in the worst-case lead to a catastrophic event.

An influx of formation fluids into the wellbore during drilling occurs if the formation pressure in an open wellbore section exceeds the hydrostatic mud pressure. This can be tolerated as long as it is considered to be a controlled influx. However, if an uncontrolled influx takes place it is known as a kick. Type of formation fluids includes water, oil and gas. If a kick is detected it is essential to swiftly initiate appropriate corrective actions to avert the kick in a controlled manner. Uncontrolled kicks might in worst-case result in a blowout.

Uncontrolled flow of formation fluid from the wellbore to surface causes blowouts, which are the most feared incidents to happen on a drilling rig. The consequences of a flammable and explosive flow of hydrocarbons reaching the surface is catastrophic, as history shows. Figure 7.1 shows a picture taken after the worst blowout in recent times, respectively referred to as the Macondo blowout. This further emphasizes why properly handling kicks are of upmost importance.

Figure 7.1: A blowout occurring on the rig DeepWater Horizon in 2010 [42].

This chapter will cover kick theory, signals and indicators of a kick, how to detect them in the earliest phase of development, which furthermore will be the basis the automated kick-detection model created - seeking to aid the operator by increasing detection-accuracy. The progress made in regards to kick-detection automation will also be touched on. With the main focus being on constructing a detection-model in MATLAB in correlation with OpenLab Simulator [26] to assist the operator with detecting kicks.

7.1 Influx and Kick Theory

When drilling through a formation, the normal operating procedure is to use mud weight that creates a hydrostatic pressure column greater than the formation pressure, to avoid influx of formation fluids. Influx is defined as a flow formation fluids into the wellbore from the porous formation rock. This section will describe the initiating factors of fluid influx, signs of a kick and possible sources of false kick indications.

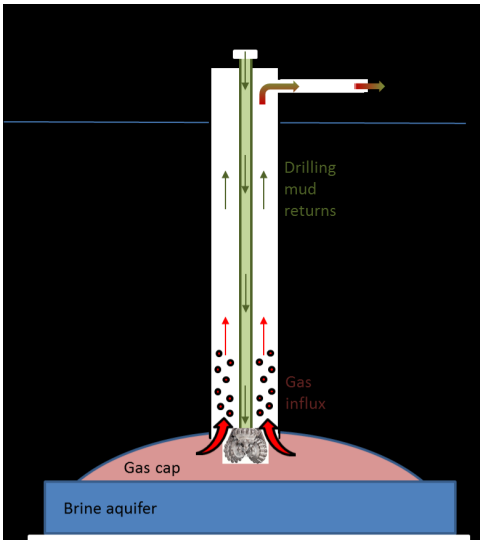

Figure 7.2: Visualization of a kick [43].

7.1.1 Initiating Factors of Downhole Pressure Variations

A flow of fluid from the formation into the wellbore is dependent on the formation pressure exceeding the pressure in the wellbore. Initiating factors for downhole pressure variations which might induce fluid influx are listed below, and will be further elaborated.

- Insufficient mud weight entering a new zone
- Improper hole filling during tripping
- Swabbing
- Cut Mud
- Lost Circulation

Insufficient mud weight entering a new zone

Insufficient mud weight when entering a new zone is the main contributor to initiating a kick. The operators drills into a permeable formation while still using mud weight estimated for the previous, completed zone. Drilling into a high pressured

zone where the hydrostatic mud pressure falls below pore pressure and creates an underbalanced situation. Furthermore, given that the new zone is permeable, an uncontrolled flow of formation fluid enters the wellbore, initiating a kick if the influx volume is large enough [28].

To prevent the hydrostatic mud weight from falling below the pore pressure, an obvious solution is using heavier mud. However, there is an upper limit to avoid unwanted incidence. Firstly, if the mud weight exceeds the fracture pressure the formation breaks, resulting in lost circulation, which can induce a kick [44]. Secondly, the mud weight has an inverse relationship with rate of penetration (ROP) and thus slowing down the operation [45].

For an openhole section, the preferable mud weight is lies within the mud weight window[7]. An example mud weight window is properly visualized in Figure 7.3.

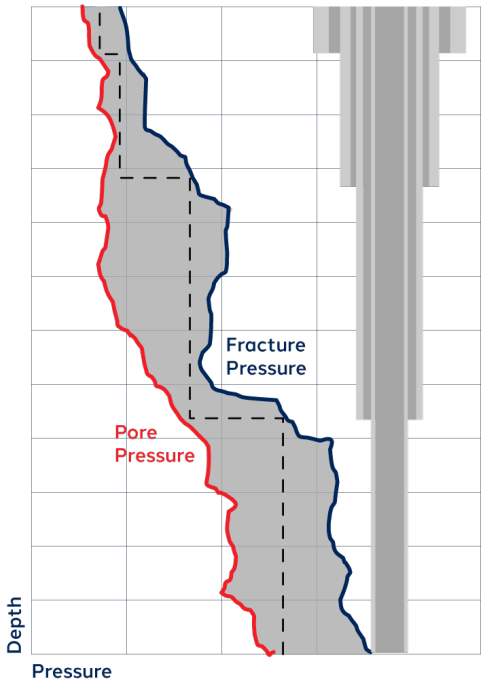

Figure 7.3: Mud weight window [47].

[7] A mud weight window commonly defines the pore- and fracture pressures as the upper and lower limits, to avoid influx and lost circulation[46].

Improper hole filling during tripping

Another significant cause initiating kicks occur during tripping. When pulling out of hole the annular mud levels decreases as a result of the drillstring no longer displacing the mud. This correlates to the water levels decreasing when stepping out of the bathtub.

The wellbore should continuously be filled with new mud when tripping, to assure that the annular hydrostatic mud pressure does not fall below the pore pressure. Calculating the exact mud volume pumped into the well is challenging. Two methods commonly used, include observing the number of pump-strokes and trip-tank volume.

Number of pump-strokes can be estimated using a positive-displacement pump to periodically fill up the hole. The device automatically shuts off the pump when the hole is sufficiently filled with mud[48].

A calibration sensor is used to monitor the mud volume currently in the trip-tank, and based on this the mud volume pump into the wellbore is estimated. The advantage of using a trip-tank rather than mud tanks, is that the trip-tank contains a smaller volume hence is easier to monitor [49].

Swabbing

Swab pressure is induced when tripping out of hole, creating local reductions of the hydrostatic pressure. If these local variations are large enough, the hydrostatic pressure might fall below the defined pore pressure.

Swabbing is most commonly mitigated by decreasing the tripping speed. Other factors affecting the extent of swabbing, which will not be further elaborated, are [50]:

- Mud rheology.
- Wellbore dimensions.

- Bit balling [8].

Cut mud

Mud often contains some gas particles. As the density of gas is less than the drilling fluid, the invasion of smaller amounts of gas will decrease the overall mud weight. The invasion of gas comes from porous formations or drilled cuttings releasing gas into the drilling mud [28].

Lost circulation

Lost circulation is defined as a lack of returned mud to surface. Commonly this happens when the drill bit runs into natural fractures, caverns, or in case of self-induced fractures. Consequently, if the hydrostatic column decreases rapidly the well moves out of an overbalanced situation, which might result in a large influx of hydrocarbons [52].

7.1.2 Warning Signs

It is important to recognize the physical behavior of the wellbore to detect a kick as early as possible. Many wellbore measurements are constantly being recorded during drilling, thus it is important to know what to look for. Some of the warnings signs are significant, while others are difficult to spot. Key warnings signals for detecting kicks are listed below, and will be further elaborated.

- Increase in flow rate.
- Increase in pit volume.
- Flowing well with pumps off.
- Change in standpipe pressure.
- Improper fill-up during tripping.
- Change in string weight.

[8] Accumulation of material on the face of the cutting structure that interferes with depth of cut [51].

- Abrupt break in drilling.

Increase in flow rate

As long as the flow rate into the well is kept constant, the returns are maintained. Hence, if the return rate suddenly increases it is a primary indicator of a kick occurring. The sudden increase can be explained as an influx of formation fluid into the wellbore, pushing the drilling fluid out of the well [53].

Increased pit volume

A method for detecting an increase in return flow rate, is observing if the pit volume changes. As described above a sudden increase in returns is a kick indicator, subsequently the pit volume also increases. If no operational action is taken, a sudden pit volume increase should be alarming [53].

Flowing well with pumps off

If the mud pumps are shut off during an operation, but the return flow continues, it is a strong indication that a kick is initiated. However, there are exceptions describing the increase in return flow, including u-tube effect[9] and well ballooning[10].

Change in standpipe pressure

Another indication of kick is when the standpipe pressure encounters sudden changes. Occasionally, the standpipe pressure temporarily increases due to influx of formation fluid which causes the mud to flocculate. Essentially what happens is that the influx changes pressure downhole, which is displayed on the standpipe pressure readings at topside [53].

[9] When the mud inside the drillpipe is heavier than the annular, and as a result pushes the annular fluid upwards [25].

[10] A natural phenomenon occurring when formations collect mud while the pumps are on, and as they are turned off it flows back to the wellbore [54].

Improper fill-up during tripping

During tripping, it is essential for the decrease in pit volume to correspond to the volume of steel being removed. If the pit level decreases less than the calculated volume necessary to fill the well, it is assumed that a kick is initiated [53].

Change in string weight

The drillstring is always effected by the buoyancy effect. The buoyancy effect affects the hook-loads such that, if the mud weight increases, the correlating response is an increase in the buoyancy which makes the drillstring ”lighter” and vice versa [55]. Hence, if the operator observes a sudden decrease in hook-load, it is an indication of formation flow into the wellbore.

Drilling break

If the operator observes a sudden increase in ROP, it can be assumed that the drill bit has entered a new formation. This requires a flow check to be conducted, as properties of the new formation are unknown and the possibility of kick is present [28, 25].

Overview

The significance of a warning sign indicating a kick varies, thus they are separated into primary and secondary indications, presented in Table 7.1.

Table 7.1: An overview of primary and secondary kick indicators [56].

Primary Indicator	Secondary indicator
Flow rate increase	Standpipe pressure change
Pit volume increase	String weight change
Flowing well with pumps off	Drilling break
Improper fill up during tripping	

Be aware that other drilling phenomenons may cause sudden changes in the properties mentioned above. Either way, if an uncontrolled influx is suspected the

proper health, safety and environment (HSE) procedure is to always implement the available safety barriers, and investigate whether a kick was initiated.

7.1.3 False-Positive Kick Sources

During a drilling operation, the operator will occasionally observe signs suggesting a kick is initiated. However, some responses are similar to the warning signs elaborated in section 7.1.2, but are in fact so-called false-positives. Relevant false-positives are covered below.

Cuttings accumulation in the annulus

During drilling, rock fragments may end up accumulating in the annulus, creating an increase in standpipe pressure similar to when a kick is imminent. However, this pressure increase is due to the high-density cuttings contributing to a heavier hydrostatic pressure column in the annulus. Subsequently, creating a higher bottomhole pressure.

Bit plugging

Small particles that are not filtered out in the shakers, might enter the mud pumped back into the wellbore. Through an accumulation of particles, the bit nozzles can partially- or fully plug the bit. Such an incident will increase the measured standpipe pressure in the same pattern as an occurring kick [57].

Pipe connections

During the process of connecting pipe, topside measurements suggest that a kick is occurring, however they are false-positives. Mud pumps are turned off when connecting pipe, which will temporarily decrease bottomhole pressure. This might lead to formation fluids entering the wellbore, but as the pumps turn back on the hydrostatic pressure increase and the influx will be reduced [58].

7.2 Criteria for Kick Detection

The influx and kick theory described in section 7.1, is the basis for defining three criteria, to be utilized in the automatic kick detection system. Appropriate conditions allow for defining the safety barrier necessary to execute a safe operation, such that the proper action is taken to prevent kick or worst-case blowouts. Ibarra [59] defined three criteria significant to consider in an automated system, these were: peak in standpipe pressure, followed by a slight downward trend and increase in mud returns.

7.2.1 Criterion 1: Peak In Standpipe Pressure

A peak in the standpipe pressure is observed as a result of sudden influx of formation fluid into the wellbore.

Figure 7.4 illustrates an example of a time-based log recorded during drilling. The pink line represents the return flow rate, while the blue line is the standpipe pressure. A peak in standpipe pressure is commonly associated with a kick, but there are some exceptions as mentioned above. This peaking-behavior therefore defines the first criterion of automated kick detection.

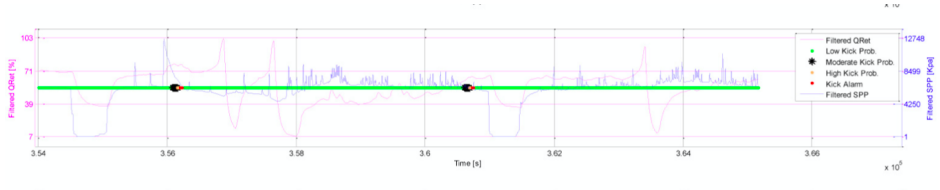

Figure 7.4: Time-based log during drilling with automated kick detection [59].

7.2.2 Criterion 2: Slight Downward Trend in Standpipe Pressure

After the standpipe pressure peaks, a slow declining behavior is observed. This is a result of lighter formation fluid partially displacing the mud column in the annulus. The slow declination in standpipe pressure can be used as a continuance of criterion one, to further confirm a kick [59].

7.2.3 Criterion 3: Increase in Mud Returns

The third criterion for detecting kicks is if the returned flow rate increases abruptly. Meaning that the fluid influx pushes the mud upwards the annulus, causing an increase of flow [52].

The example shown in Figure 7.4 set of the kick alarm twice when all three criteria were met. The first kick detected is easily spotted as the variations are huge, while the second despite smaller variations made the kick alarm go off.

7.3 Previous Work with Automatic Kick-Detection

Automatic kick-detection has been an objective in research communities for some years. Studies have shown that the most challenging part of automated kick-detection is the recognition of false-positives. Two studies covering automatic kick-detection are presented below.

A study conducted by Ibarra [59] covered 18 field-cases with kick occurrence. It was based on 7 wells, and the model delivered a kick detection accuracy of 94%, i.e. 17 out of 18 kicks were detected using the three criteria mentioned in section 7.2. The alarming part of the results obtained was that 7 of them were false-positives. However, it is stated that the false-positives do not undermine the accuracy of the algorithm, and with future work, the model can be improved and will carry out kick-detection with increased accuracy.

Fjetland [60] conducted a study concerning kick-detection utilizing machine learning. Trigger parameters for different influx volumes are discussed, with their relation to the occurring number of false alarms. Two models are developed based on different trigger values. Model A uses lower trigger values, making it sensitive to change, which reduces the number of false-negatives, i.e. the model recognizes more and smaller kick as well as an increasing number of false-positives. Model B almost completely removes false-positives by increasing the trigger values, unfortunately, the number of false-negatives increases.

Results obtained from these studies show that detecting a kick is not the concerning issue, but rather the challenge of distinguishing false alerts from real ones. It is suggested that detection algorithms can either be very sensitive towards anomalies increasing the number of false-positives, or the trigger values defined are too high, which increases the number of false-negatives.

7.4 Kick-Detection Model

An automated kick-detection model is created in MATLAB, using knowledge based on the presented theory and findings covered in the sections above. This model uses the OpenLab simulator, covered in section 5.2, to generate drilling simulation data. The model uses the three criteria defined as the trigger parameters for detecting kicks. Additionally, it has been tuned to avoid prompting false-positive occurrences, as well as reducing false-negatives.

7.4.1 Configuration and Inputs

To initialize an OpenLab simulation model, it needs to be configured. The model configurations are listed in Table 7.2, where those not specified are set to their default values according to Table 5.1.

Table 7.2: Model configurations and its user inputs.

Description	User value
Initial bit depth	2500 m
Reservoir model	true
Manual mass rate	Will vary kg/s
Manual total mass	Will vary kg
Manual depth	Initial bit depth
Reservoir kick-off time	40 s

Influx rate and total influx mass are inputs that are essential for tuning the model. As kicks occur in different rates and sizes, these parameters will vary throughout testing the model.

After the simulation model has been configured, it opens up for specifying set-points. The set-point that can be defined by the user are listed in Table 7.3. Those not specified, are set to their default values presented in Table 5.2. Hereunder, set-points such as blow-out preventer (BOP) status, inlet fluid density and managed pressure drilling (MPD) properties are included.

Table 7.3: User inputs for kick-detection model.

Parameter	MATLAB variable	Unit
Flow rate in	FlowRateIn	m^3/s
Top-off String Velocity	TopOffStringVelocity	m/s
ROP	ROP	m/s
Surface RPM	SurfaceRPM	rev/s

7.4.2 Triggering Criteria

With the use of the three criteria associated with an incoming kick defined in section 7.2, the model considers the increase in return flow rate, standpipe pressure and annulus pressure acquired from the along string measurementss (ASMs).

The model's triggering value, α, is defined as follows:

$$\alpha < \frac{x_i - x_{i-1}}{x_{i-1}} \tag{7.1}$$

The algorithm checks if there is an increase in the measurements, x, from $i-1$ to step i. The value of α defines model-sensitivity, and is updated by the user accordingly.

7.4.3 Probability-Levels of Kick

The model created detects a kick shortly after its occurrence, and is inspired by the model developed by Ibarra [59].

The significance of the increase in measurement between two steps corresponds to the possibility of a kick occurring. Four categories are defined based on this

from ”low probability” to ”high probability” of a kick to finally a kick alarm going off. The kick probability-level is represented with color-coding:

- Green: Low probability
- Orange: Medium probability
- Black: High probability
- Red: Kick alarm

7.4.4 Test Well

The test well used for the simulations is configured in the OpenLab user interface (UI). How to configure a well is described in section 5.2.1, while this section summarizes the chosen properties of the test well configuration.

Hole section and well path

The test well is a 2500 meter vertical well, with seafloor located 80 meters below rotary kelly bushing (RKB). A 10 $^{3}/_{4}$” casing is hung off at surface, with its shoe depth at 2200m. The 8 $^{1}/_{2}$” section is drilled 300m out of the surface casing. Furthermore, 2500mTVD is defined as the starting point of the simulation. An illustration of the well is shown in Figure 7.5, in addition to a detailed description of the hole section presented in Table 7.4.

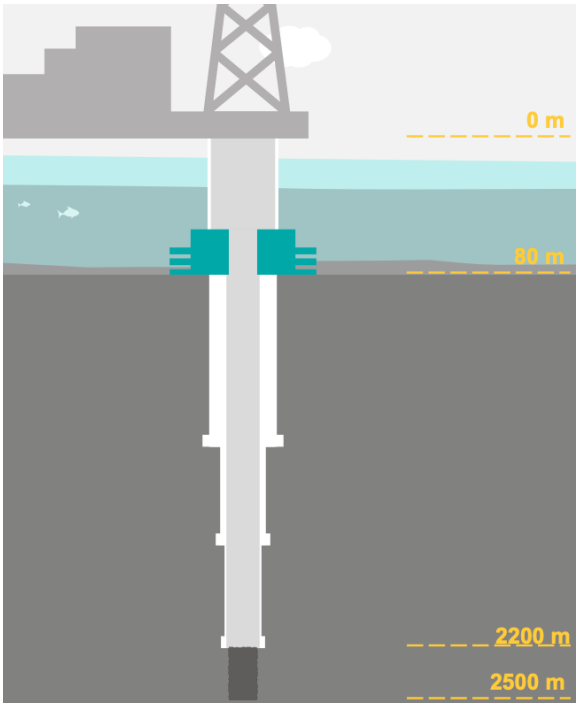

Figure 7.5: Setting depth of riser and casing, with openhole length of 300m.

Table 7.4: Detailed configuration of hole section.

Type	Depth [m]	OD [in]
Riser	80	21
Casing 1	1055	20
Casing 2	1616	13 ⅜
Casing 3	2200	10¾
Openhole	2500	8 ½

Fluid

The drilling fluid used is an oil-based mud with a density of 1.63 sg; a detailed description of the drilling fluid composition is shown in Figure 7.6.

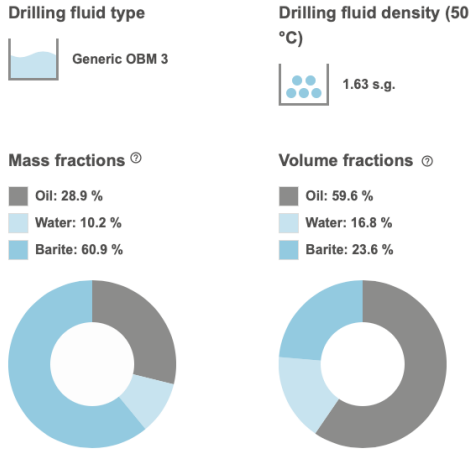

Figure 7.6: Drilling fluid composition for the test well.

Drillstring

The drillstring used for the simulations is of high importance, as the detection model relies on utilizing wired drillpipe (WDP) technology. It consists of 5" drillpipe joints, in addition to downhole measurement tools, such as measurements while drilling (MWD), logging while drilling (LWD) and ASM, located in the bottom hole assembly (BHA). The ASM is an essential part of the BHA, as it measures the annular pressure at its current depth.

The drillstring consists of a BHA with a cumulative length of 160 meters; beyond that, it consists of drillpipe joints. Drillbit diameter is 8 ½ inches and its length is 0.3 meters.

Geology

The geo-pressure window for the test well is shown in Figure 7.7, is used to choose appropriate mud weights.

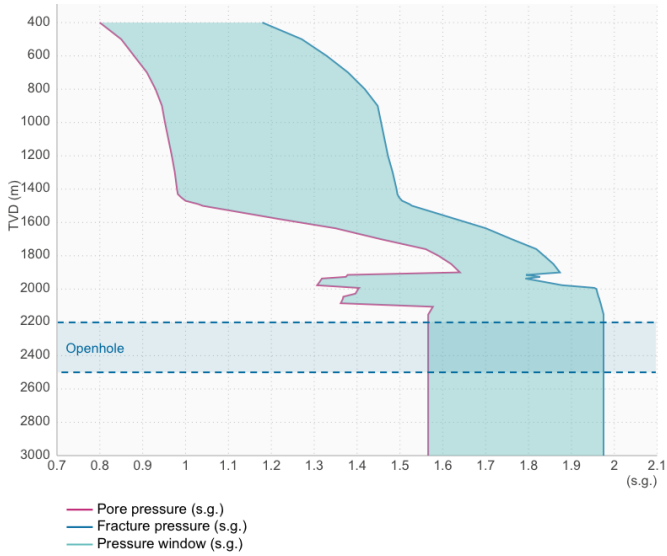

Figure 7.7: Mud Window

7.5 Results and Discussion

Four cases are considered for testing the automated kick-detection model. The different cases will show the sensitivity-level of the model, as well as its weak-points and where it performs at a satisfying level. The results from all cases will be presented and discussed in this section.

7.5.1 Input Values

Table 7.5 presents the defined user inputs, utilized through the entire operation for all cases. The bit starts drilling at 2500mTVD, which corresponds to the depth where influx is initiated. Mud flow rate into the wellbore is 2200 liter per minute, and it is kept constant throughout the operation. This is also applicable for the surface revolutions per minute (RPM) - 120 RPM. As mentioned in section 7.4.1 the kick mass and total influx rate values are changed depending on the test case description.

Table 7.5: Constant user inputs for kick-detection model testing.

Parameter	Value	Unit
Flow rate in	2200	lpm
Surface RPM	120	rpm
Top of string velocity	0.1	m/s
ROP	20	m/hr

The model will be tested using different influx rates, kick mass, bit plugging and a manually initiated kick. These tests are performed to challenge the model's accuracy and see if it reports false-positives or false-negatives.

7.5.2 Influx Rate Test

The influx rate test will investigate the model's ability to detect kicks with varying influx rates. Kicks occurs in different influx volumes and rates.

User input

The set-points for the influx rates are: 0.6, 1.0, 5.0, and 10.0 kg/s. While the total mass of the kick is 150 kg for all rates.

Results & discussion

Results from the tests conducted are presented in Figure 7.8. The kick-detection model was able to detect the occurrence of kicks at the 40-second mark correctly for 3 of the 4 cases. Figure 7.8b, 7.8c and 7.8d indicates this by the red alarm signal.

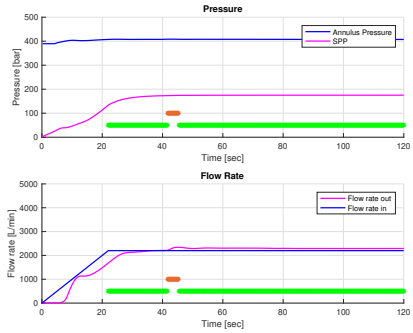

(a) Influx Rate: 0.6 kg/s.

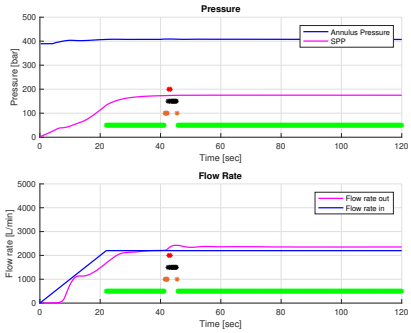

(b) Influx Rate: 1 kg/s.

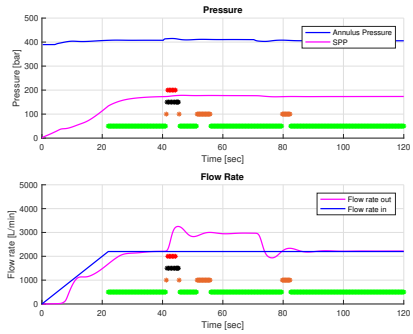

(c) Influx Rate: 5 kg/s.

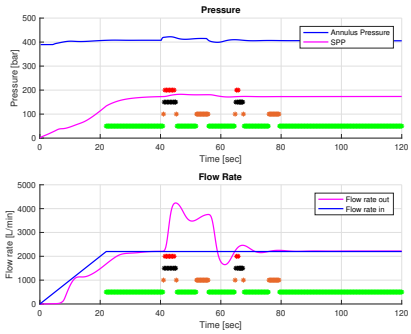

(d) Influx Rate: 10 kg/s.

Figure 7.8: Kick-detection test results with varying influx rates, but constant volume.

In Figure 7.8d, the algorithm correctly detects the kick occurring at the 40-second mark. Furthermore, another kick alarm is triggered at the 65-second mark. This is approximately around the time the kick exits the wellbore, causing the flow rates to destabilize. And while this is happening, a spike in flow rate is observed, causing the kick-detection model to alert a false-positive. The algorithm recognizes this as a kick because of the behavior induced by stabilizing the well, which is similar to what a kick looks like. However, this is not too concerning, as the operators would have taken appropriate action to mitigate the kick initiated at the 40-second mark.

The simulation performed with an influx rate of 0.6 kg/s did not detect the kick, this is shown in Figure 7.8a. Only a slight increase in flow rate out is observed. This shows that the model has a high trigger-setting, not sensitive enough to recognize smaller rates of influx.

7.5.3 Kick-mass Test

In this test, the total mass of the kick will be the changing variable, while the influx rate will remain constant. This means that the kick will last longer with increasing mass, leading to the flow rate out taking longer to stabilize towards normal conditions after the kick has been initiated.

User input

The set-points for the mass of the kick is: 10, 50, 500, and 1000 kg. The influx rate of the kick is kept constant at 1 kg/s.

Results & discussion

The algorithm was successfully able to detect kicks initiated at all four cases. The set-off time for the kick is still at the 40-second mark, which is shown in Figure 7.9 the red alarm is triggered for all cases.

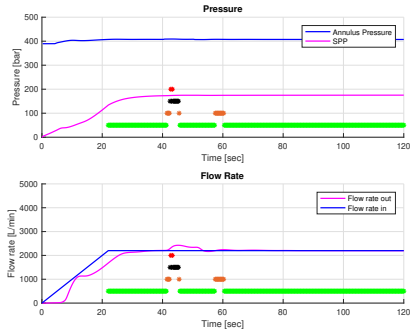

(a) Mass of kick: 10 kg.

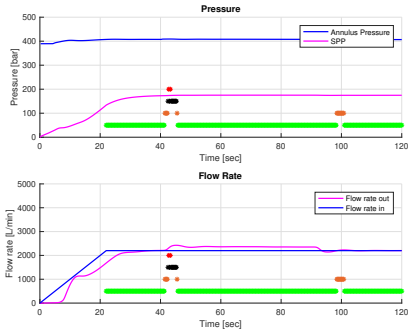

(b) Mass of kick: 50 kg.

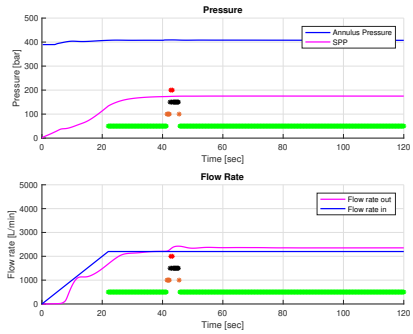

(c) Mass of kick: 500 kg.

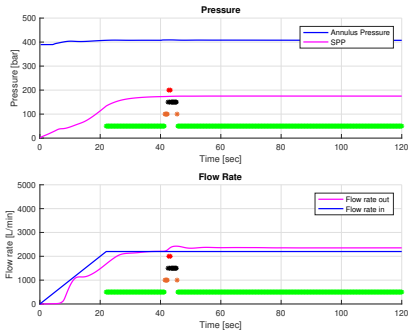

(d) Mass of kick: 1000 kg.

Figure 7.9: Kick-detection test results with varying mass, but a constant influx rate of 1 kg/s.

Results from this test did not fluctuate as much compared to the influx rate test. Moreover, the prediction of prolonging the increase in flow rate out is proven to be correct. This can easily be observed by comparing Figure 7.9a and 7.9b. In Figure 7.9a, the flow rate out returns to normal conditions after about 10 seconds, which is how long the fluid influx lasts. In Figure 7.9b the flow rate out drop does not return to normal conditions until the 90-second mark. The same pattern is observed for the two remaining cases, but here the flow rate out does not decrease, as there still is flow of formation fluid into the wellbore at simulation end.

7.5.4 Bit Plugging Test

Bit plugging is an option among the ”Incident”-alternatives in the OpenLab UI, described in section 5.2.3.

Plugging of the bit nozzles usually corresponds to an increase in standpipe pressure, as a result of an increase in pressure drop over the bit - the flow rate remains the same. This creates a standpipe pressure behavior similar to an uncontrolled influx, and may induce a false-positive kick alarm.

User input

In all of the cases performed, the bit plugging is manually induced close to the 40-second mark, and it is unplugged close to the 80-second mark. Set-points for the bit plugging are as follows: 0, 30, 50, and 60%. This test will not initiate a kick during simulation, as it could disturb the objective of triggering a false-positive alarm.

Results & discussion

The results from all simulations were satisfying, as none of the cases evoked a false-positive kick alarm. Figure 7.10 shows that the plugging of the bit was not even able to raise the threat level to medium probability.

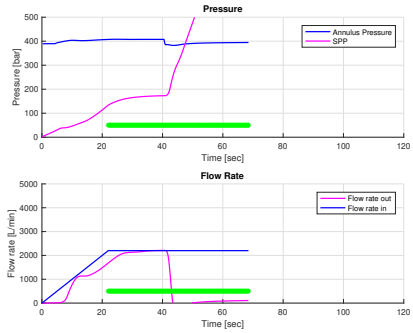

(a) Bit plugged: 0%.

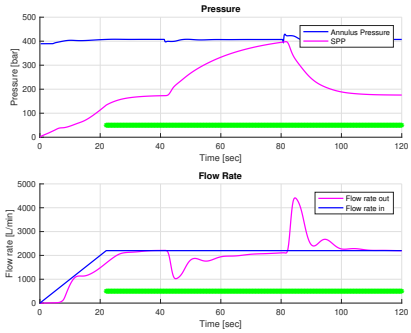

(b) Bit plugged: 30%.

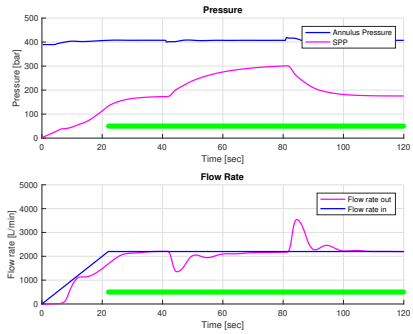

(c) Bit plugged: 50%.

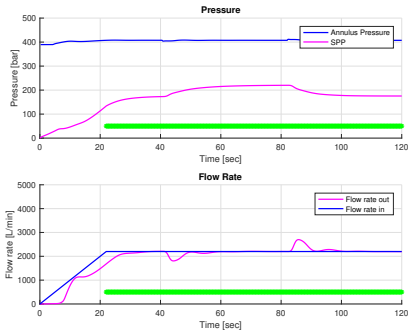

(d) Bit plugged: 60%.

Figure 7.10: Kick-detection test results where the bit is being plugged at an attempt to trigger false-positive kicks.

The non-raising behavior is due to the flow rate out decreasing. Bit plugging reduces the volume of flow into the annulus which conflicts with one of the three criteria defined in section 7.2.

In Figure 7.10a, 0% flow through the nozzles is manually activated, which causes a tremendous increase in standpipe pressure, while the flow rate out drops towards zero. This caused the simulator to crash and the test did not finish. But the result is not to be overlooked; the kick-detection model did not trigger a false-positive alarm.

7.5.5 Manual Kick Initiated Test

In addition to bit plugging incident, the OpenLab simulator had the option of turning off pre-planned prompting of a kick, and instead initiate a kick manually as the user desire. The effect of a manual kick differs compared to the tests performed in section 7.5.2 as the kick is initiated in the OpenLab simulation UI

User Input

The different cases change the influx rate to the following: 0.5, 1.0, 3.0, and 5.0 kg/s. The total mass of the kick is to remain constant at 150 kg.

Results & Discussion

The kick-detection algorithm delivered the correct result in 3 out of the 4 cases, not unlike the results achieved in section 7.5.2.

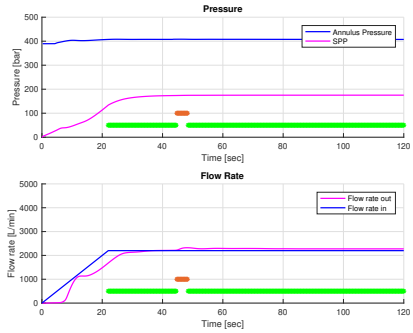

(a) Manual Kick: 0.5 kg/s

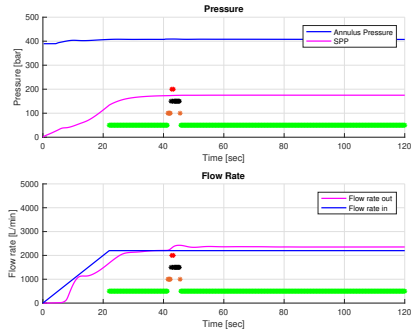

(b) Manual Kick: 1 kg/s

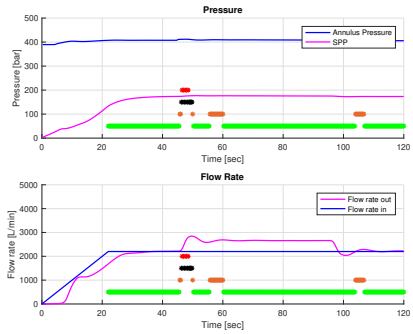

(c) Manual Kick: 3 kg/s

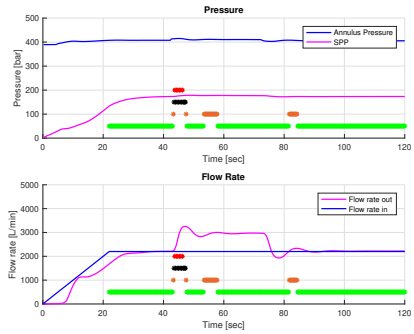

(d) Manual Kick: 5 kg/s

Figure 7.11: Kick-detection test results where a kick is manually prompted. Constant total mass with varying influx rates.

The algorithm did once again fail to recognize the smallest of the kicks - in the sense of low influx rate, indicating that it allows for large rates of influx from the formation to enter the wellbore before alerting a kick. section 7.3 discusses the possibility of using different kick-detection models, where the main factor of difference between them are their ”sensitivity”. By the looks of it, this detection model seems to lean toward a high trigger value, as it does not seem to have a problem with the kicks that have 1 kg/s or higher influx rate.

This test case strengthens the findings in section 7.5.2. Comparing the test results from both section 7.5.2 and Figure 7.11, no significant difference is noticeable, concluding that the manual kick incident draws similar effects as the one initiated in the MATLAB model.

7.6 Subsequent Handling of Kick

Once a kick is detected, the operator must take appropriate action. This section will cover this, as well as propose possible supplementary additions to the kick-detection model already created to further automatize the process of handling a kick.

When the kick alarm is activated and the influx is moving up the wellbore, the operators need to take appropriate action. The standard procedure for closing the well is as follows, according to Hovda [44]:

1. Hoisting the drillstring up at least 5 meters.
2. Stop pumps and check for flow.
3. First priority-closing elements.
   (a) Close upper annular ram.
   (b) Close drillstring if not already closed.
   (c) Open inner- and outer fail safe valve and slowly close adjustable chokes in the choke manifold.
   (d) Observe maximum allowable annular surface pressure (MAASP).
4. Close remaining BOP-valves, hang off drillstring tool joint at the BOP.
5. Read shut-in casing pressure (SICP), shut-in drillpipe pressure (SIDP) and kick volume.

The procedures presented above should be implemented as a continuation of the kick-detection model presented in this chapter. As the subsequent operational steps are mainly consisting of initiating mechanical tasks, monitoring well behavior as well as recording measurements, it has the potential of being included in the kick-detection models.

7.7 Kick-Detection Conclusion

The kick-detection model is a program designed to detect any potential kicks that might occur during a drilling operation. Handling of kicks is one of the most important safety measures operators must do, as a potential blowout might end up being fatal. As the oil and gas industry gradually transition into utilizing digital technology and automated solutions, one of the main objectives is to increase the accuracy of successfully detecting kick. The purpose of the algorithm presented in this chapter is to show that autonomous detection of kicks, to assist the operator, is definitely possible to achieve. Furthermore, the models can be built upon to increase their functionality and accuracy.

The tests completed presented in section 7.5 had a success rate of 87.5%, respectively 14 out of the 16 cases gave the expected result. This is presumed satisfying. The results showed that the algorithm was designed with a high trigger rate, as it was not able to detect the smallest kicks in regards to influx rates.

The algorithm did not get triggered by the bit getting plugged and shows promise of reducing the number of false-positives.

To rely upon a kick-detection model, it needs to be extremely accurate as reporting a false-negative subsequently could result in a blowout. Moving towards a fully automated process requires more real-time data acquired from downhole sensors. WDP has slowly entered the market, and this chapter presents that a detection model would heavily benefit from the continued development of instruments related to that.

Chapter 8

Automated Friction Test System

With the high cost and associated safety hazards, the drilling operation is recognized among the most comprehensive phases encountered in the lifetime of a well. As a consequence, the oil and gas industry strives to discover new efficient and cost-effective solutions to optimize the operation while maintaining the same level of safety. Studies have shown that most non-productive time (NPT) is related to hole cleaning, wellbore instabilities, and drillstring failures [61]. To reduce NPT, and successively well cost, it is important to detect possible downhole problems as early as possible in order to take preventive actions. Friction test is an operational procedure that gives information about possible changes in drillstring friction along the wellbore. The test results can be used to identify downhole problems by comparing a series of tests, and look for discrepancies. The friction test has several factors that might affect the test results, where most of them are related to the operator and drilling parameters used.

This chapter will present how friction tests are performed today and apparatuses used for obtaining relevant measurements. An automated friction test will be presented at the end of this chapter. This algorithm is programmed in MATLAB and runs simulations linked up to the OpenLab drilling simulator. The system will be used to investigate the impact of different drilling parameters have on the friction test results.

8.1 Drillstring Torque and Drag Theory

Torque and drag (T&D) are among the most important drilling parameters, which are constantly used as indicators of the downhole drilling conditions. Drillstring drag is a force that is generated by the weight of the drillstring, and it is affected by buoyancy, friction and potential fluid flow. On the other hand drillstring torque is the moment required to rotate the string at the desired revolutions per minute (RPM) level. The magnitudes of the T&D measurements correlates, consequently high drag forces and excessive torque loads often occurs together [62]. This section will describe how field measurements of T&D are performed and factors influencing them.

8.1.1 Field Measurements

Accurate T&D interpretations are highly dependent on accurate real-time readings, and therefore depend on the accuracy of the measurement equipment. This section will describe today's T&D measurement technology, as well as introducing improved measurement solutions needed for a future autonomous friction test system.

Hook-load measurement

Today's industry standard of hook-load measurement is based on a tensiometer clamped mechanically to the wire at the hanging point of the top drive, or a compression cell at the dead line anchor [63]. The typical location of the two sensors are shown in Figure 8.1, where the dead line sensor is the most used [62].

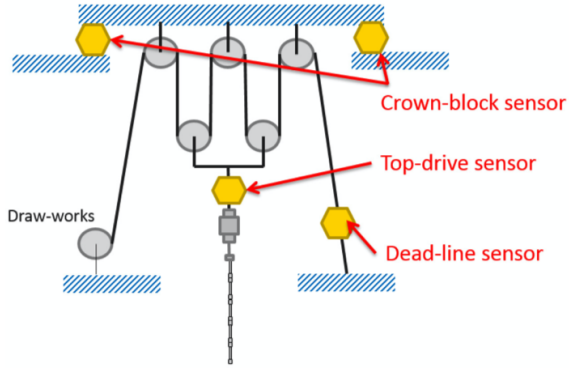

Figure 8.1: Typical position of indirect hook-load measurements in a draw-works hoisting system [64].

Using technology available today, the hook-load measurements displayed at top-side do not correlate with their true values. The hook-load value reported from the compression cell is the sum of all load-generating forces. These load-generating forces can be the weight from umbilicals attached to the top drive, the top drive weight itself, frictional forces in the tackle system, as well as and forces associated with weight and rotation of the drillstring [64]. Downhole problems are associated with small hook-load deviations from the trend, i.e. a few tons, and should be investigated further. Hook-load measurement technology available today is located too far from the target load, which ultimately increases the overall uncertainty of the reading, and causes problems to detect smaller deviations.

Torque measurement

The most common torque measurement technique is to monitor the electrical current, which is measured at the powered portion of the top drive [65]. Motor current is displayed as motor amperage, to perform the conversion to torque values motor curves are used. The motor curves apply to a newly manufactured motor, but does not account for wear or degradation of the specific motor. Another shortcoming is that the current is measured at the motor shaft, this measurement includes the losses through the gearbox and bearings located prior to the drillstring. Due to this, the measurement is counted as an indirect value [63].

Instrumented internal blowout preventer

An optimized drilling system is only as efficient as the quality and accuracy of the measurement reported to the system. Industry standards available today related to T&D measurement contain too high uncertainties, as the sensors are placed too far from the target load. Wylie et al. [63] present a new system designed to provide accurate drilling measurements directly from the target load, i.e. top of the drillstring. The presented system, referred to as instrumented internal blow-out preventer (IIBOP), will provide the high demanding accuracy needed for today's modern control systems.

The IIBOP is a modified top drive system, able to measure six different drilling parameters: tension/compression, torsion, pressure, rotational speed, acceleration, and bending. With this solution, the string weight measurements exhibited a 65% reduction in signal noise compared to the dead-line sensor, giving a clearer picture of drillstring dynamics. Such improvements were also demonstrated for real-time torque measurements [63].

Stepping towards autonomous drilling operations requires more accurate measurements than what is provided by today's solutions. The IIBOP provides readings closer to the actual target load, subsequently providing higher accuracy results. This new type of measurement technology is essential for the industry in order to transition into automated operations.

8.1.2 Wellbore Friction

Along the wellbore there are several contact points between the wellbore wall and the drillstring. At these contact points, the forces exerted are defined as friction forces. All the local friction forces have one thing in common - they strive to resist motion. The hook-loads and torques measured at the surface are the results of all the local friction forces along the drillstring in addition to the string's weight. Several factors influence the friction test readings, which complicates the interpretation of the results. Therefore, to correctly interpret the test, it is important to know the different types of wellbore frictions, which can be divided into [66]:

- Dry friction: Friction between two solid surfaces in contact, which can be both static (non-moving surfaces) and kinetic (moving surfaces) friction.
- Skin friction: The force resisting fluid motion across a surface.
- Fluid friction: Friction between layers moving relative to each other within a viscous fluid.
- Lubricated friction: Friction with a lubricating fluid in-between two solid surfaces.
- Internal friction: Resisting force between elements within a solid material undergoing deformation.

When analyzing wellbore friction, the types listed above are of varying importance. The main frictions impacting a drilling operation will be further elaborated below.

Dry friction

In a well with good hole conditions, drillstring T&D are primarily caused by dry friction [62]. The occurrence of dry friction increases with increasing wellbore deviation. Figure 8.2 illustrate the concept of dry friction along an inclined plane, where the friction is denoted as F_f.

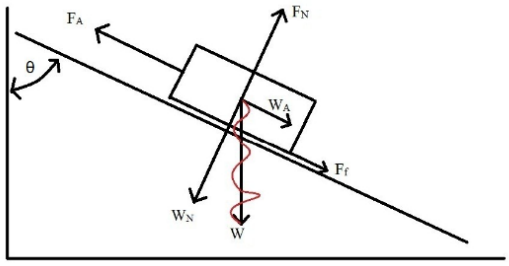

Figure 8.2: Forces acting on an object pulled along an inclined plane [66].

The dry friction is created by the drillstring tool joints in contact with the borehole wall at several places along the string, as shown in Figure 8.3a. In case of bad hole

cleaning the cuttings might accumulate on the low side of the borehole, as shown in Figure 8.3b. Consequently, the dry friction will include both the wall contact friction and the force needed to displace the cutting particles with the tool joints [67].

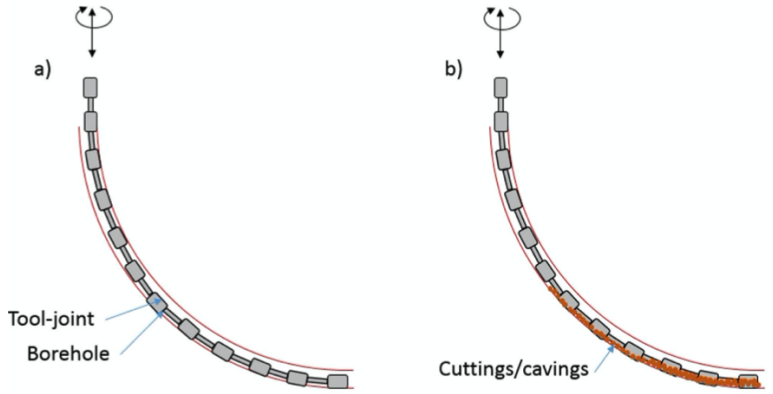

Figure 8.3: a) Clean hole where contact between tool joints and borehole limited to friction. b) Cuttings accumulation on low side of well, tool joints need to displace the cuttings in addition to the contact friction [67].

Skin friction

Skin friction, also known as hydraulic drag, is the force exerted by the wellbore fluids when pulling a solid object through. The high viscous drilling fluid sticks to the drillstring and hinders movement [66]. In addition to the hydraulic drag, a viscous drag force transpires with this movement. The displaced volume of the pipe has to be refilled, this effect is known as swab. Displaced volume reduces the local pressure and results in a net downward force, given that the pumped fluid volume exceeds the displaced volume the force will act in the opposite direction [68]. The hydraulic drag phenomenon is illustrated by a velocity curve in Figure 8.4, where the fluid velocity vector prevents upward pipe movement.

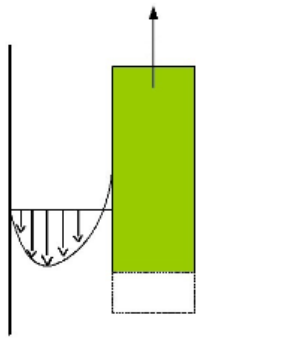

Figure 8.4: Drillstring pulled upwards creating hydraulic and viscous drag forces [66].

Lubricated friction

The lubricating effect tends to reduce friction. Related to drilling operations, the drilling fluid and particles in the well will act as a lubricating substance [66]. Studies show that friction coefficients are affected by mud quality, mudcake and lubricant additions, as well as the lubricating effect often being difficult to predict [69].

8.1.3 Torque and Drag Friction Model

Torque and drag models have always been an important part of a drilling operation, especially with the introduction of extended-reach, high-angle wells introduced in the 1980s. T&D models are usually used to estimate expected downhole T&D during drilling operations, with different friction coefficients. In addition, the model is used in correlation with friction test data obtained. A friction coefficient for the entire well can be estimated using the model presented in this section; the model is provided by Aadnøy et al. [55].

An important factor in the T&D model is the buoyancy factor. Buoyancy is a phenomena constantly present in a drilling operation and it is essential to predict accurate T&D values [70]. The buoyancy factor, β, is the ratio of effective- and unit pipe weight. With equal fluid density on both sides of the pipe, the buoyancy factor is defined as:

$$\beta = 1 - \frac{\rho_f}{\rho_{pipe}} \tag{8.1}$$

Where ρ_f is the fluid density and ρ_{pipe} is the pipe's material density.

Straight wellbore sections without pipe rotation

The normal weight component is the only component contributing to friction in straight sections, therefore straight sections are weight dominated [55]. Figure 8.5 illustrates an element along a straight wellbore section.

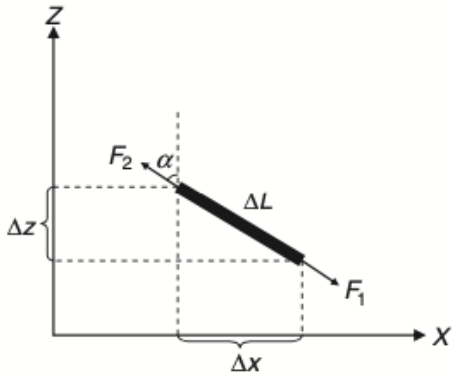

Figure 8.5: Element pulled along straight section [55].

The top force of a pipe element in a straight section, without rotational pipe movement, is given by:

$$F_2 = F_1 + \beta \Delta L w(cos\alpha \pm \mu sin\alpha) \tag{8.2}$$

Where $\pm$ represents pipe hoisting and pipe lowering respectively. F_1 is the force at the lower end, ΔL is the pipe element length, the unit pipe weight is w, the wellbore inclination is α and μ is the friction factor [55].

Straight wellbore sections with pipe rotation

The top force of a rotating pipe element, in a straight section, is given as:

$$F_2 = F_1 + \beta \Delta L w cos\alpha \tag{8.3}$$

Torque is defined as the normal weight component multiplied by the pipe radius,

r, and the coefficient of friction. The torque for straight wellbore sections, without axial movement, is given as:

$$T = \mu r \beta w \Delta L sin\alpha \tag{8.4}$$

Curved wellbore sections without pipe rotation

The pipe's normal force in a curved section is strongly dependent on the axial loading, thus making it a tension dominated process. The situation of an element pulled along a curved surface is illustrated in Figure 8.6.

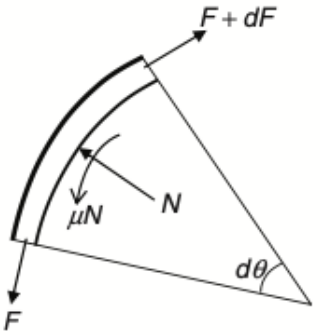

Figure 8.6: Element pulled along curved section [55].

Top force of a pipe element in a curved section is dependent on azimuth as well as inclination, and given by:

$$F_2 = F_1 e^{\pm|\phi_2 - \phi_1|} + \beta w \Delta L \frac{sin\alpha_2 - sin\alpha_1}{\alpha_2 - \alpha_1} \tag{8.5}$$

The dogleg angle ϕ is given as:

$$\phi = cos^{-1}(sin\alpha_1 sin\alpha_2 cos(\theta_1 - \theta_2) + cos\alpha_1 cos\alpha_2) \tag{8.6}$$

Where θ is the azimuth angle.

Curved wellbore sections with pipe rotation

A rotating curved pipe element's top force is given as:

$$F_2 = F_1 + \beta w \Delta L \frac{sin\alpha_2 - sin\alpha_1}{\alpha_2 - \alpha_1} \tag{8.7}$$

Further the element's torque is expressed as:

$$T = \mu r F_1 |\phi_2 - \phi_1| \tag{8.8}$$

By separating the well into straight and curved elements, the friction for any wellbore shape can be calculated by utilizing Equation 8.2 through 8.8.

8.2 Friction Test

During a drilling operation, it is crucial to carefully monitor the cuttings transported out of the well as this increases the possibility to detect downhole problems. Accumulation of cuttings as a result of poor hole cleaning and/or hole collapse will increase the wellbore friction, as the number of contact points increases. A friction test is a test procedure used to detect changes in wellbore friction, and it might indicate downhole problems at an earlier stage rather than by monitoring cuttings out of the well.

A friction test is a procedure where the driller record surface values such as free rotating torque (FRT), free rotating weight (FRW), pick-up weight (PUW) and slack-off weight (SOW). The test results provide information about possible changes in wellbore friction by comparing the recorded values with earlier test results. Friction testing is a repetitive task performed at regular intervals decided by the operator. To obtain recordings sufficient enough for comparison, all tests should ideally be performed with equivalent drilling parameters and procedures. The operation is rated with the lowest level of automation (LOA) (L1), where the operator's function is to monitor, generate, select, and implement.

8.2.1 Procedure

When the bit is off bottom, it is assumed zero T&D at the lower end of the drillstring. The measured surface values of hook-load and torque will then represent the buoyed drillstring T&D, where the effect of friction along the wellbore is

present [67]. The test is divided into three sub-tests: free rotating test, pick-up test, and slack-off test. Figure 8.7 illustrates a typical friction test sequence, starting out with a free rotating test, followed by a pick-up test and finally conducting a slack-off test. Movement of the drillstring, either rotational or axial, results in variations in the measured hook-load. These periods are called transition periods and last until the drillstring reaches steady-state movement, which is recognized by stabilization in the recorded values.

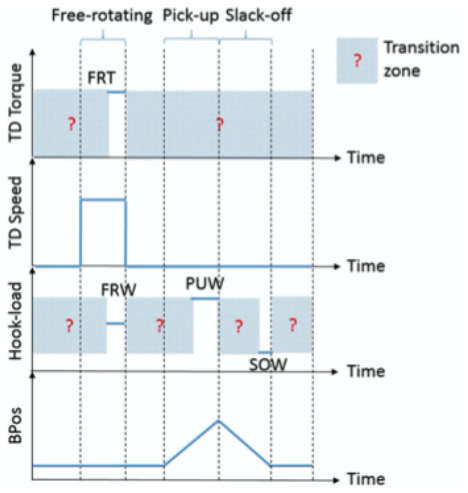

Figure 8.7: Typical sequence for a friction test [67].

When the FRT, FRW, PUW and SOW recordings are obtained, the values can be used to calculate the mechanical friction by utilizing the T&D model presented in section 8.1.3. By applying the model to the relevant string motion of the friction test, and dividing it into straight and curved elements, the friction coefficient can be estimated. This is done by subtracting the T&D forces starting with the recorded values at topside. As mentioned, the bottom end condition is zero torque and zero drag.

8.2.2 Steady-State Requirement

Steady-state movement when recording the test results is an important requirement, as it affects the measured values and furthermore complicates the interpre-

tation of the results [64]. As the drilstring is elastic, it will experience a transition period before reaching steady-state when motion is applied.

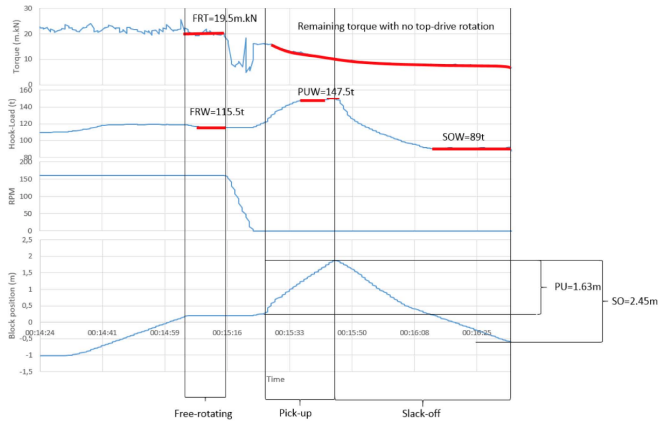

Figure 8.8: Example of PUW taken with remaining torque in drillstring [67].

Figure 8.8 shows an example of a sub-test conducted prior to the steady-state requirement is fulfilled. The pick-up test sequence starts with stopping the top drive rotation, i.e. setting RPM to zero. When the RPM reaches zero, the system initiates string pick-up. When the surface RPM reaches zero, the string will contain leftover torque due to wellbore frictions. When the string is picked up there is a combination of axial and rotational movement, due to the leftover torque inducing unwinding of the drillstring. A PUW recorded at this point will not represent the true PUW as the steady-state requirement is yet to be fulfilled [67]. This behavior is recognized in the example recording shown in Figure 8.8. Specifically, the PUW is recorded as the value starts to stabilize, however just before the slack-off sequence is initiated, the hook-load increases. This indicates drillstring unwinding, and as the hook-load increases, the unwinding rotational speed decreases.

8.2.3 Interpretation Challenges

The interpretation in relation to earlier observations has several sources of variation to be considered when analyzing the wellbore friction. Drilling fluid conditions impact the test readings as different flow rate and mud rheology affects the forces applied on the drillstring.

Cayeux et al. [67] analyzed friction tests from an 8 $^1/_2$" section drilled in the North Sea. The test was performed for every stand drilled, some performed by an automated system, and some manually by the driller. In one of the tests, it was noticed a discrepancy in the hook-load from the other tests, therefore the time-based log of the test was investigated. The log showed two test recordings, one executed by the automatic system and one by the driller. Figure 8.9 shows the time-based log around the mentioned friction test, this emphasizes how the flow rate can influence the friction test recordings. Due to different flow rates used during testing, the difference in the recorded hook-load was as high as 6 tons.

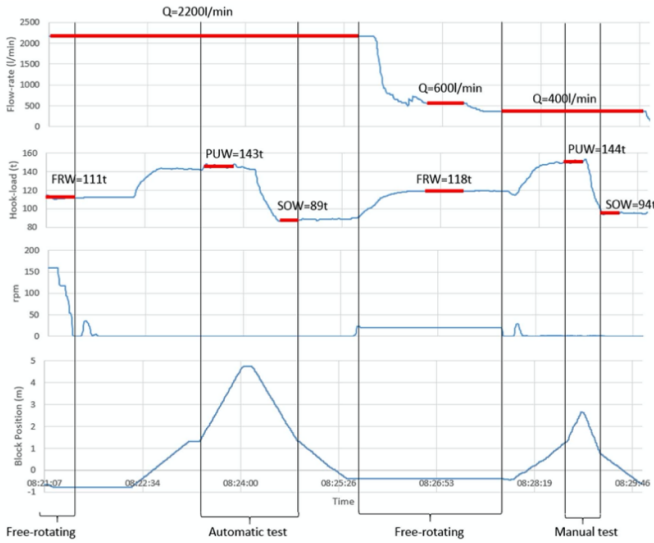

Figure 8.9: Time-based log of friction test taken in the North Sea [67].

8.3 Automated Friction Test Model

The friction test model is programmed and connected to the OpenLab simulator with the use of MATLAB. The model is set up to perform a friction test sequence in the order described in section 8.2.1. Recording of test results and proceeding to the next test sequence rely on the stabilization of flow rate, surface torque, and hook-load.

8.3.1 Configuration and Inputs

To be able to initialize a simulation from MATLAB, there needs to exist a configuration in the OpenLab user interface (UI). The different configuration possibilities are mentioned in section 5.2.2. Table 8.1 show the test model configuration, where those not specified are set to their default values described in Table 5.1.

Table 8.1: Friction test model configurations.

Model configuration	Model value
Initial bit depth	Target depth - 4 m
Reservoir model	false
Transient mechanical model	true

When a configuration has been constructed, the model can be initiated using MATLAB. To initialize the model it should be given appropriate initial set-points. Some set-point properties are not of importance to the test conducted and thus set to the default values presented in Table 5.2. These properties are rate of penetration (ROP), managed pressure drilling (MPD) properties, blow-out preventer (BOP) status and inlet fluid density. The relevant parameters that should be defined for each test sequence are shown in Table 8.2.

Table 8.2: User inputs to friction test model.

Parameter	MATLAB variable	Unit
Flow rate in	FlowRateIn	m^3/s
Pick-up velocity	PickUpVelocity	m/s
Slack-off velocity	SlackOffVelocity	m/s
Surface RPM	SurfaceRPM	rev/s

Flow rate in is given as an initial set-point at start of the simulation, which is the value the simulator seek to achieve. Surface RPM, pick-up velocity and slack-off velocity are kept at zero when initializing the simulator, and kept at zero except when the relevant test sequence is executed.

8.3.2 Data Handling

The OpenLab simulator is applicable for all types of different drilling operations, therefore it is important to correctly handle the data important for the relevant operation performed. The following section will present how the model handles the data and its stabilization criteria.

Storing data

The friction test model depends on three data recordings computed by the OpenLab simulator, respectively hook-load, surface torque, and flow rate out. The model handles the data such that the last twenty recordings of hook-load, torque, and flow rate out are saved and accessible at all times. This provides the possibility to detect stabilization in the recorded data.

Stabilization criteria

The data stabilization criterion in the model is based on mean absolute deviation (MAD) and the mean of the data-set. The MAD of a data-set is the absolute average distance between each data point and the mean [71]. The MAD of a data-set x, with n data points are expressed as:

$$MAD = \frac{\sum_{i=1}^{n} |x_i - \overline{x}|}{n} \tag{8.9}$$

The different types of simulation data varies with different order of magnitude, therefore the model's data stabilization criteria are given as the MAD's fraction of the mean. The criteria used in the model is given as:

$$\epsilon = \frac{MAD(x)}{MEAN(x)} = \frac{\sum_{i=1}^{n} |x_i - \overline{x}|}{\sum_{i=1}^{n} x_i} \tag{8.10}$$

Test results

If the criteria is satisfied, the model saves the result of FRT, FRW, PUW and SOW. These are given as the mean of the last twenty data points recorded. Furthermore, they are printed in the command window and plotted on their relevant graphs created by the model.

8.3.3 Model States

As mentioned in section 8.2.1 the friction test consists of three sub-tests. The model is therefore built up by different states, where it only proceeds to the next state if one or more of the requirements are fulfilled. The different states are bit-off bottom, free rotating test, pick-up test and slack-off test.

State 1 : Bit-off bottom

The first state is getting the bit off bottom. This assures that the assumption of zero weight and torque at the bottom end of the drillstring is valid. In this state the simulator picks up the drillstring until the bit is four meters above bottom, which is the defined state requirement. Drillstring will start rotating when this requirement is fulfilled and furthermore proceed to the free rotating test.

Due to limitations of running the simulator in MATLAB, the initial bit depth is always set such that state 1 requirements is fulfilled when starting the simulator. At the current time, it is not possible to adjust the top of the string position when initializing the simulator with MATLAB. This will then limit the movement of the drillstring at later stages of the tests, which leads to some tests not being completed as the drillstring hits the top of the derrick.

State 2 : Free rotating test

The objective of the second state is to record FRT and FRW. In order to obtain a true reading of the torque and hook-load the drillstring steady-state requirement must be fulfilled. At this state the drillstring is rotating with a predefined RPM until the torque, flow rate and hook-load have stabilized within one percent deviation from the mean as shown in Table 8.3.

Table 8.3: State criteria for free rotating test.

Data type	Stabilization criteria
Torque	1%
Hook-load	1%
Flow rate	1%

When the state criteria are fulfilled, FRT and FRW will be recorded, subsequently setting the RPM set-point to zero and proceeding to the next state.

State 3 : Pick-up test

The objective of the third state is to record the PUW, which is the drillstring weight when it is picked up with the predefined pick-up velocity. In this state, the model waits for the RPM to reach zero, before starting to pick-up the drillstring. The steady-state requirement at the pick-up test is dependent on stable readings of hook-load and flow rate out, the test criteria are shown in Table 8.4. In addition to the stabilizing criteria, this test has to take in to account the drillstring unwinding when the RPM has reached zero. Taking into account the drillstring unwinding, the recordings will not be performed until the surface torque is below 1 Nm.

Table 8.4: State criteria for pick-up test.

Data type	Stabilization criteria
Hook-load	3%
Flow rate	1%
Torque	$>$1 Nm

When the PUW is recorded, the model changes the top of string velocity to the slack-off velocity value and proceeds to the last state.

State 4 : Slack-off test

The last stage of the friction test is to record the SOW. The SOW recording is conducted when the flow rate and hook-load stabilizes in accordance to the criteria presented in Table 8.5.

Table 8.5: State criteria for slack-off test.

Data type	Stabilization criteria
Hook-load	3 %
Flow rate	1 %

When the model has recorded the SOW it will stop the simulation and display the recorded data in text form and corresponding plots.

8.3.4 Test Well

The well path, casing design, fluid description, geology and drillstring for the test well is configured in the OpenLab UI.

Well path

The test well is configured with a 500 meters horizontal reservoir section and a constant azimuth angle of 0°. The well path starts out with a 300 meter vertical section followed by a build-up section. A 43° tangent section starts at 1370 meters measured depth (MD) and ends at 1840 mMD, where the second build-up section starts. The well path reaches 90° inclination at 2720 mMD and ends with a 500 meters reservoir section to target depth at 3220 mMD. The well path is shown in Figure 8.10a

Hole section

The well design at the simulation start is shown in Figure 8.10b. The 10 $^{3}/_{4}$" production casing is hung off at wellhead, 200 meters below rotary kelly bushing (RKB), with shoe depth at 2500 mMD. The 8 $^{1}/_{2}$" section is drilled out of the production casing and down to 3000mMD. This is the starting point for each simulation.

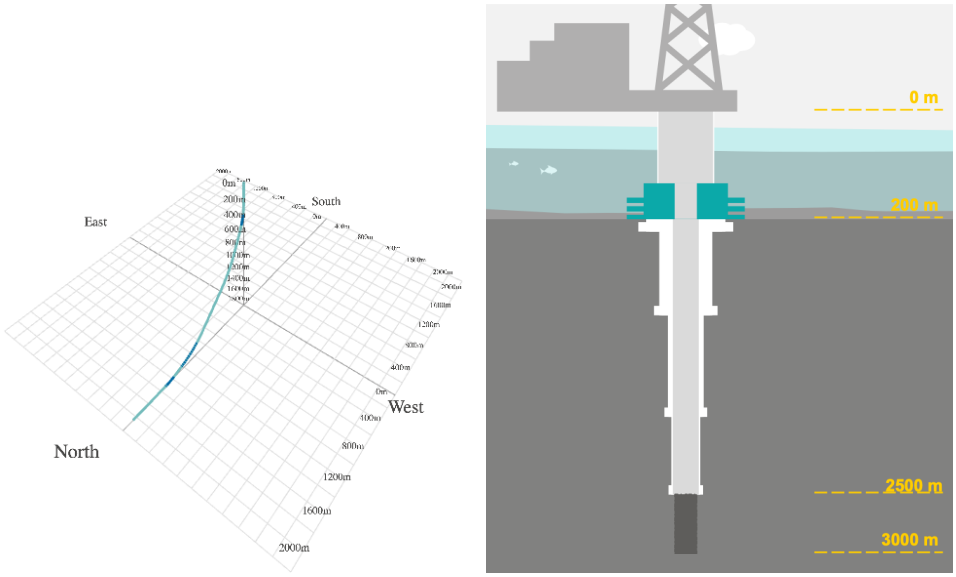

(a) Flow rate : 1000 lpm. **(b)** Flow rate : 2500 lpm.

Figure 8.10: Well path and hole section for test well.

Fluid selection

All simulations are executed using an oil-based mud, with varying fluid densities. The friction test fluid density dependence will be tested using the simulator. Therefore the fluid density is to be changed during the fluid density dependence test. For other tests, the drilling fluid density is set to 1.2 sg and the composition is shown in Figure 8.11

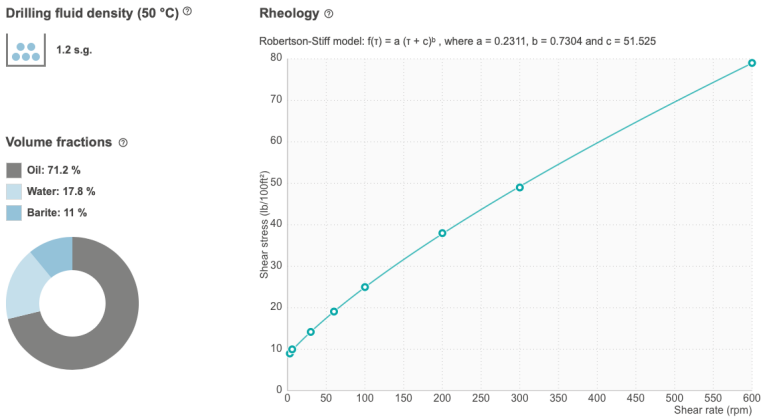

Figure 8.11: Casing design for friction test.

Drillstring

The drillstring consists of a 150 m long bottom hole assembly (BHA) with a 8 $^1/_2$" drillbit. Furthermore, 5" OD drillpipe joints, with a linear weight of 34.2 kg/m are chosen.

Geology

Figure 8.12 show the geo-pressure window for the well configuration. This pressure window is used to choose the appropriate drilling fluid densities, relevant for testing the density dependence.

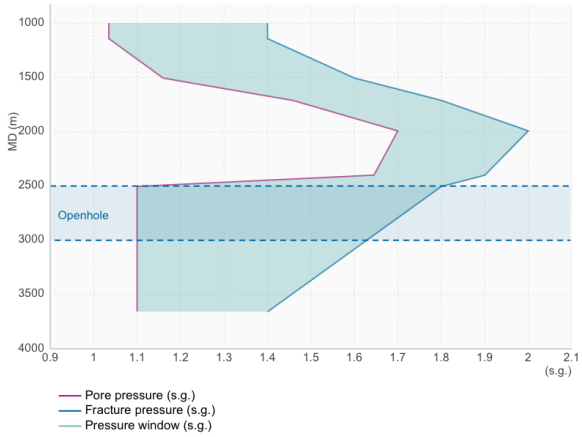

Figure 8.12: Geo-pressure window.

8.4 Results and Discussion

The friction test results are dependent on several different factors, some of those related to hydraulic drilling conditions. This section will present two different test cases, one with varying flow rates and one with varying fluid densities. Test results from the tests will be presented and analyzed to quantify how much impact the different hydraulic conditions have on the results.

8.4.1 Flow Rate Dependence

Flow rate is a drilling parameter in constant change due to different operational precautions and procedures, respectively maintaining the bottom-hole pressure at the desired level and pipe connections. A friction test should ideally be performed with equivalent flow rates. Due to operational limitations this might not be possible, therefore it is necessary to determine the impact of flow rate variations on the results.

User input

The flow rate dependence test is to perform several tests with varying flow rate set-points. User inputs for the test sequence are shown in Table 8.6, where the only variation between the tests are the flow rate in value.

Table 8.6: User inputs to friction test model with varying flow rates.

Parameter	Value	Unit
Initial bit depth	2996	m
Flow rate in	500-3000	lpm
Pick-up velocity	-0.15	m/s
Slack-off velocity	0.15	m/s
Surface RPM	150	rpm
Mud density	1200	kg/m^3

The flow rate set-points used in the test are: 500, 1000, 1500, 2000, 2500 and 3000 lpm. The model simulates one simulation for each flow rate value, this assures identical start conditions.

Results & discussion

The test result from two of the tests conducted are shown in Figure 8.13. Hook-load is plotted in the upper figure, whereas torque and current state in the lower.

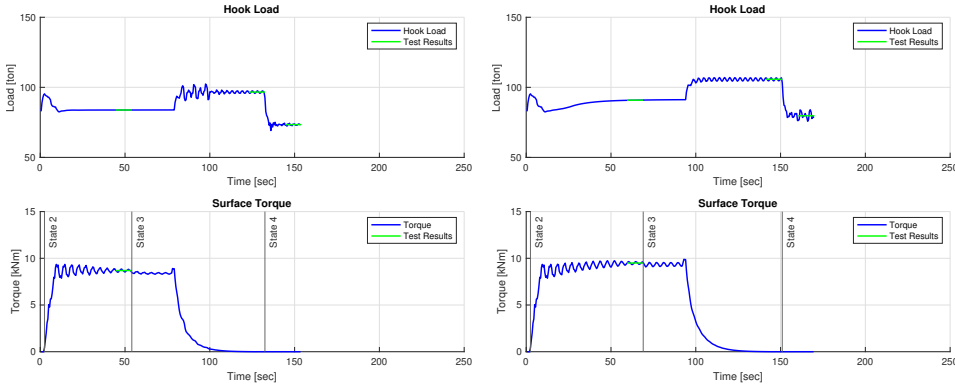

(a) Flow rate : 1000 lpm.

(b) Flow rate : 2500 lpm.

Figure 8.13: Friction test results with varying flow rates.

Table 8.7 summarizes the test results with the correlating flow rates. The test initiated with 500 lpm flow rate did not obtain hook-load stabilization to record a SOW value and therefore missing the SOW recording.

Table 8.7: Friction test results with varying flow rates.

Flow rate [lpm]	FRT [kNm]	FRW [ton]	PUW [ton]	SOW [ton]
500	8.58	82.76	95.39	-
1000	8.69	83.81	96.62	73.40
1500	8.86	85.37	98.66	75.19
2000	9.02	87.38	101.64	77.46
2500	9.49	90.83	105.78	79.70
3000	10.11	94.33	110.76	83.19

The results obtained from the test sequence showed that drillstring T&D increased with an increasing flow rate. This indicates that the downward force generated by the internal diameter continuously changing, within the drillstring, is greater than the upward force generated by annular fluid flow. The friction test has considerable variations in the recordings obtained depending on which flow rate used. Looking at the SOW results collected from the tests presented in Figure 8.13, the SOW difference is 6.3 tons respectively. 6.3 tons is equivalent to 216 meters of additional drillpipe in the vertical wellbore section, which is estimated using Equation 8.2. If these values were to be compared without being aware of flow rate changes, it would be reasonable to assume a change in wellbore friction and thus indicate downhole problems.

The flow rate dependence test shows that the rate has a considerable impact on the test results. In a drilling operation with friction tests performed for each stand, changing the flow rate in one of the tests should show a deviation from the trend which can be misinterpreted as a downhole problem.

8.4.2 Fluid Density Dependence

Drilling fluid density is an important drilling parameter as its main function is to provide hydrostatic pressure, to prevent formation fluids entering the wellbore. There might be small changes in mud density while drilling a section, therefore it is important to be familiar with the impact of fluid densities on the results.

User input

The fluid density test performs several friction tests with fluid densities ranging from 1.15 sg. to 1.35 sg. The fluid density range is chosen based on the configuration's geo-pressure gradients shown in Figure 8.12. Table 8.8 shows the user inputs used to execute the test.

Table 8.8: User inputs to friction test model with varying fluid densities.

Parameter	Value	Unit
Initial bit depth	2996	m
Flow rate in	2000	lpm
Pick-up velocity	-0.15	m/s
Slack-off velocity	0.15	m/s
Surface RPM	150	rpm
Mud density	1150-1350	kg/m^3

Results & discussion

Table 8.9 show the friction test results with varying fluid densities. The results indicates a slight decrease in T&D with increasing fluid density. The buoyancy effect is demonstrated in this test, respectively with increasing fluid densities, the buoyancy will decrease and thus decrease the buoyed T&D. Comparing the results shows that the change is considerable with changing the fluid densities. However, the tests utilizes extreme changes in density and where the density of the entire will is changed between simulations. In a real drilling situation, changing the fluid density does not happen instantaneously, as the previous mud needs to circulate out of the wellbore. However, such a significant change in fluid density is not common during a normal operation, rather the change ranges from 0.01 to 0.02 sg.

Table 8.9: Friction test results with varying fluid densities.

Fluid density[kg/m^3]	FRT [kNm]	FRW [ton]	PUW [ton]	SOW [ton]
1150	9.15	88.11	101.87	77.31
1200	9.02	87.38	101.64	77.46
1250	8.97	87.20	101.25	77.32
1300	8.92	87.02	101.14	77.17
1350	8.86	86.86	100.63	77.63

Figure 8.14 shows tests conducted with fluid densities 1150 kg/m^3 and 1350 kg/m^3 respectively. The biggest difference between the tests are with a density of 1150 kg/m^3 the model requires more time to stabilize the torque value, as oppose to a test with density of 1350 kg/m^3. This shows that the use of lighter drilling fluids affects the torque stabilization criteria, as the drillstring torque requires more time to stabilize, hence the total test time increases.

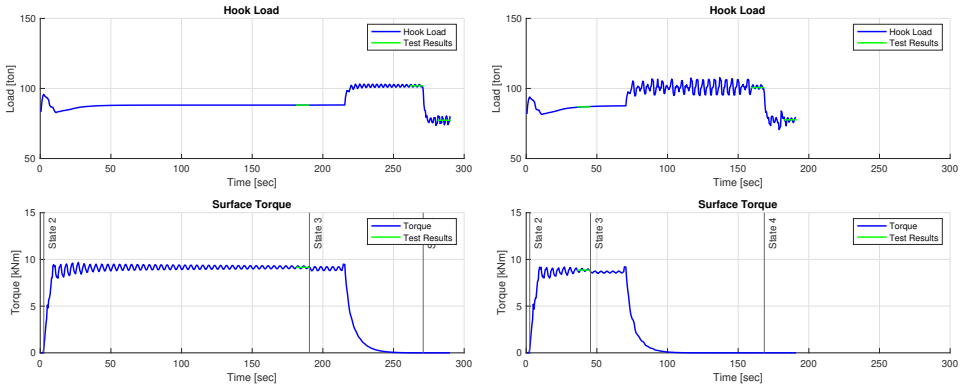

(a) Fluid density : 1150 kg/m^3.

(b) Fluid density : 1350 kg/m^3.

Figure 8.14: Friction test results with varying fluid densities.

Tests conducted show that the friction test results are not highly dependent on the fluid density defined. There are observed differences between the tests, but they are not significant enough to be relevant in a full-scale drilling operation. The biggest impact observed, of the defined densities, is the duration of the test, whereas heavier fluid will decrease test duration.

8.5 Friction Test Conclusion

The automated friction test created, is a test procedure used to detect any occurring downhole problems. Solutions available for recording measurements today are not, standalone or even combined, accurate enough for recording downhole frictions. The presented solution of an IIBOP to automatically measure drilling parameters at top of the drillstring is an important step to enable a fully automated friction test system.

The model presented in this chapter shows that it is feasible to advance the operation to a higher LOA; this model would be classified at L8. Referring to Table 4.1 this suggests that the monitoring and generating functions are split between a human- and computer control, whereas the selecting and implementing functions are controlled solely by the computer. The only human interaction in the test model is feeding the initial inputs and monitor while the test is executed.

Dependencies of hydraulic drilling parameters are investigated. Comparing successive friction tests it is essential to be aware of which flow rate correlates to which test, as the cases presented showed a high flow rate dependence. Observations made in the fluid density test are small affections on friction test results when varying fluid density, and therefore it is not relevant to keep it stable.

The friction test is an operation with great potential to be automated in the future, as it is a repetitive task performed at pre-defined intervals. Utilizing the model presented in this chapter, along with a T&D model describing the hydraulic dynamics should remove the issue with changing drilling parameters between the friction tests. This combined with the new IIBOP technology, allows for early detection of downhole problems which subsequently will decrease the NPT in the industry.

Chapter 9

Conclusion

Based on reviewing literature as well as further investigating three areas of a drilling operation, findings observed show great potential for further implementation of automation. Which standalone is not a revolutionary discovery, however, the research conducted presents specific examples of partial automation that can easily be implemented, which will release the crew of repetitive and monotonous tasks. The oil and gas industry is rather conservative when it comes to introducing new technology, as the consequences are extensive if the system fails to maintain the required level of health, safety and environment (HSE). It is essential for the operator responsible for the task to follow along in the development to hold enough knowledge about the system, in order to execute the appropriate corrective actions if needed. Furthermore, excessive testing of the technology is critical to increase system reliability.

As oil and gas resources are becoming less accessible, extended-reach wells utilizing directional drilling is discovered to be an efficient solution to hit the desired target(s). However, this will increase the operational cost, thus it is desired to optimize the operation, such as finding a smooth corrective well path. The minimum well-profile-energy criterion is used to determine this correction path, as opposed to common automated control algorithms such as proportional-integral-derivative (PID) and fuzzy controllers. The advantage with the minimum-energy-method is its ability to create smooth well paths, which usually increases borehole quality.

Subsequently, inducing a reduction in drillstring failure, improved hole cleaning, and faster drilling rates. In theory, it is possible to achieve an ideal smooth well path, but this is not viable in the real world as unforeseen factors will affect the actual drill path.

To further develop the trajectory controller, it is essential to implement models capable of adjusting the bit tilt angle and toolface, to take corrective action and initiate proper steering.

Kicks that turn into blowouts are enormous safety hazards. The Deepwater Horizon is a blowout in recent times showing the fatal consequences of not taking appropriate actions in conjunction with kicks. The main objective of diminishing such dreadful events is to improve overall HSE. This thesis aims to create an automated kick-detection model. The accuracy of detecting kicks is observed to be 87.5%, which implies that spotting a kick is not the main problem, but rather detecting small kicks, as well as not reporting false-positives and false-negatives. Through extensive testing these types of automation-systems can be fine-tuned, i.e. increasing the accuracy, making it more reliable.

The next step required to further develop an automated kick-detection system is to implement conditions for taking appropriate actions when a kick is detected. Hereunder, actions for closing the well, includes hoisting the drillstring, stop the pumps, and initiate closing of primary barriers.

Early detection of downhole problems is desired to decrease the NPT of drilling operations. A friction test has great automation potential, as it is a repetitive operational task manually performed, to detection changes in downhole conditions. The operation sequence of a friction test with LOA at L8, like the one presented in this thesis, in combination with newfound measurement technology, will improve the economic feasibility of a drilling operation. Other advantages with combining the two include earlier detection of downhole problems and improved accuracy in measurements recorded. With today's computational power, engineering while drilling calculations can be performed, which enables for real-time models avail-

able on site. Allowing for drilling parameters impacting field-tests to be removed, such as variations in flow rate.

By removing irrelevant drilling parameters from the automated friction model, the probability of early detecting downhole problems should increase. As a result, NPT decreases, which ultimately reduces the total well costs. This is therefore relevant for further developing the model.

For final conclusions, the three areas investigated show great potential to optimize the drilling operation, contribute to the economic feasibility and improve HSE. Due to the time constraints related to COVID-19 the authors did not have time to perform excessive testing of the automated models created. However, the results obtained were satisfying. If the industry wants to grow along with the modernization of society, the oil and gas industry needs to take a leap of faith and commit to the benefits automation offers.

References

[1] United Nations. *The Paris Agreement — UNFCCC*. June 9, 2020. URL: https://unfccc.int/process-and-meetings/the-paris-agreement/the-paris-agreement.

[2] Pourya Farmanbar et al. "Digitalization of Detailed Drilling Operation Plans and Verification of Automatic Progress Tracking with an Online Drilling Simulator Environment". In: *IADC/SPE International Drilling Conference and Exhibition*. Society of Petroleum Engineers. 2020.

[3] SPE International, ed. *SPE - Drilling Systems Automation Technical Section*. Apr. 24, 2020. URL: https://connect.spe.org/dsats/home.

[4] Society of Petroleum Engineers (SPE) and Drilling Systems Automation Technical Section (DSATS), eds. *Drillbotics™ Guidelines*. Feb. 18, 2020. URL: https://drillbotics.com/download/guidelines/2020-Drillbotics-Guidelines.pdf.

[5] V. R. Meyer et al. "Design Report NTNU - Drillbotics 2020 Phase I". Report. Department of Geoscience and Petroleum, 2019.

[6] Drillbotics©. *European Test and Coronavirus*. Mar. 12, 2020. URL: https://drillbotics.com/european-test-and-coronavirus/.

[7] Drillbotics©. *Drillbotics© 2019-2020 Cancelled*. Apr. 10, 2020. URL: https://drillbotics.com/drillbotics-2019-2020-cancelled/.

[8] Norsk olje & gass, ed. *Recommended practice for establishing and working in the red zone on the drill floor*. June 1, 2020. URL: https://www.norskoljeoggass.no/contentassets/103bce01eb4b445da85ff042df068c7b/recommended-practice-for-establishing-and-working-in-the-red-zone-on-the-drill-floor-final-260619.pdf.

[9] Fionn Iversen et al. "Drilling automation: potential for human error". In: *SPE Drilling & Completion* 28.01 (2013).

[10] Nancy Leveson et al. "Analyzing software specifications for mode confusion potential". In: *Proceedings of a workshop on human error and system development*. Glasgow Accident Analysis Group. 1997, pp. 132–146.

[11] Charles E Billings. "Human-centered aviation automation: Principles and guidelines". In: (1996).

[12] Nathan Moralez et al. "Intelligent Pipe-Handling: A Case Study for Automation". In: *IADC/SPE International Drilling Conference and Exhibition*. Society of Petroleum Engineers. 2020.

[13] Mica R Endsley and Esin O Kiris. "The out-of-the-loop performance problem and level of control in automation". In: *Human factors* 37.2 (1995), pp. 381–394.

[14] John Thorogood et al. "Drilling automation: technologies, terminology, and parallels with other industries". In: *SPE drilling & completion* 25.04 (2010), pp. 419–425.

[15] Thomas B Sheridan. *Humans and automation: System design and research issues.* Human Factors and Ergonomics Society, 2002.

[16] Mica R Endsley. "Level of automation effects on performance, situation awareness and workload in a dynamic control task". In: *Ergonomics* 42.3 (1999), pp. 462–492.

[17] Fred Florence et al. “Drilling Systems Automation: Current State, Initiatives and Potential Impact”. In: *SPE Annual Technical Conference and Exhibition*. 2013.

[18] Alfred William Eustes et al. “The evolution of automation in drilling”. In: *SPE Annual Technical Conference and Exhibition*. Society of Petroleum Engineers. 2007.

[19] Richard Buchanan Russell et al. “’Intelligent’Wired Drill-Pipe System Allows Operators to Take Full Advantage of Latest Downhole Sensor Developments”. In: *International Petroleum Technology Conference*. International Petroleum Technology Conference. 2008.

[20] O Sehsah et al. “Intelligent Drilling System: Expanding the Envelope of Wired Drill Pipe”. In: *Abu Dhabi International Petroleum Exhibition & Conference*. Society of Petroleum Engineers. 2017.

[21] Robert Foster, Robin Macmillan, et al. “High speed telemetry on wired drill pipe, history, and impact on drilling process”. In: *Offshore Technology Conference*. Offshore Technology Conference. 2018.

[22] Tony Pink et al. “World First Closed Loop Downhole Automation Combined with Process Automation System Provides Integrated Drilling Automation in the Permian Basin.” In: *SPE/IADC Drilling Conference and Exhibition*. Society of Petroleum Engineers. 2017.

[23] Bill Chmela et al. “Safer Tripping Through Drilling Automation”. In: *IADC/SPE Drilling Conference and Exhibition*. Society of Petroleum Engineers. 2014.

[24] Nejm Saadallah et al. “OpenLab: Design and Applications of a Modern Drilling Digitalization Infrastructure”. In: *SPE Norway One Day Seminar*. Society of Petroleum Engineers. 2019.

[25] Schlumberger. *Schlumberger Oilfield Glossary*. June 5, 2020. URL: `https://www.glossary.oilfield.slb.com`.

[26] NORCE. *OpenLab Drilling*. May 15, 2020. URL: `https://openlab.app`.

[27] Farah Omar Farah. “Directional well design, Trajectory and survey calculations, with a case study in Fiale, Asal rift, Djibouti”. In: *Ministry of Energy and Natural Resources* 27 (2013).

[28] B. Brechan et al. *Drilling, Completion, Intervention and P&A - design and operations*. Department of Geosciense and Petroleum, 2017.

[29] Bill Chmela et al. “Directional Drilling Automation: Human Factors and Automated Decision-Making”. In: *IADC/SPE International Drilling Conference and Exhibition*. Society of Petroleum Engineers. 2020.

[30] K.J. Årström and R.M. Murray Murray. *Analysis and Design of Feedback System*. Caltech, 2004.

[31] Control Engineering, ed. *Modern updates in PID control tuning*. May 6, 2020. URL: https://www.controleng.com/articles/modern-updates-in-pid-control-tuning/.

[32] J.G. Balchen, T. Andresen, and B.A Foss. *Reguleringsteknikk*. Department of Engineering Cybernetics, 2016.

[33] Michael S. Stoner. “A Fuzzy Logic Controller for Drilling Directionally”. PhD dissertation. Colorado School of Mines, Golden, Colorado, July 1997.

[34] Xue Qilong et al. “Simulation Study on Fuzzy Control of Rotary Steering Drilling Trajectory”. In: 2012.

[35] Zhengchun Liu, Robello Samuel, et al. “Wellbore-trajectory control by use of minimum well-profile-energy criterion for drilling automation”. In: *SPE Journal* 21.02 (2016), pp. 449–458.

[36] Jiang Wu et al. “Drill-pipe bending and fatigue in rotary drilling of horizontal wells”. In: *SPE Eastern Regional Meeting*. Society of Petroleum Engineers. 1996.

[37] J. J. Azar and G. Robello Samuel. *Drilling Engineering*. PennWell Books, 2007.

[38] O. Vaisberg et al. “Fatigue of Drillstring: State of the Art”. In: *Oil & Gas Science and Technology* 57.1 (Jan. 2002), pp. 7–37. DOI: 10.2516/ogst:2002002. URL: https://doi.org/10.2516%5C%2Fogst%5C%3A2002002.

[39] Robello Samuel et al. “A new well-path design using clothoid spiral (curvature bridging) for ultra-extended-reach drilling”. In: *SPE Drilling & Completion* 25.03 (2010), pp. 363–371.

[40] Robello Samuel and Xiushan Liu. “Wellbore Tortuosity, Torsion, Drilling Indices, and Energy: What do They have to do with Well Path Design?” In: *SPE Annual Technical Conference and Exhibition, New Orleans, LA, Oct*. 2009, pp. 4–7.

[41] Richard Russell et al. “Improving borehole quality and drilling efficiency with a new suite of drilling tools”. In: *Abu Dhabi International Petroleum Exhibition and Conference*. Society of Petroleum Engineers. 2002.

[42] Sintef, ed. *Blowout on Deep Water horizon*. May 10, 2020. URL: https://www.sintef.no/en/projects/deepwater-horizon-accident-causes-teachings-and-ac/.

[43] SM Willson, Anand S Nagoo, Mukul M Sharma, et al. “Analysis of potential bridging scenarios during blowout events”. In: *SPE/IADC Drilling Conference*. Society of Petroleum Engineers. 2013.

[44] B. Brechan, S. Hovda, and P. Skalle. *Compendium: Introduction to Drilling Engineering*. Department of Geosciense and Petroleum, 2017.

[45] Husam H Alkinani et al. “Examination of the relationship between rate of penetration and mud weight based on unconfined compressive strength of the rock”. In: *Journal of King Saud University-Science* 31.4 (2019), pp. 966–972.

[46] Juan Gustavo Vargas, Mateus Jefferson, Mario A Serrano, et al. “Beyond Mud-Weight Window: A Geomechanical Approach to Evaluating and Achieving Drilling Goals”. In: *SPE Latin American and Caribbean Petroleum Engineering Conference*. Society of Petroleum Engineers. 2010.

[47] Beyond Energy, ed. *Beyond Energy - Mud Window*. June 8, 2020. URL: https://www.beyondenergy.ca/mpd-101/.

[48] Robert D. Grace. "CHAPTER THREE - PRESSURE CONTROL PROCEDURES WHILE TRIPPING". In: *Blowout and Well Control Handbook*. Ed. by Robert D. Grace. Burlington: Gulf Professional Publishing, 2003, pp. 90–116. ISBN: 978-0-7506-7708-0. DOI: https://doi.org/10.1016/B978-075067708-0/50004-9. URL: http://www.sciencedirect.com/science/article/pii/B9780750677080500049.

[49] Dan Fraser et al. "Early kick detection methods and technologies". In: *SPE Annual Technical Conference and Exhibition*. Society of Petroleum Engineers. 2014.

[50] Uduak Mme and Pål Skalle. "Effects of mud properties, hole size, drill string tripping speed and configurations on swab and surge pressure magnitude during drilling operations". In: *Inter J Pet Sci Technol* 5 (2012), pp. 143–153.

[51] *IADC Drilling Manual*. Vol. 12. IADC. Chap. Drilling Practices, DP–5.

[52] Oltingey Lindi. "Analysis of Kick Detection Methods in the Light of Actual Blowout Disasters." MA thesis. NTNU, 2017.

[53] MR Hornung et al. "Kick prevention, detection, and control: Planning and training guidelines for drilling deep high-pressure gas wells". In: *SPE/IADC Drilling Conference*. Society of Petroleum Engineers. 1990.

[54] Drillingformulas. *Well ballooning*. June 8, 2020. URL: http://www.drillingformulas.com/well-ballooning-wellbore-breathing-or-micro-fracture/.

[55] Bernt S Aadnoy, Mohammad Fazaelizadeh, Geir Hareland, et al. "A 3D analytical model for wellbore friction". In: *Journal of Canadian Petroleum Technology* 49.10 (2010), pp. 25–36.

[56] Petrowiki. *Kicks*. May 10, 2020. URL: https://petrowiki.org/Kicks.

[57] Anders Willersrud et al. “Early detection and localization of downhole incidents in managed pressure drilling”. In: *SPE/IADC Managed Pressure Drilling and Underbalanced Operations Conference & Exhibition*. Society of Petroleum Engineers. 2015.

[58] Dan Fraser et al. “Early kick detection methods and technologies”. In: *SPE Annual Technical Conference and Exhibition*. Society of Petroleum Engineers. 2014.

[59] Mauricio Ibarra et al. “Automatic Kick Detection Method and Preliminary Results”. In: *SPE/IADC Managed Pressure Drilling and Underbalanced Operations Conference and Exhibition*. Society of Petroleum Engineers. 2016.

[60] Andreas K Fjetland et al. “Kick Detection and Influx Size Estimation during Offshore Drilling Operations using Deep Learning”. In: *2019 14th IEEE Conference on Industrial Electronics and Applications (ICIEA)*. IEEE. 2019, pp. 2321–2326.

[61] Anirbid Sircar. *Downhole Drilling Problems*. Oct. 2012. DOI: 10.13140/RG.2.2.24291.55846.

[62] CA Johancsik, DB Friesen, Rapier Dawson, et al. “Torque and drag in directional wells-prediction and measurement”. In: *Journal of Petroleum Technology* 36.06 (1984), pp. 987–992.

[63] Robert Wylie et al. “Instrumented Internal Blowout Preventer Improves Measurements for Drilling and Equipment Optimization”. In: *SPE/IADC Drilling Conference*. Society of Petroleum Engineers. 2013.

[64] Cayeux Eric, Hans Joakim Skadsem, Roald Kluge, et al. “Accuracy and correction of hook load measurements during drilling operations”. In: *SPE/IADC Drilling Conference and Exhibition*. Society of Petroleum Engineers. 2015.

[65] Fred Florence, Fionn Petter Iversen, et al. “Real-time models for drilling process automation: Equations and applications”. In: *IADC/SPE Drilling Conference and Exhibition*. Society of Petroleum Engineers. 2010.

[66] Edvin Kristensen. “Model of hook load during tripping operation”. MA thesis. Institutt for petroleumsteknologi og anvendt geofysikk, 2013.

[67] Eric Cayeux et al. “Challenges and solutions to the correct interpretation of drilling friction tests”. In: *SPE/IADC Drilling Conference and Exhibition*. Society of Petroleum Engineers. 2017.

[68] Mohammad Fazaelizadeh. “Real Time Torque and Drag Analysis during Directional Drilling”. In: (2013).

[69] Eric E Maidla, Andrew K Wojtanowicz, et al. “Laboratory study of borehole friction factor with a dynamic-filtration apparatus”. In: *SPE drilling engineering* 5.03 (1990), pp. 247–255.

[70] Bernt Sigve Aadnoy, Eirik Kaarstad, et al. “Theory and application of buoyancy in wells”. In: *IADC/SPE Asia Pacific Drilling Technology Conference and Exhibition*. Society of Petroleum Engineers. 2006.

[71] Khan Acadaemy. *Mean absolute deviation (MAD)*. May 19, 2020. URL: https://www.khanacademy.org/math/statistics-probability/summarizing-quantitative-data/other-measures-of-spread/a/mean-absolute-deviation-mad-review.

[72] NTNU. *Koronavirus (COVID-19): Retningslinjer og råd.* Apr. 26, 2020. URL: https://www.ntnu.no/korona.

[73] Fridtjov Irgens. *Fasthetslære*. 7th ed. Tapir Akademisk Forlag, 2006.

[74] Drilling Manual. *Bent Sub and Positive Displacement Motor*. May 13, 2020. URL: https://www.drillingmanual.com/2017/11/bent-sub-and-positive-displacement-motor.html.

[75] Tan Nguyen et al. “Modeling the design and performance of progressing cavity pump using 3-D vector approach”. In: *Journal of Petroleum Science and Engineering* 122 (2014), pp. 180–186.

[76] DNV GL. *Digitalization and the future of energy*. May 20, 2020. URL: https://www.dnvgl.com/power-renewables/themes/digitalization/index.html.

[77] Petrowiki. *Directional deviation tools*. June 1, 2020. URL: https://petrowiki.org/Directional_deviation_tools.

[78] Bjørn A. Brechan et al. *Drilling, Completion, Intervention and P&A –design and operations*. NTNU - Department of Petroleum Engineering and Applied Geophysics, 2016.

[79] Drilling Formulas. *Drillers Method*. June 1, 2020. URL: http://www.drillingformulas.com/drillers-method-in-well-control/.

[80] Robert J White et al. "Bottom-Hole Pressure Reduction Due to Gas Cut Mud". In: *Journal of Petroleum Technology* 9.07 (1957), pp. 49–50.

[81] Drillbotics. *Microbits by Baker Hughes*. Apr. 3, 2020. URL: https://drillbotics.com/2020-drillbotics-microbits-from-baker-hughes/.

[82] Knut S Bjørkevoll et al. "Enhanced Well Control Potential with Along-String Measurements". In: *SPE Norway One Day Seminar*. Society of Petroleum Engineers. 2018.

[83] Junho Park et al. "Improved bottomhole pressure control with wired drillpipe and physics-based models". In: *SPE/IADC Drilling Conference and Exhibition*. Society of Petroleum Engineers. 2017.

[84] H. E. Helle, M. U. Azam, and J. M. Montoza. "Design and Implementation of an Autonomous Miniature Drilling Rig for Directional Drilling". Thesis. Department of Geoscience and Petroleum, 2019.

[85] Formlabs. *3D Printing Materials for Engineering, Manufacturing, and Product Design*. June 3, 2020. URL: https://formlabs.com/materials/engineering/.

[86] Formlabs. *Material data sheet : Grey Pro*. June 3, 2020. URL: https://formlabs-media.formlabs.com/datasheets/Grey_Pro_Technical.pdf.

[87] Formlabs. *Material data sheet : Durable*. June 3, 2020. URL: https://formlabs-media.formlabs.com/datasheets/1801084-TDS-ENUS-0P.pdf.

[88] Formlabs. *Material data sheet : Flexible*. June 3, 2020. URL: https://formlabs-media.formlabs.com/datasheets/Flexible_Technical.pdf.

[89] Formlabs. *Post-Curing with Form Cure*. June 3, 2020. URL: https://s3.amazonaws.com/servicecloudassets.formlabs.com/media/Finishing/Post-Curing/115001414464-Form%5C%20Cure%5C%20Time%5C%20and%5C%20Temperature%5C%20Settings/FormCurePost-CureSettings.pdf.

[90] Micon Downhole Tools, ed. *Positive Displacement Motors (PDM)*. May 7, 2020. URL: https://micon-drilling.de/Download/Catalog_PDM_EN.pdf.

[91] Petrowiki, ed. *Influx Gradient Guidelines*. May 19, 2020. URL: https://petrowiki.org/File:Devol2_1102final_Page_199_Image_0002.png.

[92] Researchgate, ed. *Influx Gradient Guidelines*. May 28, 2020. URL: https://www.researchgate.net/figure/Schematic-of-the-Shallow-Gas-Kick-Analyzed-in-Scenario-3_fig7_267461529.

Appendices

Appendix A

Derivations

A.1 Minimum-Curvature Method

Two equations can be derived for the correction path, defined with constant build- and drop-rates, and geometric relations:

$$\kappa_{\alpha n-1}\Delta D_{n-1} + \kappa_{\alpha n}\Delta D_n = \alpha_n - \alpha_{n-2} \tag{A.1}$$

$$\kappa_{\phi n-1}\Delta D_{n-1} + \kappa_{\phi n}\Delta D_n = \phi_n - \phi_{n-2} \tag{A.2}$$

The simple balanced tangential method is applied, which is the basis for three equations estimating the wellbore trajectory coordinates:

$$\begin{aligned}\Delta X = \frac{\Delta D_{n-1}}{2}(sin\alpha_{n-2}\, cos\phi_{n-2} + sin\alpha_{n-1}\, cos\phi_{n-1}) \\ + \frac{\Delta D_n}{2}(sin\alpha_{n-1}\, cos\phi_{n-1} + sin\alpha_n\, cos\phi_n)\end{aligned} \tag{A.3}$$

$$\begin{aligned}\Delta Y = \frac{\Delta D_{n-1}}{2}(sin\alpha_{n-2}\, sin\phi_{n-2} + sin\alpha_{n-1}\, sin\phi_{n-1}) \\ + \frac{\Delta D_n}{2}(sin\alpha_{n-1}\, sin\phi_{n-1} + sin\alpha_n\, sin\phi_n)\end{aligned} \tag{A.4}$$

$$\Delta Z = \frac{\Delta D_{n-1}}{2}(cos\alpha_{n-2} + cos\alpha_{n-1}) + \frac{\Delta D_n}{2}(cos\alpha_{n-1} + cos\alpha_n) \quad (A.5)$$

Where $\alpha_{n-1} = \alpha_n - \kappa_{\alpha n}\Delta D_n$.

A.2 Maximum Bending Stress

There are three different cases of pipe bending, or an increase of compressing load, in a build section shown in Figure A.1. Wu [36] presented equations to analyze the drillpipe bending in horizontal wells, his derivations and resulting equations are rendered in this section.

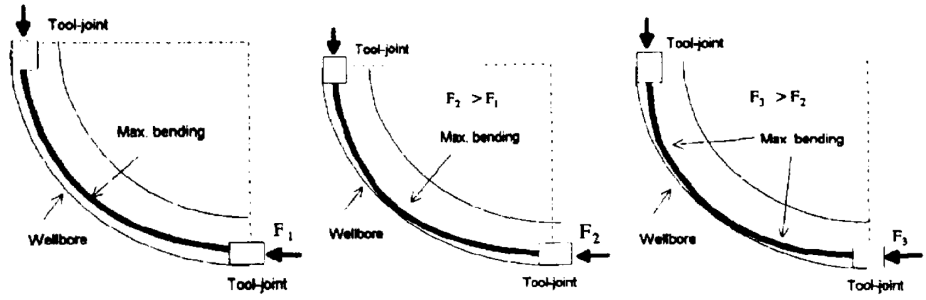

(a) No contact **(b)** Point contact **(c)** Arc contact

Figure A.1: Drillpipe bending cases as axial compression increases [36].

The differential equation for drillpipe bending in the build section of a wellbore under axial compression, illustrated in Figure A.2 is:

$$\frac{d^2y}{dx^2} + k^2y = C_o + \frac{S_o}{EI}x - \frac{w_e sin(\theta)}{2EI}x^2 \quad (A.6)$$

Where $C_o[rad/in]$ is the tool-joints bending curvature, $S_o[lbf]$ is the shear load at tool-joints, $E[psi]$ is Young's modulus, $I[in^4]$ is the moment of inertia, $w_e[lb/in]$ is the drillpipe effective weight. k is expressed as:

$$k^2 = \frac{F}{EI} \quad (A.7)$$

Where $F[lbf]$ is the axial compression load.

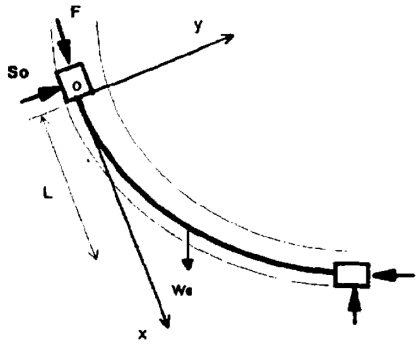

Figure A.2: Drillpipe bending model under axial compression [36].

The drillstring tool-joints are stiffer than the drillpipes and follow the wellbore trajectory, this gives the following boundary condition for drillpipe bending:

$$y|_{x=0} = 0 \tag{A.8}$$

$$\frac{dy}{dx}|_{x=0} = 0 \tag{A.9}$$

The general solution of the differential equation in Equation A.6 is:

$$y = \frac{1}{k^2}[C_c(1 - cos(kx)) + s_o(kx - sin(kx)) - \frac{q}{2}(kx)^2] \tag{A.10}$$

Where C_c, q and s_o are unknown parameters heavily affected by drillpipe wall contact, given as:

$$C_c = C_o + q \tag{A.11}$$

$$q = \frac{w_e sin(\theta)}{k^2 EI} \tag{A.12}$$

$$s_o = \frac{S_o}{kEI} \tag{A.13}$$

A.2.1 No contact

The no contact case exists under small axial load conditions. This case has two conditions kept constant and are based on the drillpipe symmetry:

$$\frac{dy}{dx}|_{x=L} = LC \tag{A.14}$$

$$\frac{d^3y}{dx^3}|_{x=L} = 0 \tag{A.15}$$

For this case are C_c and s_o are expressed as:

$$C_c = (C+q)\frac{kL}{tan(kL)} \tag{A.16}$$

$$s_o = C_c tan(kL) \tag{A.17}$$

The drillpipe bending curvature distribution is given as:

$$\frac{d^2y}{dx^2} = (C+q)\frac{kLcos(kL-kc)}{sin(kL)} - q \tag{A.18}$$

For this case is the maximum drillpipe bending stress located at the middle of the drillpipe length ($x = L$) and given as:

$$\sigma_b = \frac{ED}{2}[(C+q)\frac{kL}{sin(kL)} - q] \tag{A.19}$$

Where D is the drillpipe outer diameter.

A.2.2 Point contact

With increasing axial compression will the drillpipe be in contact with the wall, also called point contact as shown in Figure A.1b. The following two continuous conditions are, where the denotion j is for tool-joints and p for drillpipes:

$$y|_{x=L} = \frac{L^2C}{2} - \frac{1}{2}(D_j - D_p) \tag{A.20}$$

$$\frac{dy}{dx}|_{x=L} = LC \tag{A.21}$$

The parameters of C_c and s_o is solved as:

$$C_c = \frac{(C+q)kL - s_o(1-cos(kL))}{sin(kL)} \tag{A.22}$$

$$s_o = \frac{\frac{k^2}{2}[L^2C - (D_j - D_p)]sin(kL) - kLC[1-cos(kL)]}{kLsin(kL) - 2(1-cos(kL))} + \frac{qkL}{2} \tag{A.23}$$

The drillpipe bending curvature distribution is:

$$\frac{d^2y}{dx^2} = C_c cos(kx) + s_o sin(kx) - q \tag{A.24}$$

The location of maximum drillpipe bending stress at $x = L_m$ is:

$$L_m = \frac{1}{k} tan^{-1}(\frac{s_o}{C_c}) \tag{A.25}$$

The corresponding maximum drillpipe bending stress is thus:

$$\sigma_b = \frac{ED}{2}[C_c cos(kL_m) + s_o sin(kL_m) - q] \tag{A.26}$$

A.2.3 Arc contact

For the arc contact case, illustrated in Figure A.1c, there are three conditions kept constant:

$$y|_{x=L_c} = \frac{L_c^2 C}{2} - \frac{1}{2}(D_j D_p) \tag{A.27}$$

$$\frac{dy}{dx}|_{x=L_c} = L_c C \tag{A.28}$$

$$\frac{d^2y}{dx^2}|_{L \geq x \geq L_e} = C \tag{A.29}$$

Where L_c is the length of the arc in contact. A trial and error approach is used to determine L_c by the following:

$$C = C_c cos(kL_c) + s_o sin(kL_c) - q \tag{A.30}$$

and has to be satisfied while solving the following:

$$C_c = \frac{(C+q)kL_c - s_o(1-cos(kL_c))}{sin(kL_c)} \tag{A.31}$$

$$s_o = \frac{\frac{k^2}{2}[L_c^2 C - (D_j - D_p)]sin(kL_c) - kL_c C[1-cos(kL_c)]}{kL_c sin(kL_c) - 2(1-cos(kL_c))} + \frac{qkL_c}{2} \tag{A.32}$$

The drillpipe bending curvature distribution is:

$$\frac{d^2y}{dx^2} = C_c cos(kx) + s_o sin(kx) - q \qquad (L_c \geq x \geq 0) \tag{A.33}$$

$$\frac{d^2y}{dx^2} = C \qquad (L \geq x \geq L_c) \tag{A.34}$$

The location of maximum bending stress is located in the ”uncontact” portion of the drillpipe:

$$L_m = \frac{1}{k} tan^{-1}(\frac{s_o}{C_c}) \tag{A.35}$$

The corresponding maximum drillpipe bending stress, at L_m, is then:

$$\sigma_b = \frac{ED}{2}[C_c cos(kL_m) + s_o sin(kL_m) - q] \tag{A.36}$$

Appendix B

MATLAB Scripts

B.1 Automated Trajectory Controller

```
% TRAJECTORY CONTROLLER
clear variables;
clc;
close all;

%% Parameters
SurveyRecordings();

for i = 1:length(x_Act)
    err = sqrt((x_Act(i)-x_Ref(i))^2 + (y_Act(i)-y_Ref
        (i))^2 + (tvd_Act(i)-tvd_Ref(i))^2);
    errX = abs(x_Act(i) - x_Ref(i));
    errY = abs(y_Act(i) - y_Ref(i));
    errZ = abs(tvd_Act(i) - tvd_Ref(i));

   if err > 3
       A = [x_Act(i), y_Act(i), tvd_Act(i)];
       R = [x_Ref(i+7), y_Ref(i+7), tvd_Ref(i+7)];
       break
```

```
19      end
20  end
21
22  posA = find(x_Act == A(1));
23  aziA = azi_Act(posA);
24  incA = inc_Act(posA);
25  dlsA = dls_Act(posA);
26  mdA = md_Act(posA);
27
28  posR = find(x_Ref == R(1));
29  aziR = azi_Ref(posR);
30  incR = inc_Ref(posR);
31  dlsR = dls_Ref(posR);
32  mdR = md_Ref(posR);
33
34  n = 10000;
35
36  dAR = sqrt((A(1)-R(1))^2 + (A(2)-R(2))^2 + (A(3)-R(3))
        ^2);
37  dCR_min =  dAR - 30;
38  dCR_max = dAR + 30;
39  dCR = linspace(dCR_min, dCR_max, n);
40
41  %% Wellpath plots
42  WellpathPlots();
43
44  %% Calculations
45  dX = abs(A(1)-R(1));
46  dY = abs(A(2) - R(2));
47  dTVD = abs(A(3) - R(3));
48  cos_B = cosd(incA) * cosd(incR) + sind(incA) * sind(
        incR) * cosd(aziA - aziR);
49
```

```
%% Find CR
Res = zeros(12,n);
dCR_adj = [];
j = 0;
for i = 1:n
    % M = [dE, AC, incC, aziC, k_incAC, k_incCR,
        k_aziAC, k_aziCR, k_AC, k_CR, t_AC, t_CR];]
      [M] = Equations(dCR(i), cos_B, incA, incR, aziA,
          aziR, dX, dY, dTVD);
      Res(:,i) = M;
      if isreal(M)
          j = j + 1;
          Res(:,j) = M;
          dCR_adj(i) = dCR(i);
    end
end

dE = Res(1,:);
dE_adj = [];
j = 0;
for i = 1:length(dE)
    if dE(i) > 0
        j = j + 1;
        dE_adj(j) = dE(i);
  end
end

k = find(dE == min(dE_adj));
dCR = dCR_adj(k);

%% Estimating unknown variables
TC_res = Equations(dCR, cos_B, incA, incR, aziA, aziR,
    dX, dY, dTVD);
```

```
dE = TC_res(1);
dAC = TC_res(2);
incC = TC_res(3);
aziC = TC_res(4);
k_incAC = TC_res(5);
k_incCR = TC_res(6);
k_aziAC = TC_res(7);
k_aziCR = TC_res(8);
k_AC = TC_res(9);
k_CR = TC_res(10);
t_AC = TC_res(11);
t_CR = TC_res(12);

%% Plot position C
xC = A(1) + dAC/2 * (sind(incA)*cosd(aziA) + sind(incC
    )*cosd(aziC));
yC = A(2) + dAC/2 * (sind(incA)*sind(aziA) + sind(incC
    )*sind(aziC));
zC = A(3) + dAC/2 *(cosd(incA) + cosd(incC));
C = [xC, yC, zC];

PlotPosC();
```

```
% SURVEY RECORDINGS

%% Parameters from Excel Sheet, collected from OpenLab

md_Ref = xlsread('PathData.xlsx', 'RefPath', 'B3:B192'
    ).';
x_Ref = xlsread('PathData.xlsx', 'RefPath', 'G3:G192')
    .';
y_Ref = xlsread('PathData.xlsx', 'RefPath', 'H3:H192')
    .';
```

```
inc_Ref = xlsread('PathData.xlsx', 'RefPath', 'C3:C192').';
azi_Ref = xlsread('PathData.xlsx', 'RefPath', 'D3:D192').';
tvd_Ref = xlsread('PathData.xlsx', 'RefPath', 'E3:E192').';
dls_Ref = xlsread('PathData.xlsx', 'RefPath', 'F3:F192').';

md_Act = xlsread('PathData.xlsx', 'ActualPath', 'B3:B192').';
x_Act = xlsread('PathData.xlsx', 'ActualPath', 'G3:G192').';
y_Act = xlsread('PathData.xlsx', 'ActualPath', 'H3:H192').';
inc_Act = xlsread('PathData.xlsx', 'ActualPath', 'C3:C192').';
azi_Act = xlsread('PathData.xlsx', 'ActualPath', 'D3:D192').';
tvd_Act = xlsread('PathData.xlsx', 'ActualPath', 'E3:E192').';
dls_Act = xlsread('PathData.xlsx', 'ActualPath', 'F3:F192').';
```

```
% EQUATIONS

function [M] = Equations(dCR, cos_B, incA, incR, aziA, aziR, dX, dY, dTVD)
dAC = ((dX^2 + dY^2 + dTVD^2) - dCR * (dTVD*cosd(incR) + dX*sind(incR)*cosd(aziR) + dY*sind(incR)*sind(aziR))) / (dCR*(1-cos_B)/2 + (dTVD*cosd(incA) + dX*sind(incA)*cosd(aziA) + dY*sind(incA)*sind(aziA)));

```

```
6  incC = acosd((2*dTVD - dAC*cosd(incA) - dCR*cosd(incR)
       )/(dAC+dCR));
7  aziC = atand((2*dY - dAC*sind(incA)*sind(aziA) - dCR*
       sind(incR)*sind(aziR))/(2*dX - dAC * sind(incA)*
       cosd(aziA) - dCR*sind(incR)*cosd(aziR)));
8
9  k_incAC = (incC - incA)/dAC;
10 k_incCR = (incR - incC)/dCR;
11
12 k_aziAC = (aziC - aziA)/dAC;
13 k_aziCR = (aziR - aziC)/dCR;
14
15 k_incAC_dot = -(incC-incA)/(dAC^2);
16 k_incCR_dot = -(incR-incC)/(dCR^2);
17
18 k_aziAC_dot = -(aziC-aziA)/(dAC^2);
19 k_aziCR_dot = -(aziR-aziC)/(dCR^2);
20
21
22 k_AC = sqrt(k_incAC^2 + k_aziAC^2*sind(incC)^2);
23 k_CR = sqrt(k_incCR^2 + k_incCR^2 * sind(incR)^2);
24
25 t_AC = ((k_incAC*k_aziAC_dot - k_aziAC*k_incAC_dot)/(
       k_AC^2))*sind(incC) + k_aziAC*(1 + (k_incAC^2)/(
       k_AC^2))*cosd(incC);
26 t_CR = ((k_incCR*k_aziCR_dot - k_aziCR*k_incCR_dot)/(
       k_CR^2))*sind(incR) + k_aziCR*(1 + (k_incCR^2)/(
       k_CR^2))*cosd(incR);
27
28 dE = (k_AC^2 + t_AC^2)*dAC + (k_CR^2 + t_CR^2)*dCR;
29
30 M = [dE, dAC, incC, aziC, k_incAC, k_incCR, k_aziAC,
       k_aziCR, k_AC, k_CR, t_AC, t_CR];
```

```
31 end
```

```
1  % WELLPATH PLOTS
2  %% 3D plot of reference and actual drill path in x/y/z
       directions
3  figure(1)
4  plot3(x_Act(1:posA), y_Act(1:posA), tvd_Act(1:posA), '
       r', x_Ref(1:posR), y_Ref(1:posR), tvd_Ref(1:posR),
       'k', x_Ref(posR:end), y_Ref(posR:end), tvd_Ref(posR
       :end), 'k—',A(1), A(2), A(3), 'k.', R(1), R(2), R
       (3), 'k.')
5  set(gca, 'Zdir', 'reverse');
6  xlabel('x [m]')
7  ylabel('y [m]')
8  zlabel('TVD [m]')
9  legend('Actual Path', 'Reference Path', 'Continuation
       of Reference Path')
10 title('3D plot of reference and actual drill path in x
       /y/z directions')
11 grid on
12 axis([-1200 1200 -1200 1200 0 2500]);
13
14 %% Zoomed: 3D plot of reference and actual drill path
       in x/y/z directions
15 figure(2)
16 plot3(x_Act(1:posA), y_Act(1:posA), tvd_Act(1:posA), '
       r', x_Ref(1:posR), y_Ref(1:posR), tvd_Ref(1:posR),
       'k', x_Ref(posR:end), y_Ref(posR:end), tvd_Ref(posR
       :end), 'k—',A(1), A(2), A(3), 'k.', R(1), R(2), R
       (3), 'k.')
17 set(gca, 'Zdir', 'reverse');
18 xlabel('x [m]')
19 ylabel('y [m]')
```

```
zlabel('TVD [m]')
text(A(1) + 0.7, A(2) + 0.7, A(3) + 0.4, 'A');
text(R(1) + 0.7, R(2) + 0.7, R(3) + 0.4, 'R');
legend('Actual Path', 'Reference Path', 'Continuation
    of Reference Path')
title('3D plot of reference and actual drill path in x
    /y/z directions')
grid on
axis([0 50 -2 100 700 900]);

%% 2D plot of reference and actual drill path in x/y
    directions
figure(3)
plot(x_Act(1:posA), y_Act(1:posA), 'r', x_Ref(1:posR),
     y_Ref(1:posR), 'k', x_Ref(posR:posR+5), y_Ref(posR
    :posR+5), 'k--', A(1), A(2), 'k.', R(1), R(2), 'k.'
    )
xlabel('x [m]')
ylabel('y [m]')
text(A(1) - 0.8, A(2) + 0.2, 'A');
text(R(1) - 0.8, R(2) + 0.2, 'R');
legend('Actual Path','Refernce Path', 'Continuation of
     Reference Path')
title('2D plot of reference and actual drill path in x
    /y directions')
grid on

%% Zoomed: 3D plot of reference and actual drill path
    in x/y/z directions with deviation error
figure(4)
plot3(x_Act(1:posA), y_Act(1:posA), tvd_Act(1:posA), '
    r', x_Ref(1:posR), y_Ref(1:posR), tvd_Ref(1:posR),
    'k', x_Ref(posR:end), y_Ref(posR:end), tvd_Ref(posR
```

```
    :end), 'k--',A(1), A(2), A(3), 'k.', R(1), R(2), R
    (3), 'k.',x_Ref(posA), y_Ref(posA), tvd_Ref(posA),
    'k.', [A(1) x_Ref(posA)], [A(2) y_Ref(posA)], [A(3)
     tvd_Ref(posA)],'k')
set(gca, 'Zdir', 'reverse');
xlabel('x [m]')
ylabel('y [m]')
zlabel('TVD [m]')
text(A(1) + 0.7, A(2) + 0.7, A(3) + 0.4, 'A');
text(R(1) + 0.7, R(2) + 0.7, R(3) + 0.4, 'R');
legend('Actual Path', 'Reference Path', 'Continuation
    of Reference Path')
title('3D plot of reference and actual drill path in x
    /y/z directions')
grid on
axis([0 50 -2 100 700 900]);
```

```
% PlotPosC

figure(5)
plot3(x_Act(1:posA), y_Act(1:posA), tvd_Act(1:posA), '
    r', x_Ref(1:posR), y_Ref(1:posR), tvd_Ref(1:posR),
    'k', x_Ref(posR:end), y_Ref(posR:end), tvd_Ref(posR
    :end), 'k--',A(1), A(2), A(3), 'k.', R(1), R(2), R
    (3), 'k.', xC, yC, zC, 'b.')
set(gca, 'Zdir', 'reverse');
xlabel('x [m]')
ylabel('y [m]')
zlabel('TVD [m]')
text(A(1) + 0.7, A(2) + 0.7, A(3) + 0.4, 'A');
text(R(1) + 0.7, R(2) + 0.7, R(3) + 0.4, 'R');
text(C(1) + 0.7, C(2) + 0.7, C(3) + 0.4, 'C', 'Color',
     'blue');
```

```
12 legend('Actual Path', 'Reference Path', 'Continuation
       of Reference Path')
13 grid on
14 axis([0 35 -2 40 700 890]);
15
16 figure(6)
17 plot(x_Act(1:posA), tvd_Act(1:posA), 'r', x_Ref(1:posR
       ), tvd_Ref(1:posR), 'k', x_Ref(posR:end), y_Ref(
       posR:end), 'k--', A(1), A(3), 'k.', R(1), R(3), 'k.
       ', xC, zC, 'b.');
18 set(gca, 'Ydir', 'reverse');
19 xlabel('x[m]')
20 ylabel('TVD[m]')
21 text(A(1) + 0.4, A(3), 'A');
22 text(R(1) + 0.4, R(3), 'R');
23 text(C(1) + 0.4, C(3), 'C', 'Color', 'blue');
24 grid on
25 axis([0 35 700 890]);
26
27 figure(7)
28 plot(x_Act(1:posA), y_Act(1:posA), 'r', x_Ref(1:posR),
        y_Ref(1:posR), 'k', x_Ref(posR:posR+5), y_Ref(posR
       :posR+5), 'k--', A(1), A(2), 'k.', R(1), R(2), 'k.'
       , xC, yC, 'b.');
29 xlabel('x[m]')
30 ylabel('y[m]')
31 text(A(1) - 0.8, A(2) + 0.2, 'A');
32 text(R(1) - 0.8, R(2) + 0.2, 'R');
33 text(C(1) - 0.8, C(2) + 0.2, 'C', 'Color', 'blue');
34 grid on
```

B.2 Automated Kick-Detection

```
clear variables;
clc;
close all;
%% Initial setpoints
FlowRateIn = 0;   % [m3/sec]
TopOfStringVelocity = 0;  % [m/sec]
ROP = 0;  % [m/sec]
SurfaceRPM = 0;  % [revolutions per sec.]
InitialBitDepth = 2500; % [m]
%% Config
addpath(genpath(pwd));
IdentityServerURL = 'https://live.openlab.app/';
[username, api_key, license_guid] = GetLoginData();
% Influx/loss configuration
UseReservoirModel = true; % false: no influx and loss, true: influx and loss
ManualReservoirMode = true; % true: manual influx/loss, false: influx based on geo-thermal (only if UseReservoirModel is true)
ManualInfluxLossMassRate = 10; % [kg/s] (positive for influx, negative for loss)
ManualInfluxLossTotalMass = 150; % [kg]
ManualInfluxLossMD = InitialBitDepth; %2500; % [m]
ComplexReservoirKickOffTime = 40;
UseTransientMechanicalModel = false;
StepDuration = .25;

% Create simulation object
ConfigurationName = 'ASMconfig';
SimulationName = join(['Influxtest',num2str(ManualInfluxLossTotalMass)]);
diary(join(['Simulations/',SimulationName]))
```

```
28 Sim = OpenLabClient(IdentityServerURL, username,
       api_key, license_guid, ...
29         ConfigurationName, SimulationName, InitialBitDepth
               , UseReservoirModel, ...
30         ManualReservoirMode, ManualInfluxLossMassRate,
               ManualInfluxLossTotalMass, ...
31         ManualInfluxLossMD, ComplexReservoirKickOffTime,
               UseTransientMechanicalModel, StepDuration);
32
33 % Time steps to simulate
34 MaxTimeSteps = 480;
35 ASM = zeros(1,20);
36 SPP = zeros(1,20);
37 Flow = zeros(1,20);
38 timeStepAccuracy = 20;
39 i = 0;
40 Test = 0;
41 %% Create animations
42 PressureFigure = figure('name', 'Pressure');
43 subplot(2,1,1);
44 xlabel('Time [sec]');
45 ylabel('Pressure [bar]');
46 title('Pressure');
47 axis([0 MaxTimeSteps*StepDuration 0 500])
48 grid
49 ASMLine= animatedline('Color','b','linewidth',1.5,'
       Marker','none');
50 DischargeLine = animatedline(0,0,'Color','m','
       linewidth',1.5,'Marker','none');
51 GreenLineP = animatedline('Color','g','linewidth',1,'
       Marker','*','HandleVisibility','off','LineStyle','
       none');
```

```
52 OrangeLineP= animatedline('Color',[0.91 0.41 0.17],'
       linewidth',2,'Marker','*','HandleVisibility','off',
       'LineStyle','none');
53 BlackLineP= animatedline('Color','k','linewidth',2,'
       Marker','*','HandleVisibility','off','LineStyle','
       none');
54 RedLineP= animatedline('Color','r','linewidth',2,'
       Marker','*','HandleVisibility','off','LineStyle','
       none');
55 legend({'Annulus Pressure' 'SPP'})
56
57 subplot(2,1,2);
58 xlabel('Time [sec]');
59 ylabel('Flow rate [L/min]');
60 title('Flow Rate');
61 axis([0 MaxTimeSteps*StepDuration 0 5000])
62 grid
63 FlowRateOutLine = animatedline(0,0,'Color','m','
       linewidth',1.5,'Marker','none');
64 FlowRateInLine = animatedline(0,0,'Color','b','
       linewidth',1.5,'Marker','none');
65 GreenLine = animatedline('Color','g','linewidth',3,'
       Marker','*','HandleVisibility','off','LineStyle','
       none');
66 OrangeLine= animatedline('Color',[0.91 0.41 0.17],'
       linewidth',3,'Marker','*','HandleVisibility','off',
       'LineStyle','none');
67 BlackLine= animatedline('Color','k','linewidth',3,'
       Marker','*','HandleVisibility','off','LineStyle','
       none');
68 RedLine= animatedline('Color','r','linewidth',3,'
       Marker','*','HandleVisibility','off','LineStyle','
       none');
```

```
legend({'Flow rate out' 'Flow rate in'})
%% Simulation
if Sim.IsOK
    try
        for timeStep = 1 : MaxTimeSteps
            tStartStep = tic;

            % Set setpoints to the simulator
            if timeStep < 60
                FlowRateIn = 2200/60000;
                TopOfStringVelocity = 0.1;  % [m/sec]
                SurfaceRPM = 120/60;  % [revolutions
                    per sec.]
            else
                TopOfStringVelocity = 0.0;  % [m/sec]
                ROP = 20/3600;  % [m/sec]
            end
            Sim.FlowRateIn = FlowRateIn;
            Sim.TopOfStringVelocity =
                TopOfStringVelocity;
            Sim.ROP = ROP;
            Sim.SurfaceRPM = SurfaceRPM;
            % Step simulator
            Sim.Step();
            if ~Sim.IsOK % Simulator fails
                break;
            end
            i = i + 1;
            SPP(i) = Sim.SPP;
            Flow(i) = Sim.FlowRateOut;
            if i == 1
                ASM(i) = 30; % [m3]
            else
```

```
100                 ASM(i) = ASM(i-1) - (Sim.FlowRateIn -
                        Sim.FlowRateOut)*StepDuration;
101             end
102             if i > timeStepAccuracy
103                 SPP(1) = [];
104                 ASM(1) = [];
105                 Flow(1) = [];
106                 i = i - 1;
107             end
108             %% Cases
109             if FlowRateIn == Sim.FlowRateInActual
110             switch Test
111                 case 1 % Med = ORANGE
112                     if (Flow(i)-Flow(i-1))/Flow(i-1)
                            >= 0.009 && (SPP(i)-SPP(i-1))/
                            SPP(i-1) >= 0.00065 && (ASM(i)-
                            ASM(i-1))/ASM(i-1) > 0.000 %(
                            SPP(i)-SPP(i-1))/SPP(i-1) >=
                            0.00065 &&
113                         Test=2 ; % 2 = BLACK
114                         addpoints(BlackLine,timeStep*
                                StepDuration,1500) ;
115                         addpoints(BlackLineP,timeStep*
                                StepDuration,150) ;
116                     elseif (Flow(i)-Flow(i-1))/Flow(i
                            -1) < 0
117                         Test=0 ;
118                         addpoints(GreenLine,timeStep*
                                StepDuration,500) ;
119                         addpoints(GreenLineP,timeStep*
                                StepDuration,50) ;
120                     else
```

```
121                     addpoints(OrangeLine,timeStep*
                            StepDuration,1000);
122                     addpoints(OrangeLineP,timeStep
                            *StepDuration,100);
123                 end
124             case 2 % HIGH = BLACK
125                 if (Flow(i)-Flow(i-1))/Flow(i-1)
                        >= 0.009 && (SPP(i)-SPP(i-1))/
                        SPP(i-1) > 0 && (ASM(i)-ASM(i
                        -1))/ASM(i-1) > 0.00
126                     Test=3; % 3 = RED
127                     addpoints(RedLine,timeStep*
                            StepDuration,2000);
128                     addpoints(RedLineP,timeStep*
                            StepDuration,200);
129                 elseif (Flow(i)-Flow(i-1))/Flow(i
                        -1) < 0
130                     Test = 1;
131                     addpoints(OrangeLine,timeStep*
                            StepDuration,1000);
132                     addpoints(OrangeLineP,timeStep
                            *StepDuration,100);
133                 else
134                     addpoints(BlackLine,timeStep*
                            StepDuration,1500);
135                     addpoints(BlackLineP,timeStep*
                            StepDuration,150);
136                 end
137             case 3 % KICK: RED
138                 if (Flow(i)-Flow(i-1))/Flow(i-1) >
                        0.1 && (SPP(i)-SPP(i-1))/SPP(i
                        -1) > 0.1 && (ASM(i)-ASM(i-1))/
                        ASM(i-1) > 0.1
```

```
139                         addpoints(RedLine,timeStep*
                                StepDuration,2000);
140                         addpoints(RedLineP,timeStep*
                                StepDuration,200);
141                     else
142                         Test = 2;
143                         addpoints(BlackLine,timeStep*
                                StepDuration,1500);
144                         addpoints(BlackLineP,timeStep*
                                StepDuration,150);
145                     end
146                 otherwise % LOW = GREEN
147                     if (Flow(i)-Flow(i-1))/Flow(i-1)
                            >= 0.002 && (SPP(i)-SPP(i-1))/
                            SPP(i-1) >= 0.000 && (ASM(i)-
                            ASM(i-1))/ASM(i-1) >= 0 %Flow
                            >= 0.015 SPP > 0.001
148                         Test = 1;
149                         addpoints(OrangeLine,timeStep
                                *StepDuration,1000)
150                         addpoints(OrangeLineP,
                                timeStep*StepDuration,100)
151                     else
152                         addpoints(GreenLine,timeStep*
                                StepDuration,500);
153                         addpoints(GreenLineP,timeStep
                                *StepDuration,50);
154                     end
155             end
156             end
157 %               Update animation
158             addpoints(FlowRateInLine,timeStep*
                    StepDuration,Sim.FlowRateInActual*6
```

```
                    E4);
159                 addpoints(FlowRateOutLine,timeStep*
                        StepDuration,Sim.FlowRateOut*6E4);
160                 addpoints(DischargeLine,timeStep*
                        StepDuration,Sim.SPP*(10^-5));
161                 addpoints(ASMLine,timeStep*
                        StepDuration,Sim.AnnulusPressure(
                        Sim.BitDepth-103)*(10^-5));
162             display(['Total step duration: ' num2str(
                    toc(tStartStep))]);
163         end
164         % Stop simulation process
165         Sim.Stop;
166     catch exception
167         % Stop simulation
168         Sim.Stop;
169         rethrow(exception);
170     end
171 end
172 diary off
```

B.3 Automated Friction Test Model

```
1 clear variables;
2 clc;
3 close all;
4 % Initial setpoints
5 FlowRateIn = 2000/60000; %  [m3/sec]
6 TopOfStringVelocity = 0; %  [m/sec]
7 PickUpVelocity = -0.15;  %  [m/sec]
8 SlackOffVelocity = 0.15; %  [m/sec]
9 SurfaceRPM = 0/60;       %  [revolutions per sec.]
```

```
10 InitialBitDepth = 2996;  %  [m]
11
12 % Configuration info
13 addpath(genpath(pwd));
14 IdentityServerURL = 'https://live.openlab.app/';
15 [username, api_key, license_guid] = GetLoginData();
16 ConfigurationName = 'Deviated';
17 SimulationName = 'DensityDependence:1350';
18 diary(join(['Simulations/',SimulationName]))
19
20 % Choose model configuration
21 UseReservoirModel = false;
22 ManualReservoirMode = false;
23 ManualInfluxLossMassRate = 0;
24 ManualInfluxLossTotalMass= 0;
25 ManualInfluxLossMD = 0;
26 ComplexReservoirKickOffTime = 60;
27 UseTransientMechanicalModel = true;
28 StepDuration = .5;
29
30 % Create simulation object
31 Sim = OpenLabClient(IdentityServerURL, username,
       api_key,license_guid,...
32         ConfigurationName,SimulationName,InitialBitDepth
               ,...
33         UseReservoirModel,ManualReservoirMode,
               ManualInfluxLossMassRate,...
34         ManualInfluxLossTotalMass,ManualInfluxLossMD,...
35         ComplexReservoirKickOffTime,
               UseTransientMechanicalModel,StepDuration);
36
37 % Stabilization criteria
38 FRWAccuracy = 0.01;
```

```
39 FRTAccuracy = 0.01;
40 FlowAccuracy = 0.01;
41 PUWAccuracy = 0.03;
42 SOWAccuracy = 0.05;
43
44 % Time steps, preallocating and test-accuracy
45 MaxTimeSteps = 600;
46 timeStepAccuracy = 20;
47 Torque = zeros(1,20);
48 Load = zeros(1,20);
49 Flow = zeros(1,20);
50 i = 0;
51 Test = 1;
52
53 % Creating plot figures
54 FrictionFigure = figure('name', 'Friction Test');
55 subplot(2,1,1);
56 xlabel('Time [sec]');
57 ylabel('Load [ton]');
58 title('Hook Load');
59 axis([0 MaxTimeSteps*StepDuration 50 150])
60 grid
61 LoadLine = animatedline('Color','b','linewidth',1.5,'
       Marker','none');
62 FRWLine = animatedline('Color','g','linewidth',1.5,'
       Marker','none');
63 PUWLine = animatedline('Color','g','linewidth',1.5,'
       Marker','none');
64 SOWLine = animatedline('Color','g','linewidth',1.5,'
       Marker','none');
65 legend({'Hook Load' 'Test Results'})
66
67 subplot(2,1,2);
```

```
68 xlabel('Time [sec]');
69 ylabel('Torque [kNm]');
70 title('Surface Torque');
71 axis([0 MaxTimeSteps*StepDuration 0 15])
72 grid
73 TorqueLine = animatedline('Color','b','linewidth',1.5,
       'Marker','none');
74 FRTLine = animatedline('Color','g','linewidth',1.5,'
       Marker','none');
75 legend({'Torque' 'Test Results'})
76
77 if Sim.IsOK
78     try
79         for timeStep = 1 : MaxTimeSteps
80             i = i + 1;
81             Torque(i) = Sim.SurfaceTorque;
82             Load(i) = Sim.HookLoad;
83             Flow(i) = Sim.FlowRateOut;
84             if i > timeStepAccuracy
85                 Torque(1) = [];
86                 Load(1) = [];
87                 Flow(1) = [];
88                 i = i - 1;
89             end
90             switch Test
91                 case 1 % Bit Off Bottom
92                     if Sim.BitDepth >= Sim.TD - 4 &&
                           timeStep > 1
93                         TopOfStringVelocity = -0.2;  %
                               [m/sec]
94                     elseif timeStep > 1
95                         Test = 2;
96                         TopOfStringVelocity = 0;
```

```
97                          SurfaceRPM = 150/60;
98                          i = 0;
99                          xline(timeStep*StepDuration,'-
                                ','State 2','
                                HandleVisibility','off');
100                         TestTimeStep = timeStep;
101                     end
102                 case 2 % Free Rotating Test
103                     if mad(Torque)/mean(Torque) <=
                            FRTAccuracy && mad(Load)/mean(
                            Load) <= FRWAccuracy && mad(
                            Flow)/mean(Flow) <=
                            FlowAccuracy && i >=
                            timeStepAccuracy
104                         FRT = mean(Torque);
105                         FRW = mean(Load);
106                         addpoints(FRWLine,(timeStep-
                                timeStepAccuracy+1:timeStep
                                )*StepDuration,(timeStep-
                                timeStepAccuracy+1:timeStep
                                )*0+FRW*1E-3);
107                         xline(timeStep*StepDuration,'-
                                ','State 3','
                                HandleVisibility','off');
108                         addpoints(FRTLine,(timeStep-
                                timeStepAccuracy+1:timeStep
                                )*StepDuration,(timeStep-
                                timeStepAccuracy+1:timeStep
                                )*0+FRT*1E-3);
109                         fprintf('Free Rotating Test
                                Finished.\nFRT = %6.2f kNm\
                                nFRW = %6.2f ton\nTest
                                Duration = %6.2f seconds\n'
```

```
                    ,FRT*1e-3,FRW*1e-3,(
                    timeStep-TestTimeStep)*
                    StepDuration)
110                 Test = 3;
111                 TestTimeStep = timeStep;
112                 i = 0;
113                 SurfaceRPM = 0/60;  % [
                    revolutions per sec.]
114             end
115         case 3 % Pick-up Test
116             if Sim.SurfaceRPMActual == 0
117                 TopOfStringVelocity =
                    PickUpVelocity;  % [
                    revolutions per sec.]
118             end
119             if  mad(Load)/mean(Load) <=
                    PUWAccuracy && mad(Flow)/mean(
                    Flow) <= FlowAccuracy && i >=
                    timeStepAccuracy && mean(Torque
                    ) <= 1
120                 PUW = mean(Load);
121                 addpoints(PUWLine,(timeStep-
                    timeStepAccuracy+1:timeStep
                    )*StepDuration,(timeStep-
                    timeStepAccuracy+1:timeStep
                    )*0+PUW*1E-3);
122                 xline(timeStep*StepDuration,'-
                    ','State 4','
                    HandleVisibility','off');
123                 fprintf('Pick Up Test Finished
                    .\nPUW = %6.2f ton\nTest
                    Duration = %6.2f seconds\n'
                    ,PUW*1e-3,(timeStep-
```

```
                    TestTimeStep)*StepDuration)
124                 i = 0;
125                 Test = 4;
126                 TopOfStringVelocity =
                        SlackOffVelocity; % [
                        revolutions per sec.]
127                 TestTimeStep = timeStep;
128             end
129         case 4 % Slack-off Test
130             if mad(Load)/mean(Load) <=
                    SOWAccuracy && mad(Flow)/mean(
                    Flow) <= FlowAccuracy  && i >=
                    timeStepAccuracy
131                 SOW = mean(Load);
132                 addpoints(SOWLine,(timeStep-
                        timeStepAccuracy+1:timeStep
                        )*StepDuration,(timeStep-
                        timeStepAccuracy+1:timeStep
                        )*0+SOW*1E-3);
133                 fprintf('Slack-off Test
                        Finished.\nSOW = %6.2f ton\
                        nTest Duration = %6.2f
                        seconds\n',SOW*1e-3,(
                        timeStep-TestTimeStep)*
                        StepDuration)
134                 break
135             end
136     end
137     Sim.FlowRateIn = FlowRateIn;
138     Sim.TopOfStringVelocity =
            TopOfStringVelocity;
139     Sim.SurfaceRPM = SurfaceRPM;
140     Sim.Step();
```

```
141                 if ~Sim.IsOK % Simulator fails
142                     break;
143                 end
144                 % Update animation
145                 addpoints(LoadLine,timeStep*StepDuration,
                        Sim.HookLoad*1E-3);
146                 addpoints(TorqueLine,timeStep*StepDuration
                        ,Sim.SurfaceTorque*1E-3);
147             end
148             % Stop simulation process
149             Sim.Stop;
150         catch exception
151             % Stop simulation
152             Sim.Stop;
153             rethrow(exception);
154         end
155 end
156 diary off
157 saveas(FrictionFigure,join(['Simulations/',
        SimulationName]),'epsc')
```

Appendix C

Drillbotics©

Disclaimer: Some of this content is taken directly, or with minor modifications, from the project report [5].

C.1 Synopsis of Phase I

During Phase I, also referred to as the design phase, the Norwegian University of Science and Technology (NTNU) team worked together to decide on a sustainable design, based on mechanical and budget limitations as well as time constraints. An outline of the mechanical and electrical design proposed by the NTNU team will be presented below.

The final mechanical design proposed, included using a positive displacement motor (PDM) as the power section, an adjustable bent sub for steering, a self-designed drill bit and aluminum drillpipe. Last year's team experienced trouble with generating enough torque and RPM. However, as dimensions of the drill bit are increased, the team seeks to utilize the extra space to generate more power to drill through the rock sample. With last year's team disappointing results and other associated risks related to using a PDM as the downhole power section, the team decided to have an electrical miniature motor (EMM) as a back-up solution as it can swiftly be implemented.

The downhole power section, or the PDM, together with an adjustable bent sub will enable the team to steer and generate the appropriate well path to hit the competition target(s). With the uncertainties related to the coordinates, designing an adjustable bent sub should increase the possible hitting range of the drillstring.

The physical rig developed by previous NTNU teams has proven to be well designed and sustainable for the planned operation. The only planned changes are minor modifications to improve overall safety. Relevant parts to discuss on the rig include the hoisting motor which moves vertical, enabling it to control weight on bit (WOB), with the assistance from a WOB cell. The top drive servo motor controls both drillstring angular position and RPM. Below the top drive is an electrical swivel connecting the downhole electrical cables with the topside equipment. Subsequently, the drillstring, with the PDM, adjustable bent housing, drill bit, is to be connected. As for drilling fluid, the team was planning on using water.

The control system utilizes downhole sensors, gathering real-time data to be fed back to a closed-loop system for the drilling operation to be executed autonomously. The two main parts of the control system are a WOB controller and position controller. The speed of the operation will be controlled using the WOB controller which controls the ROP. Drill bit position will be known from the position controller, which will be essential to generate a well path hitting the relevant target(s). A sensor card located in the BHA will provide feedback through a wired communication scheme to a topside computer, which is the basis for the closed-loop control system. States, also known as the different phases in the control system, are used throughout different parts of the drilling operation and are mainly separated into vertical and directional phases. In order to ensure a safe operation, the control system will transition to a safety layer in case of any measurements obtained exceeds defined safety thresholds.

A more detailed description of the design and plans made in Phase I can be found in the project report [5].

C.2 Progress made in Phase II

A reliable and robust mechanical design is essential to maintain drilling efficiency of the autonomous system. Furthermore, a strong mechanical structure will improve overall system efficiency and stability, as well as maintaining borehole quality and integrity of the drillstring and the rig. Based on the design proposed in Phase I, this section will cover work done in regards to the mechanical design prior to the effects of COVID-19.

C.3 Positive Displacement Motor

The main drilling objective of this year's competition is to hit one or more target(s), utilizing X/Y coordinates and vertical depth(s) provided by the Drillbotics© committee on the competition day. The design report states solution chosen to encounter this problem, is using a downhole PDM in combination with a bent sub. As the PDM is the only source of rotational power in the tangent section, it was recognized early in Phase II that this was the most critical part of the design. In addtition, the team desired to optimize the design based on findings during testing.

C.3.1 PDM-design

The PDM is a reversed progressive cavity pump, which is based on the Moineau principle. A PDM transmits hydraulic energy to mechanical energy by the use of a rotor/stator configuration based on closed cavities. The PDM power section consist of a helical rotor and a helical stator with one more lobe than the rotor, illustrated in Figure C.1.

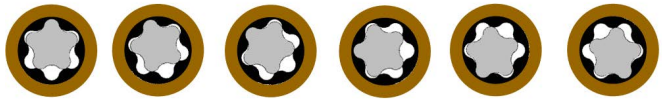

Figure C.1: Cross section of PDM with 4/5 lobe configuration [28].

A hypocycloid is the basis for designing the PDM rotor, and it is defined as a special plane curve generated by a rolling generator circle inside of a base circle as shown in Figure C.2a.

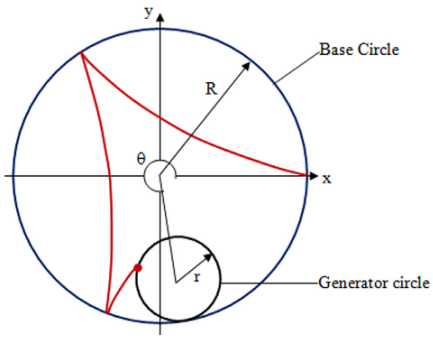

(a) Generation of a hypocycloid [75].

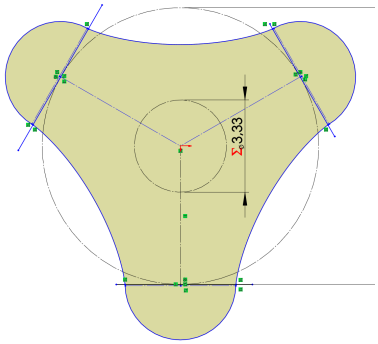

(b) Modified hypocloid generating contour of a 3-lobe rotor.

Figure C.2: Friction test results with varying flow rates.

Nguyen et al. [75] created modified hypocycloid equations to describe a N-lobe rotor's cross sectional area, using a 3-D vector approach. Equation C.1 and C.2 generates the cross section plane curve for a N-lobe PDM rotor, where r is the generator circle radius and d the diameter of the semi circles at each cusp. These equations will generate the contour of a N-lobe PDM as shown in Figure C.2b.

$$x_n = r[(N-1)cos\theta + cos((N-1)\theta)] + \frac{cos\theta + cos((N-1)\theta)}{\sqrt{2}\sqrt{1-cos(N\theta)}}\frac{d}{2} \tag{C.1}$$

$$y_n = r[(N-1)sin\theta - sin((N-1)\theta)] + \frac{sin\theta + sin((N-1)\theta)}{\sqrt{2}\sqrt{1-cos(N\theta)}}\frac{d}{2} \tag{C.2}$$

C.3.2 Material Selection

Last year's team experienced high wear rates on the PDM [84]. This provoked the most challenging aspect of designing the PDM, respectively the material selection.

This year's team were equipped with a brand new resin 3D-printer. This should reduce the experienced wear, as the printing resolution is increased compared to last year's 3D printer.

Figure C.3: First prototype of 3D-printed PDM rotor.

In the early stages of designing the PDM it was discovered that the current printing resin provides a brittle product, shown in Figure C.3. Therefore, the team acquired additional printing resin more applicable for its intended use. Three types of resins where purchased and delivered by Formlabs, designed for engineering purposes [85]. The respective types of resins purchased were: Grey Pro, Flexible and Durable. Resins post-cured material properties, and their corresponding recommended post-curing procedures, are presented in Table C.1.

Table C.1: Post-cured material properties and recommended post-curing procedures of Formlabs resins [86, 87, 88, 89].

Resin type	**Grey pro**	**Flexible**	**Durable**
Ultimate tensile strength [MPa]	61	7.7-8.5	28
Elongation at failure [%]	13	75-85	55
Compression strength [%]	-	0.40	-
Full cure time [min]	15	60	60
Full cure temperature [°C]	80	60	60

Initially, the different types of resin were intended to be used for different parts of the PDM design. The grey pro resin gave a post-cured product with moderate elongation and resistance to deformation over time. It was intended to use the grey pro raisin as a prototype for testing parts of the design, which was intended to be manufactured in steel when the final design was determined. The motivation for using a substitute for steel is the decrease in manufacturing cost per part, and decrease in the production time as it is done in-house.

The durable resin used for applications requiring minimal friction, which is ap-

plicable for a PDM. This resin was planned to be used as either the rotor- or the stator material. Finally, the flexible resin was initially thought to function as the stator material, as it produces parts possible to bend and compress.

As the different resins were acquired, the test printing of those started. Findings from testing the resins included that the flexible resin was too brittle to function as a material in any of the PDM parts. Therefore, it was planned to use the durable resin for both rotor- and stator material during the testing phase, due to its low friction application.

C.3.3 Test Plan

A plan for testing the PDM design was created, with the intention of performing tests using BHA parts designed and developed last year. A prototype design to be used during testing was created to fit the dimensions last year's BHA design, these components are shown in Figure C.4.

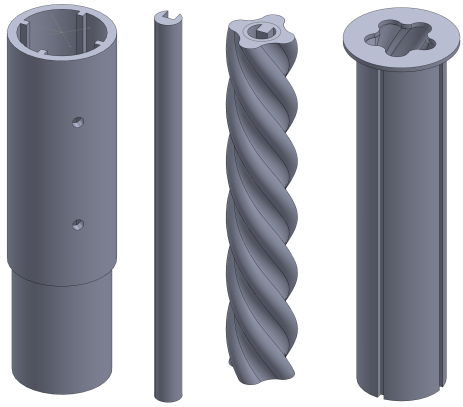

Figure C.4: PDM test design. From left to right; housing, shaft, 4-lobe rotor and 5-lobe stator.

The PDM housing was designed to fit into the power section steel tubular of last year's BHA, and the component should be printed using the grey pro resin due to its resistance to deformation. The shaft component will fit into the rotor's cavity, this will also be printed using the grey pro resin. Printing the shaft separately, as oppose to printing it together with the rotor, is due to utilizing a more solid

material for the shaft. Both the rotor and stator will be printed in durable resin for the testing phase, as mentioned above.

C.3.4 Test Phase

The PDM is designed such that small adjustments can easily be implemented. Excessive testing of the PDM will improve the overall design, making it more sustainable and robust PDM. This will be achieved based on observations and knowledge obtained during the test phase. Hereunder, different designs, respectively with varying sizes, lengths, lobe configuration and materials, will be tested during this phase. When a robust and sustainable design is created, the material of each component should be determined, specifically which parts should be manufactured in steel. This is due to the production time of these materials. Additionally, the dimensions of the BHA design are increased, which means the PDM should be adjusted to fit this; this mostly relates to an increase in diameter.

C.3.5 Final Design

The final PDM design was expected to change during the testing phase. However, the team's initial thoughts in this regard included a final design consisting of a 3D-printed steel rotor and a 3D-printed stator, printed in durable resin. The power section housing was intended to be an integral part of the BHA, designed and produced at the NTNU workshop.

C.4 Bent sub

As the main objectives in the 2020 Drillbotics© competition is to autonomously drill a well and hit multiple directional target(s), the design must be able to change the trajectory of the wellbore to hit the competition targets. Most commonly used for this is a PDM in combination with a bent sub. A bent sub is a short length of pipe manufactured so that the lower connection is slightly offset as opposed to the upper connection, this is referred to as a tilt angle. The bent sub will also contribute to the drill bit being offset from the center line of the drillstring, meaning it will not be possible to rotate the drill bit by rotating the drillstring from surface. Therefore, the bent sub must be used in conjunction with a PDM [74].

There are two possible solutions for a bent sub, respectively a fixed angle and an adjustable angle. As target coordinates will not be given prior to the competition, the team proposed designing an adjustable bent sub in Phase I to avoid limitations related to the trajectory. A possible idea for an solution is illustrated in Figure C.5. However, there are challenges related to this solution in regards to small dimensions, in combination with the limited time available. To simplify the design the team considered adjustments that could be made. Discussed were options of simplifying the locking mechanism, but a major challenge is making related to leakage. Therefore, after consulting with the mechanical engineer the team decided on using a fixed bent sub instead.

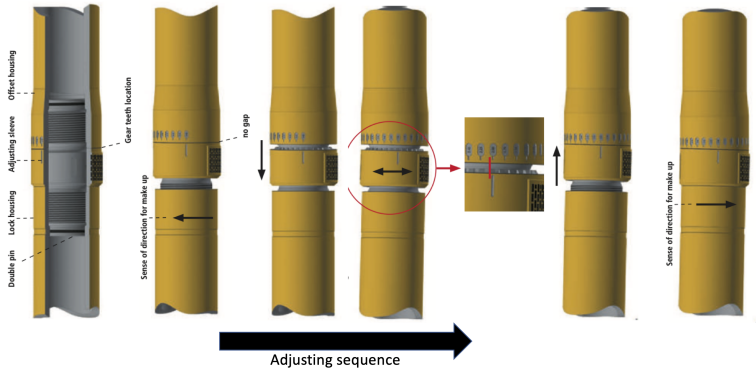

Figure C.5: Adjustable bent housing [90].

A fixed bent sub is illustrated in Figure C.6. The concept is self-explanatory, i.e. a length of steel pipe with a fixed angle. The fixed sub was to be manufactured in the NTNU workshop.

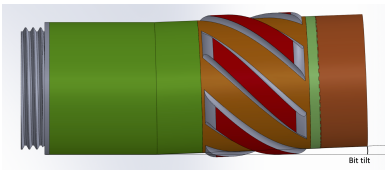

Figure C.6: Bent sub with fixed angle.

C.4.1 Bit Tilt

Bit tilt is by definition misalignment of bit face away from the drillstring axis [77]. This angle can be estimated based on the "three-point curvature" calculation:

$$\theta = \frac{DLS(L_1 + L_2)}{2} \tag{C.3}$$

$DLS[^\circ/m]$ is the dogleg severity (DLS). The length of the BHA is divided into two sections, were $L_1\,[m]$ is the length of the section above the bend and $L_2\,[m]$ is the length of the section below the bend. The estimated lengths of the sections are respectively $L_1 = 15\,cm$ and $L_2 = 8.5\,cm$. Figure C.7 shows all variables used in Equation C.3.

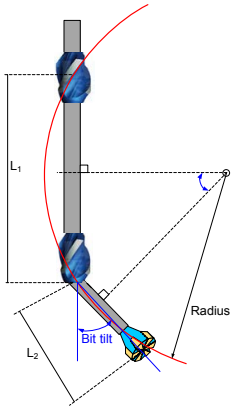

Figure C.7: Variables used in "three-point curvature" calculations, based on BHA configurations [28]

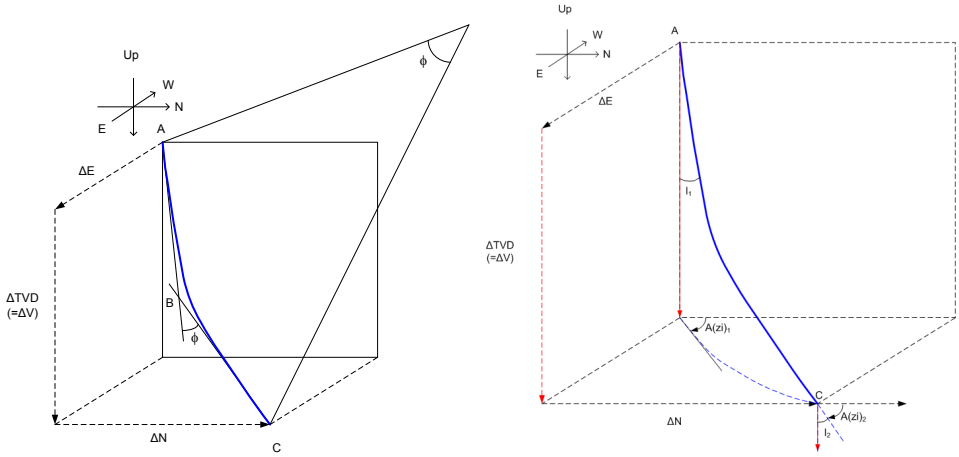

(a) Dogleg Angle (ϕ)

(b) Inclination (I) and Azimuth (A)

Figure C.8: Relevant parameters when developing a well path [28].

Equation C.4 is used to predict the DLS.

$$DLS = \frac{\phi}{CL} \tag{C.4}$$

Where $\phi\,[°]$ is the dogleg angle. $CL\,[m]$ is the course length and is estimated using Equation C.5 below:

$$CL = \frac{RC\pi(I_2 - I_1)}{180} \tag{C.5}$$

$RC\,[m]$ is the radius of curvature (RC), which is estimated based on the axial stress as a result of bending compared to the material yield strength. Based on calculations done in Phase I, it was proposed to use aluminium[11] drillpipe as oppose to stainless steel[12]. Minimum RC for aluminium is significantly less, compared to stainless steel, which corresponds to a larger horizontal displacement. Figure C.9 illustrates the minimum RC in order for the pipe to stay within its elastic zone, based on the axial stress from bending versus the material yield strength. Axial bending stress is calculated with the following equation:

$$\sigma_z^b = \frac{E}{RC} y \tag{C.6}$$

[11] Aluminium 6061-T6

[12] Stainless steel grade 316

Where $E\,[Pa]$ is the Young's Modulus for the material, in this case for aluminum, and $y\,[m]$ is the distance from the cross-sectional center to point of interest.

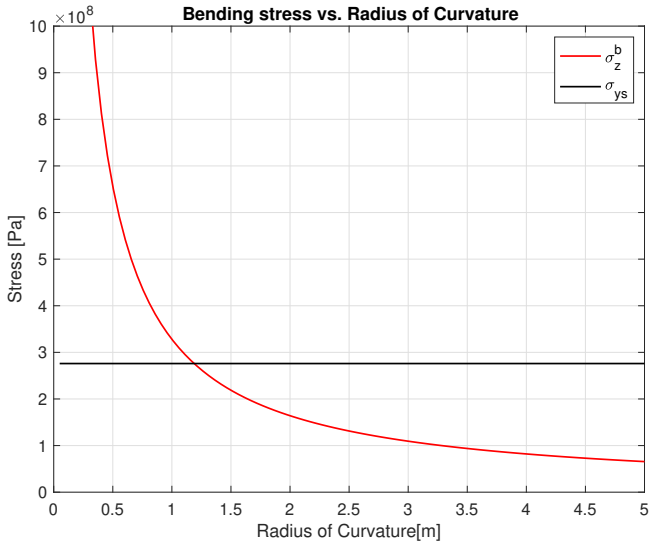

Figure C.9: Axial stress from bending to different values of RC, compared to material yield strength.

From Figure C.9, the minimum RC is found to be $1.19\,m$ for the aluminum drillpipe to stay within its elastic zone, which is equivalent to a horizontal displacement of 4.48". However, as the estimated RC is the absolute minimum to avoid deformations of the pipe, a safety factor is applied as a precaution. For further calculation, the RC is $1.32\,m$ which corresponds to a horizontal displacement of 4". This is equivalent to an exit angle of $22.6°$.

Using Equation C.5, where $RC = 1.32\,m$, $I_2 = 22.6°$, and $I_1 = 0°$ predicts a course length of $52.1\,cm$. DLS can now be estimated with Equation C.4 to $43.4°/m$. The maximum required bit tilt angle is therefore:

$$\theta = \frac{DLS(L_1 + L_2)}{2} = 5.1° \tag{C.7}$$

C.5 Drill bit

As for the drill bit, there were two options. Either utilizing the bit provided by Baker Hughes, which respectively was a PDC micro-bit designed specifically for the Drillbotics© by DSATS. Or if desired the team could design their own drill bit.

The team was motivated to design their own bit. The Drillbotics© guidelines stated that each team could design their own bits, but are not allowed to seek assistance from third-parties. However, third-parties can manufacture the designed bit. The NTNU team started designing the bit in Solidworks. The collaboration with Lyng Drilling from previous last year was continued, and they had already offered to manufacture the designed miniature bit.

Prior to the designed bit being ready for testing the team would utilize the PDC bit provided by Baker Hughes for testing other components of the drillstring.

C.5.1 Baker Hughes micro-bit

Baker Hughes supplied all teams with two micro-bits, with a 1.5” bit diameter which is increased from last year’s 1.25” bit.

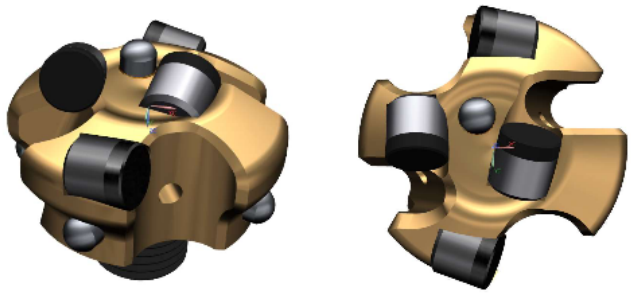

Figure C.10: The PDC Micro-bit supplied by Baker Hughes.

It consists of four nozzles used as fluid ports, and informed by the datasheet, is said to have shortened bit length, but with a rather high bit anisotropy. A quite unique feature is its option to configure and adjust the aggressiveness of its sides by changing the amount of exposure of the cutters.

C.5.2 Bit profile

The shape of a drill bit's face in addition to the spreading of the cutters are called the bit profile and is often referred to as one of the more essential parts of the bit design. The bit profile mainly influences a bit's performance, durability, ROP and steerability.

The way the profile is designed impacts how hydraulic flow from the drilling fluid will behave across the bit's surface. The main purpose of the fluid is to clean the bottom-hole as the bit penetrates the rock while simultaneously cooling down the cutters. Without the use of a hydraulic fluid, an accumulation of cuttings will gather in the bottom of the hole, causing problems to the BHA in the form of decreased ROP or make the whole drill bit completely stuck. Illustrated below in Figure C.11 are the two most common types of bit profiles.

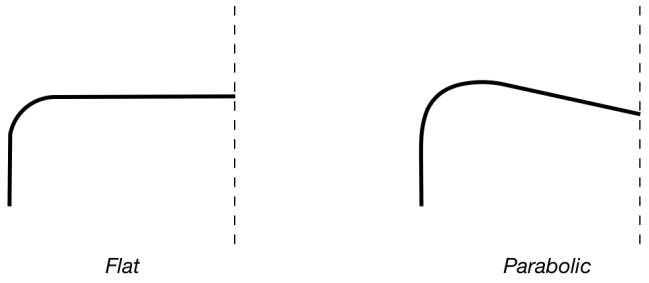

Figure C.11: Flat profile vs. Parabolic profile

C.5.3 Cutter Density

The cutters on the bit are spread around the bit profile to make sure the head of the bit covers the whole formation. This is so that nothing down hole will remain uncut. The frequency of how close to each other the cutters are placed is defined as cutter density.

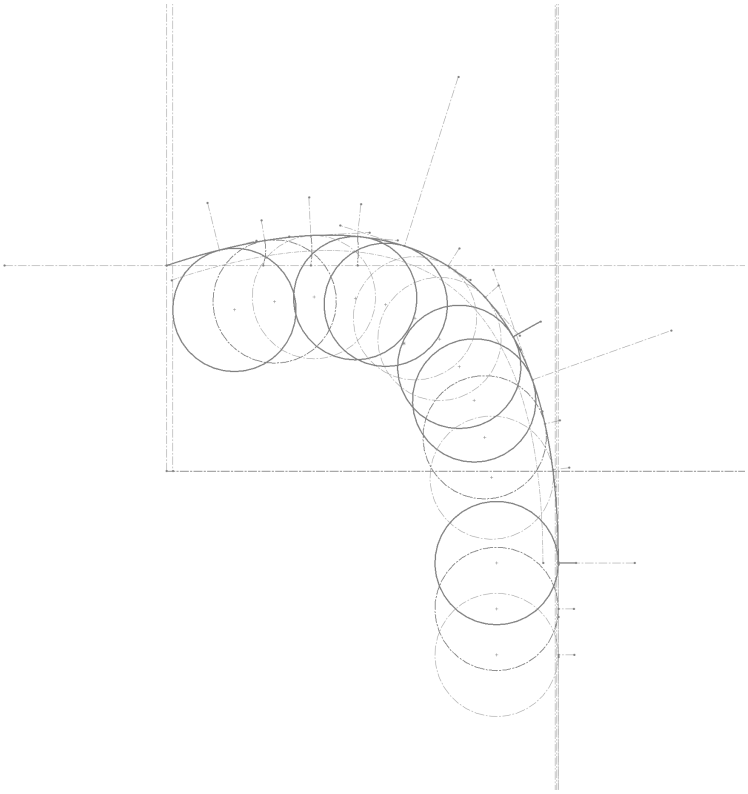

Figure C.12: The current work on the Lyng custom made bits' cutter density layout.

Figure C.12 shows the progress made by the time prior to COVID-19. The design-sketch is from Solidworks. A distance of 6 mm was used between the cutters on each line.

A. Hiwa, J. Mannsverk, V. R. Meyer

Transitioning to an automated drilling system.

NTNU
Norwegian University of
Science and Technology